



# **NAVAL POSTGRADUATE SCHOOL**

**MONTEREY, CALIFORNIA**

## **THESIS**

**THE ROLE OF SUBTROPICAL INTRUSION IN THE  
DEVELOPMENT OF TYPHOON USAGI (5W) 2007**

by

Raymund P. DeLeon

March 2008

Thesis Advisors:

Michael Montgomery  
Patrick Harr

**Approved for public release; distribution is unlimited.**

THIS PAGE INTENTIONALLY LEFT BLANK

<b>REPORT DOCUMENTATION PAGE</b>			<i>Form Approved OMB No. 0704-0188</i>	
Public reporting burden for this collection of information is estimated to average 1 hour per response, including the time for reviewing instruction, searching existing data sources, gathering and maintaining the data needed, and completing and reviewing the collection of information. Send comments regarding this burden estimate or any other aspect of this collection of information, including suggestions for reducing this burden, to Washington headquarters Services, Directorate for Information Operations and Reports, 1215 Jefferson Davis Highway, Suite 1204, Arlington, VA 22202-4302, and to the Office of Management and Budget, Paperwork Reduction Project (0704-0188) Washington DC 20503.				
<b>1. AGENCY USE ONLY (Leave blank)</b>		<b>2. REPORT DATE</b> March 2008	<b>3. REPORT TYPE AND DATES COVERED</b> Master's Thesis	
<b>4. TITLE AND</b> The Role of Subtropical Intrusion in the Development of Typhoon Usagi (5W) 2007			<b>5. FUNDING NUMBERS</b>	
<b>6. AUTHOR(S)</b> Raymund P DeLeon				
<b>7. PERFORMING ORGANIZATION NAME(S) AND ADDRESS(ES)</b> Naval Postgraduate School Monterey, CA 93943-5000			<b>8. PERFORMING ORGANIZATION REPORT NUMBER</b>	
<b>9. SPONSORING /MONITORING AGENCY NAME(S) AND ADDRESS(ES)</b> N/A			<b>10. SPONSORING/MONITORING AGENCY REPORT NUMBER</b>	
<b>11. SUPPLEMENTARY NOTES</b> The views expressed in this thesis are those of the author and do not reflect the official policy or position of the Department of Defense or the U.S. Government.				
<b>12a. DISTRIBUTION / AVAILABILITY STATEMENT</b> Approved for public release; distribution is unlimited.			<b>12b. DISTRIBUTION CODE</b>	
<b>13. ABSTRACT (maximum 200 words)</b>  <p>During July 2007, fields from both the NCEP GFS final analyses and ECMWF model of OW and SF analyses suggests the development of two distinct areas with sub-tropical intrusion from remnants of a decaying baroclinic system in the WNP.</p> <p>This analysis of the formation of Usagi points to sub-tropical intrusion of a strong lower-tropospheric baroclinic system undergoing decay as potential seedlings for typhoon formation in areas of high sea surface temperatures, weak low-level vertical wind shear, and persistent convection. As the PV anomalies is stretched and detached from the baroclinic source region, it is wrapped around a strong tropospheric anticyclone in the subtropics. This constitutes a different type of baroclinic initiation process than has been previously identified in Atlantic cyclone formation events associated with TT, which are induced by upper-level troughs.</p> <p>The area of high values of OW at the tip of a PV streamer favors sustained deep convection, which will enhance the low-level vorticity and moisten the mid-level thereby producing high values of SF. The area of strong vorticity at the tip of the second PV streamer possessed both high OW and SF, favoring deep convection and cyclonic vortex tube stretching that appeared to culminate in an enhancement of lower tropospheric cyclonic vorticity.</p> <p>Although this analysis was originally motivated by initial analyses suggesting that ex-hurricane Cosme underwent a direct vorticity interaction with the second PV streamer, our revised hypothesis on the role of Cosme is that it may have enlarged the wave pouch and helped preserve the mid-tropospheric circulation from hostile outside influences. In this sense, the Cosme wave may have played an important indirect role in the formation of Usagi. This hypothesis requires further investigation.</p>				
<b>14. SUBJECT TERMS</b> Tropical Cyclones, Tropical Transition, Subtropical intrusion Typhoon Usagi, Potential Vorticity, Marsupial Paradigm, Okubu-Wiess, Saturation Fraction			<b>15. NUMBER OF PAGES</b> 118	
			<b>16. PRICE CODE</b>	
<b>17. SECURITY CLASSIFICATION OF REPORT</b> Unclassified	<b>18. SECURITY CLASSIFICATION OF THIS PAGE</b> Unclassified	<b>19. SECURITY CLASSIFICATION OF ABSTRACT</b> Unclassified	<b>20. LIMITATION OF ABSTRACT</b> UU	

NSN 7540-01-280-5500

Standard Form 298 (Rev. 8-98)  
Prescribed by ANSI Std. Z39.18

THIS PAGE INTENTIONALLY LEFT BLANK

**Approved for public release; distribution is unlimited.**

**THE ROLE OF SUBTROPICAL INTRUSION IN THE DEVELOPMENT OF  
TYPHOON USAGI (5W) 2007**

Raymund P. DeLeon  
Captain, United States Air Force  
B.S., Valdosta State University, 2000

Submitted in partial fulfillment of the  
requirements for the degree of

**MASTER OF SCIENCE IN METEOROLOGY**

from the

**NAVAL POSTGRADUATE SCHOOL  
March 2008**

Author: Raymund P. DeLeon

Approved by: Michael Montgomery  
Thesis Advisor

Patrick Harr  
Thesis Advisor

Philip A. Durkee  
Chairman, Department of Meteorology

THIS PAGE INTENTIONALLY LEFT BLANK

## **ABSTRACT**

During July 2007, fields from both the NCEP GFS final analyses and ECMWF model of OW and SF analyses suggests the development of two distinct areas with sub-tropical intrusion from remnants of a decaying baroclinic system in the WNP.

This analysis of the formation of Usagi points to sub-tropical intrusion of a strong lower-tropospheric baroclinic system undergoing decay as potential seedlings for typhoon formation in areas of high sea surface temperatures, weak low-level vertical wind shear, and persistent convection. As the PV anomalies is stretched and detached from the baroclinic source region, it is wrapped around a strong tropospheric anticyclone in the subtropics. This constitutes a different type of baroclinic initiation process than has been previously identified in Atlantic cyclone formation events associated with TT, which are induced by upper-level troughs.

The area of high values of OW at the tip of a PV streamer favors sustained deep convection, which will enhance the low-level vorticity and moisten the mid-level thereby producing high values of SF. The area of strong vorticity at the tip of the second PV streamer possessed both high OW and SF, favoring deep convection and cyclonic vortex tube stretching that appeared to culminate in an enhancement of lower tropospheric cyclonic vorticity.

Although this analysis was originally motivated by initial analyses suggesting that ex-hurricane Cosme underwent a direct vorticity interaction with the second PV streamer, our revised hypothesis on the role of Cosme is that it may have enlarged the wave pouch and helped preserve the mid-tropospheric circulation from hostile outside influences. In this sense, the Cosme wave may have played an important indirect role in the formation of Usagi. This hypothesis requires further investigation.

THIS PAGE INTENTIONALLY LEFT BLANK

# TABLE OF CONTENTS

I.	INTRODUCTION.....	1
A.	ATLANTIC TT AND WNP CYCLONE FORMATION.....	3
B.	THE MARSUPIAL PARADIGM.....	8
C.	ELEMENTS OF THE GENESIS SEQUENCE.....	10
1.	Dynamical Fields - OW Parameter.....	10
2.	Thermodynamical Fields - SF.....	11
D.	OBJECTIVES OF CURRENT STUDY.....	11
E.	PRE-STORM SITUATION.....	12
1.	Hurricane Cosme (6E).....	12
2.	Baroclinic Extratropical Low.....	12
3.	Tropical System Non-developer (Gyre).....	13
4.	Tropical Cyclogenesis of Typhoon Usagi (5W).....	13
II.	DATA AND METHODOLOGY.....	15
A.	SATELLITE DATA PROCESSING.....	17
1.	MTSAT Infrared-Red Imagery.....	17
2.	Tropical Rainfall Measuring Mission (TRMM).....	18
B.	NUMERICAL MODEL FIELDS.....	18
1.	GFS.....	19
2.	NOGAPS and UKMET.....	19
3.	ECMWF.....	20
C.	LIMITATIONS.....	20
III.	ANALYSIS AND DISCUSSION.....	21
A.	OVERVIEW OF INITIATING BAROCLINIC SYSTEM.....	24
1.	The Large-Scale Lower Tropospheric Environment of Usagi.....	24
2.	The Local Environment of Usagi.....	28
3.	Lower Tropospheric Interactions within the Non-Developer (Gyre) and Developer (Usagi).....	30
B.	DYNAMIC AND THERMODYNAMIC EVOLUTION OF USAGI.....	47
C.	OW CRITERION AND SF PARAMETERS TO DISTINGUISH THE NON DEVELOPER (GYRE) AND DEVELOPER (USAGI).....	61
1.	OW Parameter Comparison.....	62
2.	SF Comparison.....	71
3.	Time Series Analysis.....	75
IV.	SUMMARY AND RECOMMENDATION.....	79
A.	SUMMARY.....	79
B.	FURTHER STUDIES.....	81
APPENDIX A.	OW PLOTS.....	83
APPENDIX B.	RELATIVE VORTICITY PLOTS.....	87

APPENDIX C.	SF PLOTS .....	91
APPENDIX D.	TRMM PLOTS .....	93
LIST OF REFERENCES.....		95
INITIAL DISTRIBUTION LIST .....		99

## LIST OF FIGURES

Figure 1.	(a) Visible satellite and Tropical Rainfall Measuring Mission (TRMM) Microwave Imager (TMI) 85-GHz polarized corrected temperature (PCT) imagery at 1145 and 1209 UTC 10 Sep 2000, respectively; (b) (upper right), as in (a) but for visible and TMI 85-GHz PCT at 1245 and 1335 UTC 15 Oct 2000; (c) IR and Special Sensor Microwave/Imager 85-GHz PCT at 0015 and 0219 UTC 10 Sep 2002; and (d) IR and TMI 85-GHz PCT at 2045 and 2132 UTC 11 Oct 2001. In all panels, the “L” indicates the position of surface low. Images obtained courtesy of Naval Research Laboratory: 14 February 2008. ....	6
Figure 2.	VORTRACK analysis of Usagi and Cosme interaction on 1200 UTC 26 July 2007 48 hours before Usagi was named as TD 05W. Shadings are relative vorticity (unit: $1 \times 10^{-5}$ ), winds @ 850 hPa plotted if relative vorticity is $> 0$ , and black dots are track (12 hour steps) where relative vorticity is $1.5$ (unit $1.5 \times 10^{-5}$ ). ....	22
Figure 3.	VORTRACK analysis of Usagi and Cosme interaction on 0000 UTC 27 July 2007 36 hours before Usagi was named as TD 05W. Shadings are relative vorticity (unit: $1 \times 10^{-5}$ ), winds @ 850 hPa plotted if relative vorticity is $> 0$ , and black dots are track (12 hour steps) where relative vorticity is $1.5$ (unit $1.5 \times 10^{-5}$ ). ....	23
Figure 4.	VORTRACK analysis of Usagi and Cosme interaction on 1200 UTC 27 July 2007 24 hours before Usagi was named as TD 05W. Shadings are relative vorticity (unit: $1 \times 10^{-5}$ ), winds @ 850 hPa plotted if relative vorticity is $> 0$ , and black dots are track (12 hour steps) where relative vorticity is $1.5$ (unit $1.5 \times 10^{-5}$ ). ....	24
Figure 5.	From mid-May into early August, weak to moderate Madden-Julian Oscillation (MJO) activity was observed as velocity potential anomalies propagated eastwards. ....	27
Figure 6.	The MJO index indicates that the MJO signal has weakened rapidly. July is indicated in blue and June in green. Courtesy of <a href="http://www.bom.gov.au/bmrc/clfor/cfstaff/matw/maproom/RMM/index.htm">http://www.bom.gov.au/bmrc/clfor/cfstaff/matw/maproom/RMM/index.htm</a> 1 December 2007. ....	28
Figure 7.	Streamlines of horizontal flow at 850 hPa and MTSAT satellite for 0000 UTC 22 July. Shadings are temperature values from $-20^{\circ}\text{C}$ to less than $-70^{\circ}\text{C}$ . ....	30
Figure 8.	Streamlines of horizontal flow at 850 hPa and MTSAT satellite for 1800 UTC 23 July. Shadings are temperature values from $-20^{\circ}\text{C}$ to less than $-70^{\circ}\text{C}$ . ....	32
Figure 9.	Streamlines of horizontal flow at 850 hPa and MTSAT satellite for 1200 UTC 24 July. Shadings are temperature values from $-20^{\circ}\text{C}$ to less than $-70^{\circ}\text{C}$ . ....	33

Figure 10.	Streamlines of horizontal flow at 850 hPa and MTSAT satellite for 0600 UTC 25 July. Shadings are temperature values from -20°C to less than -70°C.....	34
Figure 11.	Streamlines of horizontal flow at 850 hPa and MTSAT satellite for 1200 UTC 25 July. Shadings are temperature values from -20°C to less than -70°C.....	35
Figure 12.	Streamlines of horizontal flow at 850 hPa and MTSAT satellite for 1800 UTC 25 July. Shadings are temperature values from -20°C to less than -70°C.....	36
Figure 13.	Streamlines of horizontal flow at 850 hPa and MTSAT satellite for 0000 UTC 26 July. Shadings are temperature values from -20°C to less than -70°C.....	38
Figure 14.	Streamlines of horizontal flow at 850 hPa and MTSAT satellite for 0600 UTC 26 July. Shadings are temperature values from -20°C to less than -70°C.....	39
Figure 15.	Streamlines of horizontal flow at 850 hPa and MTSAT satellite for 1200 UTC 26 July. Shadings are temperature values from -20°C to less than -70°C.....	40
Figure 16.	Streamlines of horizontal flow at 850 hPa and MTSAT satellite for 0000 UTC 27 July. Shadings are temperature values from -20°C to less than -70°C.....	41
Figure 17.	Streamlines of horizontal flow at 850 hPa and MTSAT satellite for 0600 UTC 27 July. Shadings are temperature values from -20°C to less than -70°C.....	42
Figure 18.	Streamlines of horizontal flow at 850 hPa and MTSAT satellite for 1200 UTC 27 July. Shadings are temperature values from -20°C to less than -70°C.....	43
Figure 19.	Streamlines of horizontal flow at 850 hPa and MTSAT satellite for 1800 UTC 27 July. Shadings are temperature values from -20°C to less than -70°C.....	44
Figure 20.	Streamlines of horizontal flow at 850 hPa and MTSAT satellite for 0600 UTC 28 July. Shadings are temperature values from -20°C to less than -70°C.....	45
Figure 21.	Streamlines of horizontal flow at 850 hPa and MTSAT satellite for 1200 UTC 28 July. Shadings are temperature values from -20°C to less than -70°C.....	46
Figure 22.	Potential vorticity in units of PVU at 850-500 hPa overlay for 1800 UTC 25 July.....	50
Figure 23.	Potential vorticity in units of PVU at 850-500 hPa overlay for 0000 UTC 26 July.....	51
Figure 24.	Potential vorticity in units of PVU at 850-500 hPa overlay for 0600 UTC 26 July.....	52
Figure 25.	Potential vorticity in units of PVU at 850-500 hPa overlay for 1200 UTC 26 July.....	53

Figure 26.	Potential vorticity in units of PVU at 850-500 hPa overlay for 1800 UTC 26 July.....	54
Figure 27.	Potential vorticity in units of PVU at 850-500 hPa overlay for 0000 UTC 27 July.....	55
Figure 28.	Potential vorticity in units of PVU at 850-500 hPa overlay for 0600 UTC 27 July.....	56
Figure 29.	Potential vorticity in units of PVU at 850-500 hPa overlay for 1200 UTC 27 July.....	57
Figure 30.	Vis5D trajectories between Usagi and Cosme during 0600 UTC 26 July. Streamlines are 850 hPa. The orange figures are absolute vorticity ( $10^{-4}\text{S}^1$ ). The white strips are trajectories with Usagi and the yellow are trajectories associated with Cosme from the last 72 hours. ....	59
Figure 31.	Vis5D trajectories between Usagi and Cosme during 1200 UTC 27 July. Streamlines are 850 hPa. The orange figures are absolute vorticity ( $10^{-4}\text{S}^1$ ). The white strips are trajectories with Usagi and the yellow are trajectories associated with Cosme from the last 72 hours. ....	60
Figure 32.	Vis5D trajectories of Usagi during 1800 UTC 28 July. Streamlines are 850 hPa. The orange figures are absolute vorticity ( $10^{-4}\text{S}^1$ ). The white strips are trajectories with Usagi and the yellow are trajectories associated with Cosme from the last 72 hours.....	61
Figure 33.	Streamlines of horizontal flow at 600 hPa for the genesis sequence of the non-developer from 1800 UTC 23 July to 1200 UTC 24 July. The shadings indicate high values of OW parameter (units: $10^{-10}\text{s}^{-2}$ ) as defined in Eq. (1.1). This quantity, like vorticity, is invariant with respect to translation, therefore identical in translating and moving frames. Red areas are strong values and blue values areas are weak. ....	66
Figure 34.	Streamlines of horizontal flow at 600 hPa for the genesis sequence of the Usagi system from 0600 UTC 27 July to 0000 UTC 28 July. The shadings indicate high values of OW parameter (units: $10^{-10}\text{s}^{-2}$ ) as defined in Eq. (1.1). This quantity, like vorticity, is invariant with respect to translation, therefore identical in translating and moving frames. Red areas are strong values and blue values areas are weak. ....	66
Figure 35.	Streamlines of horizontal flow at 850 hPa for the genesis sequence of the non-developer from 1800 UTC 23 July to 1200 UTC 24 July. The shadings indicate high values of OW parameter (units: $10^{-10}\text{s}^{-2}$ ) as defined in Eq. (1.1). This quantity, like vorticity, is invariant with respect to translation, therefore identical in translating and moving frames. Red areas are strong values and blue values areas are weak. ....	67
Figure 36.	Streamlines of horizontal flow at 850 hPa for the genesis sequence of the Usagi system from 0600 UTC 27 July to 0000 UTC 28 July.	

	The shadings indicate high values of OW parameter (units: $10^{-10} \text{ s}^{-2}$ ) as defined in Eq. (1.1). This quantity, like vorticity, is invariant with respect to translation, therefore identical in translating and moving frames. Red areas are strong values and blue values areas are weak. ....	67
Figure 37.	Streamlines of horizontal (rotational + divergent) flow and Zeta at 600 hPa of the non-developer from 1800 UTC 23 July to 1200 UTC 24 July. Shading indicates relative vorticity (units: $10^{-5} \text{ s}^{-2}$ ). ....	68
Figure 38.	Streamlines of horizontal (rotational + divergent) flow and Zeta at 600 hPa of the Usagi system from 0600 UTC 27 July to 0000 UTC 27 July. Shading indicates relative vorticity (units: $10^{-5} \text{ s}^{-2}$ ). ....	68
Figure 39.	Streamlines of horizontal (rotational+divergent) flow and Zeta at 850 hPa of the non-developer from 1800 UTC 23 July to 1200 UTC 24 July. Shading indicates relative vorticity (units: $10^{-5} \text{ s}^{-2}$ ). ....	69
Figure 40.	Streamlines of horizontal (rotational+divergent) flow and Zeta at 850 hPa of the Usagi System from 0600 UTC 27 July to 0000 UTC 28 July. Shading indicates relative vorticity (units: $10^{-5} \text{ s}^{-2}$ ). ....	69
Figure 41.	Relative vorticity Hovmöller diagram 3 days before development of Usagi from 26 -30 July.....	70
Figure 42.	Streamlines of horizontal flow 600 hPa for the genesis sequence of the non-developer, with high values of saturation fraction from 1800 UTC 23 July to 1200 UTC 24 July. Red areas are strong values and white areas are weak values of SF.....	73
Figure 43.	Streamlines of horizontal flow 600 hPa for the genesis sequence of the Usagi system, with high values of saturation fraction from 0600 UTC 27 July to 0000 UTC 28 July. Red areas are strong values and white areas are weak values of SF.....	74
Figure 44.	Streamlines of horizontal flow 850 hPa for the genesis sequence of the non-developer, with high values of TRMM 3-hour accumulated precipitation indicated by shading from 1800 UTC 23 July to 1200 UTC 24 July. Red areas are strong values and white areas are weak values of precipitation. ....	74
Figure 45.	Streamlines of horizontal flow 850 hPa for the genesis sequence of the Usagi system, with high values of TRMM 3-hour accumulated precipitation indicated by shading from 0600 UTC 27 July to 0000 UTC 28 July. Red areas are strong values and white areas are weak values of precipitation. ....	75
Figure 46.	Relative humidity time series diagram of non-developer from 22 -25 July. ....	77
Figure 47.	Relative humidity time series diagram of Usagi from 26 -28 July. ....	77
Figure 48.	CAPE time series diagram of non-developer from 22 -25 July. ....	78
Figure 49.	CAPE time series diagram of Usagi from 26 -29 July.....	78

## LIST OF ABBREVIATIONS

AFWA	Air Force Weather Agency
AVOR	Absolute Potential Vorticity
UTC	Coordinated Universal Time
COLA	Center for Ocean-Land-Atmosphere Studies
IR	Infra-Red
N	North
E	East
W	West
S	South
TC	Tropical Cyclone
TS	Tropical Storm
WV	Water Vapor
WEC	Weak Extratropical Cyclone
WISHE	Wind-induced Surface Heat Exchange
WNP	Western North Pacific
JTWC	Joint Typhoon Warning Center
JAAWIN	Joint Air Force and Army Weather Information Network
NCEP	National Centers for Environmental Prediction
NHC	National Hurricane Center
NOGAPS	Navy Operational Global Atmospheric Prediction System
NRL-MRY	Naval Research Laboratory-Monterey
NCEP	National Climate Environmental Prediction
ET	Extratropical Transition
GEMPAK	General Meteorological Package
GARP	GEMPAK Analysis and Rendering Program
GFS	Global Forecast System
GDAS	Global Data Assimilation System
K	Degrees Kelvin
C	Celsius
Kt	Nautical Miles per hour
M	Meter
s	Second
ECMWF	European Centre for Medium-Range Weather Forecasts
UW	University of Wisconsin
CIMSS	Cooperative Institute for Meteorological Satellite Studies
NOAA	National Oceanic and Atmospheric Administration –
HRD	Hurricane Research Division
MJO	Madden-Julian Oscillation
FNL	Final analysis
ENSO	El Nino Southern Oscillation
SST	Sea-surface Temperatures
IGrADS	Interactive Grid Analysis and Display System

TT	Tropical Transition
T	Temperature
TUTT	Tropical Upper Tropospheric Trough
TRMM	Tropical Rainfall Measuring Mission
P	Pressure
TD	Tropical Depression
TCFA	Tropical Cyclone Formation Alert
TY	Typhoon
LAT	Latitude
LON	Longitude
RH	Relative Humidity
hPa	hecto-Pascals
PVU	Potential Vorticity Anomaly
OW	Okubu-Weiss Parameter
SF	Saturation Fraction
SEC	Strong Extratropical Cyclone
VISSR	Visible and Infrared Spin Scan Radiometer
UKMET	United Kingdom Meteorological Office
RMM1	Real-time Multivariate MJO series 1
EOF	Empirical Orthogonal Function
OLR	Outgoing Long-wave Radiation
PC	Principal Component
Flops	FLoating point Operations Per Second
MTSAT	Multi-Functional Transport Satellite
CAPE	Convective Available Potential Energy
SI	Subtropical Intrusion
GASP	Global Assimilation Prediction

## ACKNOWLEDGMENTS

The completion of this thesis would not have been possible without the support of a number of individuals, some of whom have become close friends during my twenty month-long academic endeavor at the US Naval Postgraduate School. The weekend group “brown bag” lunch study sessions allowed me to incorporate a lot of useful information and made learning fun. To all, I would like to express my sincerest thanks and appreciation.

Professors Michael T Montgomery and Patrick A. Harr, my thesis advisors, for their mentorship and advice during the entire year I was conducting my research. The Advanced Tropical Meteorology class, as well as the afternoon tropical weather briefings during T-PARC dry-runs, was inspiring and time well spent learning Tropical Meteorology.

Professor Russell L. Elsberry, my Tropical Meteorology professor, his Tropical Meteorology class was so interesting I took it twice.

Doctors Zhuo Wang and Tim Dunkerton, my thesis committee members, their insights provided me the edge to explore uncharted territories within the scope of my ground-breaking thesis.

Mr. Robert Creasey, his technical expertise provided me access to Vis5D, GFS, and GARP capabilities to run my data sets.

To my wife, Moli, for her patience and support throughout the years; Monty and Reane, for making an uncharacteristic sacrifice by allowing Daddy to be always number one priority.

THIS PAGE INTENTIONALLY LEFT BLANK

# **I. INTRODUCTION**

Improved forecast of tropical cyclogenesis is vital to US military interest in the western North Pacific (WNP) and other maritime activities in this region. A weather phenomenon such as a tropical cyclone (TC) can have dangerous winds, flood-causing heavy rain, and destructive storm surge over large areas so the degree of impact can be high. An approaching Typhoon can curtail the civilian economy, military operations, and all routine day-to-day living along several hundred miles of coastline and inland areas. The duration of the impact can be several days to several months depending on the damage.

During 22 -28 July 2007 two distinct areas of disturbed weather associated with a subtropical intrusion (SI) emerged out of remnants of a decaying baroclinic system in the WNP. In this thesis, key events that led to the non-development of the initial invest area and the development of Typhoon Usagi (5W) are investigated. This work will explore the usefulness of satellite data and model analysis to include the first testing in the WNP of Okubo-Weiss (OW) criterion and saturation fraction (SF), which are parameters that diagnose factors hypothesized to have aided in the formation of Typhoon Usagi.

The genesis of Usagi was initially analyzed using the GFS model and the analysis of relative vorticity at 850 hPa with the VORTRACK vorticity tracking system. The initial hypothesis was that Usagi was a tropical transition (TT) of a strong equatorial cyclone (SEC) that moved southwest as a decaying mid-latitude baroclinic system. It was then hypothesized that Usagi intensified due to vortex merger and axisymmetrization between the tail-end of the decaying baroclinic system and remnants of Hurricane Cosme (5E) that formed in the eastern North Pacific and moved westward across the dateline. A more detailed discussion of this possible sequence will follow in Chapter III. Based on high-resolution model analysis, this initial hypothesis was revised to include the circulation of Cosme as a factor that widened a “pouch” of vorticity anomalies of

Usagi. Some preliminary tests of this hypothesis are presented using the model analyses. The high time-resolution analysis will demonstrate no direct vorticity connection between the two systems; and satellite imagery reveals a persistent area of clearing between the two systems that is consistent with a region of subsidence. This evidence suggests that the wave-like remnants of Cosme are too far away from the baroclinic system (its closest proximity was approximately 1000 km on 0600 UTC 26 July) to be a deciding influence in the formation of Usagi. This study suggests an alternative hypothesis that the enlarged wave pouch created a favorable condition for the genesis of Usagi, especially at 600 hPa.

The tip of the potential vorticity (PV) streamer, which is dominated by curvature vorticity, is believed to be the key factor leading to the formation of Typhoon Usagi. A natural question is whether or not Usagi would have eventually developed without Cosme in widening the vorticity pouch. These questions are beyond the scope of this paper and should be the focus of further studies.

This study will highlight the difference between Atlantic and WNP TT cases and suggest why the TT model as defined in the literature for the Atlantic sector fails to give useful forecast rules for the WNP. This case offers a new example of a genesis sequence from an extratropical system in the WNP. While the frequency of this weather sequence is believed to be relatively low, the formation of any typhoon can have severe impact.

The series on TC genesis described in Dunkerton, Montgomery and Wang (2008; hereafter DMW08) examined the TC genesis pathway in association with easterly waves and instability of the Inter-tropical Convergence Zone in the Atlantic and eastern Pacific sectors. Their three-year analysis of developing cases in these sectors revealed a common occurrence of the creation of a closed gyre or “pouch” that is protected to some degree from hostile environmental influences.

This analysis of the formation of Usagi points to SI of a decaying baroclinic systems as potential seedlings for typhoon formation in areas of high sea-surface temperatures, weak low-level vertical wind shear, and persistent convection. In the case of Usagi, a large-scale anticyclone alone in the west side of the baroclinic zone is apparent. This work will use MTSAT satellite, PV, OW, SF, and TRMM retrieval analyses to show that the stretched PV anomalies that get detached from their baroclinic source region and subsequently wrapped around the large anticyclone is a different type of baroclinic initiation mechanism than the TT Atlantic cyclone formation model, which are induced by upper-level troughs. Thus, the cyclogenesis of Usagi in the WNP is not consistent with TT cases in the Gulf of Mexico or Atlantic region.

Prior to the formation of Usagi, an initial disturbance was labeled as an invest region for possible tropical cyclogenesis formation. However, this non-developing system exhibited less organization and weaker vorticity than the developing (Usagi) case. The failure of the initial SI to develop may occur due to the cyclone translating over cool waters, an area of strong vertical wind shear, a lack of moisture, or insufficient cyclonic vorticity, as the cyclone becomes detached from the main vorticity reservoir in the decaying baroclinic system.

#### **A. ATLANTIC TT AND WNP CYCLONE FORMATION**

According to Davis and Bosart (2004; hereafter DB04), TT refers to the formation of a warm core tropical cyclone from a cold-core disturbance, usually of extratropical origin. Some of the largest forecast errors of track and intensity occur with these events. Their proximity to the North American coast produces significant adverse consequences for poor forecasts, namely, minimal time for coastal warnings and inland flood preparations. DB04 define two TT scenarios based on the amplitude and structure of the precursor seedling disturbance: SEC and weak equatorial cyclone (WEC). In SEC scenarios, the extratropical cyclogenesis produces a surface cyclone capable of wind-induced surface heat exchange (WISHE). In contrast, WEC situations have the baroclinic cyclone as

the organizing agent for convection. This convection must then undergo self-organization to create a disturbance capable of self-amplification. DB04 suggest no clear threshold exist between SEC and WEC cases, since these cases represent points on a spectrum. Once an appropriately strong surface vortex is formed, no clear distinction was found in the ensuing tropical cyclone intensification in either SEC or WEC situations.

In these stronger extra-tropical cases, baroclinic and diabatic processes combine to produce an intense mesoscale cyclone, which then transitions to a tropical cyclone (Davis and Bosart 2003, hereafter DB03) as the WISHE process develops a low-level, warm-core circulation center. DB04 showed that SEC cases have a more consistent and repeatable evolution than WEC cases, and strong tropical cyclones tend to form most often with SEC scenarios.

In contrast, the baroclinic WEC situations act as the organizing agent for convection. This convection must then undergo self-organization to create a disturbance capable of self-amplification. DB04 suggest no clear threshold exist between SEC and WEC cases, since these cases represent points on a spectrum. Once an appropriately strong surface vortex is formed, no clear distinction was found in the ensuing tropical cyclone intensification in either SEC or WEC situations.

The TT cases discussed above reside within a broader continuum of marine cyclogenesis that comprise a range from baroclinic cyclones to hurricanes initiated from weak extratropical systems (DB04). Although storm-induced surface heat and moisture fluxes play a key role in TT, the key role in TT seems to be determined by baroclinicity as long as the circulation is over a sufficiently warm ocean. However, forecasting the TT of various baroclinic systems in different areas such that of this WNP case is rather challenging.

In SEC instances, the low-latitude frontal cyclone has intensity sufficient to begin the WISHE process. DB03 showed diabatic processes serve to eliminate the vertical wind shear present over the cold-core low. The decrease in shear is

caused by both the upper-tropospheric outflow from convection, and from the diabatic redistribution of PV. Both of these processes help to homogenize the horizontal gradients of PV directly above the low-level circulation. As a result, an equilibrated cyclone resembling an occluded system in a sub-synoptic “cocoon” of weak shear is generated. This Usagi case takes place within this favorable environment, and eventually a tropical cyclone forms.

The occlusion before TT is different from the classical model of occlusion in which surface cyclone moves poleward toward colder air beneath an upper-tropospheric jet. In contrast, the jet in the TT cases is rearranged via diabatic processes and results in an apparent migration of the surface cyclone toward warmer tropospheric air (DB04).

The rainfall and cloud signatures just before TT began in the four SEC cases discussed in DB04 are reproduced here in Figure 1. In each situation, a marked asymmetry exists in the rainfall, with a proclivity for a “bent back” frontal structure, and heavy rainfall on the west side of the still extratropical surface low. This structure was observed prior to some of the stronger hurricanes generated from the TT process. The pre-hurricane Florence structure in Figure 1a most resembles the pre-typhoon Usagi seedling.

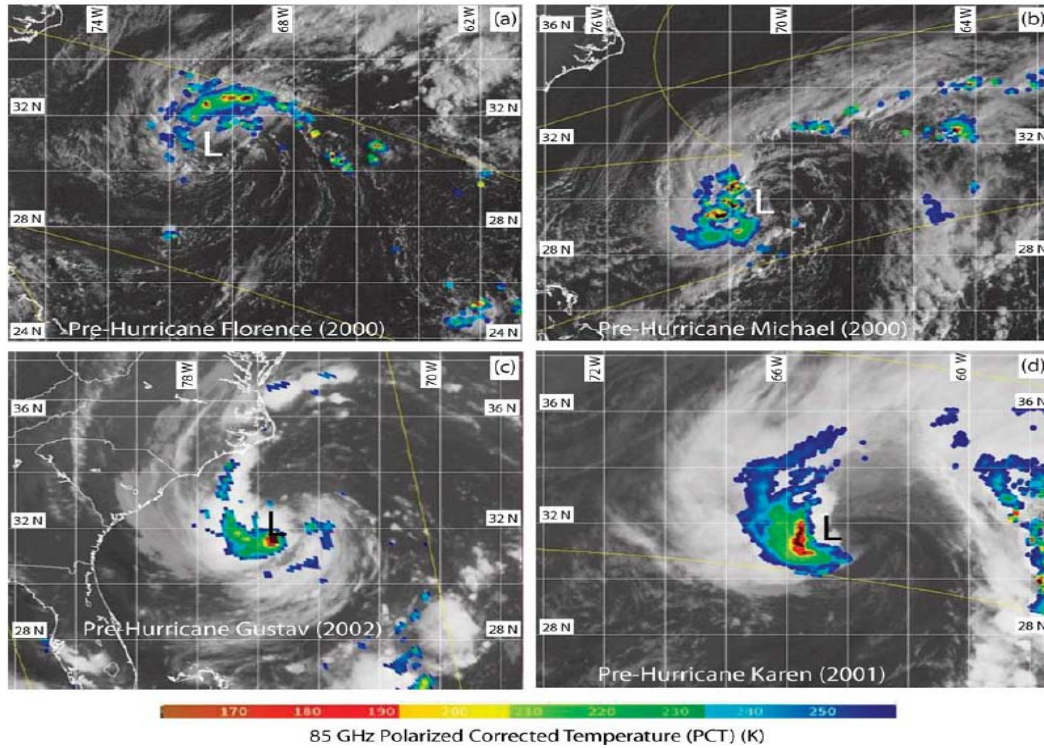


Figure 1. (a) Visible satellite and Tropical Rainfall Measuring Mission (TRMM) Microwave Imager (TMI) 85-GHz polarized corrected temperature (PCT) imagery at 1145 and 1209 UTC 10 Sep 2000, respectively; (b) (upper right), as in (a) but for visible and TMI 85-GHz PCT at 1245 and 1335 UTC 15 Oct 2000; (c) IR and Special Sensor Microwave/Imager 85-GHz PCT at 0015 and 0219 UTC 10 Sep 2002; and (d) IR and TMI 85-GHz PCT at 2045 and 2132 UTC 11 Oct 2001. In all panels, the “L” indicates the position of surface low. Images obtained courtesy of Naval Research Laboratory: 14 February 2008.

In WEC cases, precursor disturbances can be weak baroclinic waves, or mid-tropospheric vortices that simply have insufficient amplitude to create a surface cyclone capable of amplifying by WISHE without invoking an intermediate process to enhance mesoscale vorticity. The mechanism responsible for the warm-core transition in WEC cases is unclear. The production of cyclonic vorticity centers on scales of 10-20 km, so-called rotating hot towers (Hendricks et al. 2004, Montgomery et al. 2006), may be the preferred means by which the convective scale influences the development of the primary, larger-scale vortex. Mid-tropospheric convectively generated vortices have also been observed to initiate tropical cyclogenesis in lower latitudes (e.g., Simpson et

al. 1997). DB04 argue that it is through understanding the initiation of tropical cyclogenesis by mesoscale vortices at higher latitudes that the link with tropical cyclone formation in the deep tropics can be made. Just as there is a continuum between the weak and strong baroclinic precursors, there is a range of realizations between mesoscale vortices and weak baroclinic systems. Numerical simulations of Diana (1984) (Powers and Davis 2002) showed that the path to tropical cyclogenesis required a lower-middle-tropospheric vortex that formed within convection initiated by an extratropical precursor. The distinguishing character between cases, the mid-tropospheric vortex existed for more than two days before tropical cyclogenesis began. In such cases, the vortex must organize new convection through its interaction with vertical shear. When a weak extratropical cyclone is maintained, the organization of convection occurs through a superposition of vortex and cyclone-induced ascent. In the cases studied, there were multiple lower tropospheric vortices formed within a mesoscale ascent region, and the coalescence and growth of these vortices formed the nascent tropical storm (TS) (Hendricks et al. 2004). Considerable research remains to understand how convection organizes in systems with weak precursors. Therefore, it is difficult to derive a set of forecast rules. However, it is apparent that PV “debris” extruded from the mid-latitude jet is common over the warm oceans of the subtropical Atlantic, even as far south as 15°N on occasion. Overall then, favorable conditions for WEC cases of TT involve mid-upper-tropospheric cyclone PV anomalies encountering lower-tropospheric baroclinity (and, hence, vertical shear). In the cases that develop into tropical cyclones, the shear remains either roughly 10 m s<sup>-1</sup> or less, or it is reduced to such values following convection organization (Powers and Davis 2002). DB04 noted that at lower latitudes, convection has also been observed to organize when upper-tropospheric disturbances approach easterly waves, wherein systematic baroclinity is hard to identify. There are almost certainly other factors involved in WEC cases of TT, but research has yet to fully clarify them. Although in the Gabrielle (2001), the period is relatively short (about 6 hours); the depression

undergoes a full warm-core transformation (not shown). It is believed that the ongoing convection is somehow responsible for this decrease in shear.

One of the critical forecast challenges, then, is to anticipate a favorable environmental modification, since it usually occurs on the timescales of less than one day. DB04 proposed a primary empirical forecast rule to aid in the forecast challenge of predicting SEC TT cases: “The precursor cyclone must occlude and remain over warm water ( $>26^{\circ}\text{C}$ ) for at least a day after the occlusion.” DB03 hypothesized that the initially strongly sheared environment, which is hostile to tropical cyclone formation, is significantly modified as the incipient cyclone progresses. After about one day, the vertical shear is markedly decreased, which facilitates the creation of a finite amplitude vortex in the lower troposphere that is able to enhance the moist entropy fluxes from the ocean surface.

Hurricane Diana provided a useful illustration of this process. Diana was a modest baroclinic cyclogenesis event that stimulated organized convection, which led to the coherent vortices in the lower troposphere that formed the seed for tropical cyclogenesis (DB03, Hendricks et al. 2004). Another prime example of TT was in the case of Hurricane Michael (2001) (not shown). The pre-Michael cyclone was a robust baroclinic cyclone that was able to generate a finite amplitude mesoscale surface cyclone so the transition to a warm-core system could begin almost as soon as the vertical shear weakened.

Failure of TT may occur because of two reasons. Transition will fail if the occluding cyclone translates over cool water before TT can occur (thus, the “1-day rule” above). Secondly, transition will fail if the primary cyclone is prevented from occluding due to an increase in vertical wind shear over its center from short waves approaching the surface cyclone (DB04).

## **B. THE MARSUPIAL PARADIGM**

Summarizing the DMW08 theory, the relevant theoretical paradigm is the formation of a closed proto-vortex or “embryo” (Emanuel, 2007; Montgomery,

2006) within the wave in the lower troposphere. Subsequent eddies that are shed from the vortex, become energized further by deep convective heating to become detached from the baroclinic wave. In the following section, we will refer to this as the marsupial paradigm. The marsupial paradigm is a rudimentary understanding of the Lagrangian flow and its dynamical and thermodynamical properties in the neighborhood of the developing storm.

DMW08 proposed three main hypotheses for TC formation that synthesized existing knowledge and advanced new insight on the flow kinematics and dynamics, moist thermodynamics, and wave/vortex interactions during the transformation into a tropical depression-strength vortex. First, the proto-vortex cyclonic eddies instrumental in TC formation are hypothesized to be intimately associated with the parent wave's critical latitude in the lower-troposphere. The critical level/layer is generally a surface in three dimensions, but the word level has been used in this study to represent one of these dimensions, e.g., latitude. This structure forms a critical layer because of the wave's finite amplitude interaction with its own critical latitude. The critical layer is a region of cyclonic rotation and weak strain/shearing deformation in which synoptic and mesoscale anomalies move together and amplify on a nearly zero relative mean flow. This multi scale interaction provides a dynamical pathway to bottom-up development of the proto vortex. The second hypothesis is that the critical layer of the parent wave provides a set of closed material contours inside of which air is repeatedly moistened by convection. The wave is protected to some degree from lateral intrusion of dry air impinging vertical shear, and able to keep in pace with the parent wave until the proto-vortex has strengthened into a self-maintaining entity. The third hypothesis is that the parent wave is maintained and possibly enhanced by diabatically amplified eddies within the wave. This process is favored in regions of small intrinsic phase speed. This hypothesis, agrees with the common observation that the tropical wave is considerably weakened or eliminated when the diabatic vortex leaves the pouch, having acquired its own identity and propagation characteristics independent of the parent wave.

The ex-hurricane Cosme disturbance is an illustrative example in which a westward propagating wave carried its proto-vortex over time. Once the depression ensued, the strengthened and enlarged vortex (Usagi) acquired a poleward component of propagation while its zonal component begins to slow relative to the phase speed of the parent wave.

## C. ELEMENTS OF THE GENESIS SEQUENCE

### 1. Dynamical Fields - OW Parameter

The relative vorticity ( $\zeta$ ) and OW fields at 600 hPa and 850 hPa will be examined to single out curvature vorticity compared to shear vorticity. The large positive values of OW parameter suggest regions where curvature vorticity is dominant. Perhaps the most important conclusion to draw from the OW parameter inside the translating gyre is that the flow within it is relatively free of strain and shear (McWilliams 1984), favoring nominally the formation of smaller proto-vortical structures within.

The moving frame of reference is optimal to display the Lagrangian flow and the evolution of the storm vortex. This enables one to estimate the Lagrangian parcel motions that are affecting the dynamics and thermodynamics of the transformation process.

The OW parameter is defined as

$$OW = \zeta^2 - S^2 \quad (1.1)$$

where

$$S^2 = \left( \frac{\partial u}{\partial x} - \frac{\partial v}{\partial y} \right)^2 + \left( \frac{\partial v}{\partial x} + \frac{\partial u}{\partial y} \right)^2 \quad (1.2)$$

is the square of the horizontal strain deformation and

$$\zeta = \frac{\partial v}{\partial x} - \frac{\partial u}{\partial y} \quad (1.3)$$

is the relative vertical vorticity.

Negative values of the Okubo-Weiss parameter for the simulation period are regions that are strain dominated, whereas positive values indicate strain-free rotationally dominant regions. The vortex cores are characterized by strongly positive values of OW (Weiss, Pasquero, and Provenzale 2002). In the following, we identify the vortex cores as those circular regions with positive OW.

## **2. Thermodynamical Fields - SF**

The saturation fraction of the lower troposphere, defined as the ratio of precipitable water to saturated precipitable water, from case studies concluded by David Raymond (2002), the saturation fraction appears to be the primary control on precipitation in the ECMWF model and the surface moisture flux is acting in a secondary fashion via its effect on the SF. In this thesis, we use 600 hPa SF as a benchmark to focus on the lower tropospheric moisture anomalies.

## **D. OBJECTIVES OF CURRENT STUDY**

1. To present the facts that led to the development of Usagi; examine model analysis data, and satellite imagery in observing the conditions leading to WNP TC formation

2. To explore the usefulness high-resolution model analyses of OW and SF in order to assess these hypothesized factors in the formation of Typhoon Usagi (5W).

3. To propose an explanation on how the remnants of Hurricane Cosme (6E) created a favorable condition for the genesis of Usagi.

More generally, we wish to increase the forecast capability of the Joint Typhoon Warning Center (JTWC) and we believe that further investigation and qualitative documentation of the various pathways to tropical cyclone formation

will prove useful to the forecasting community as well. This includes identifying synoptic patterns favorable for tropical cyclone formation and providing guidance on mesoscale conditions that may enhance or inhibit tropical cyclone formation in the WNP (Non-developer and developer cases).

The organization of the thesis is as follows. In Chapter II, an overview of the satellite and model data is presented, and this is followed by discussion of the data processing used in the thesis. In Chapter III, the case studies used in the thesis are presented. Finally, the summary of results, conclusions, and recommendations for future research are contained in Chapter IV.

## **E. PRE-STORM SITUATION**

### **1. Hurricane Cosme (6E)**

On 14 July 2007, the National Hurricane Center (NHC) identified Tropical Depression (TD) (6E) as an area of disturbed weather about halfway between Mexico and the Hawaiian Islands. The area of disturbed weather acquired a surface circulation and sufficiently deep convection for the NHC to designate it as a TD, what then became TS Cosme.

On 24 July, the JTWC was still tracking the weak remnants of Cosme 810 nautical miles east of Wake Island. Animated infrared satellite imagery depicted improved consolidation with persistent deep convection near the partially exposed low-level circulation center.

### **2. Baroclinic Extratropical Low**

This extratropical low moving southwest out of the mid-latitudes into the tropics had a low-level circulation that was already near the surface and rather strong. Thus, it did not take much to transition this cold-core low into a tropical system given that it was moving southward into an area with warm sea-surface temperatures (SSTs), high ocean heat content, low vertical wind shear, and the approaching remnants of Cosme.

On 22 July, an area of deep convection emerged out of this system but never developed. However, on 28 July, JTWC issued a Tropical Cyclone Formation Alert (TCFA) from the same extratropical low, and then designated the system a TD later that day.

### **3. Tropical System Non-developer (Gyre)**

As mentioned earlier, two noted systems of deep convection developed from remnants of a decaying baroclinic extratropical low. The initial system on 22 July gets detached but never develops and the second identified system on 28 July eventually became Typhoon Usagi. To look at the two systems, a simple strategy is to compare the precursors of the two tropical system formations

### **4. Tropical Cyclogenesis of Typhoon Usagi (5W)**

According to JTWC (2007), on 1200 UTC 28 July the system quickly strengthened as a TD as it approached 260 nautical miles northeast of Saipan and had tracked westward at 14 knots over the past 6 hours with maximum sustained winds at 25 knots gusting to 35 knots. At 0000 UTC 29 July, JTWC upgraded it to TS strength.

One of the most interesting aspects of tropical cyclogenesis that is not understood, especially in the western North Pacific (WNP) sector, is SI or TT events. According to DB04, the development of almost half (26 out of 57) of all Atlantic tropical cyclones from 2000 to 2003 relied on an extratropical disturbance. Majorities of these systems were of a baroclinic origin and were initially cold-core systems. A kinematic and thermodynamic (cold core to warm core) transformation of these disturbances was required. DB04 consider this process to be the definition of TT, and contrast it to extratropical transition (ET), in which a TC transitions into an extratropical cyclone. However, this has not been considered as a dominant formation type in the WNP. The thesis will examine the formation of Usagi relationship to the TT conceptual model.

THIS PAGE INTENTIONALLY LEFT BLANK

## **II. DATA AND METHODOLOGY**

The General Meteorological Package (GEMPAK) Analysis and Rendering Program (GARP) was used to generate plots of fields from the National Center for Environmental Prediction (NCEP) Global Forecast System (GFS) 30-day global analysis. Additionally, the Navy Operational Global Atmospheric Prediction System (NOGAPS) model analysis and the United Kingdom Meteorological Office (UKMET) model were also examined. All of the model data was examined from 0000 UTC 22 July through 1800 UTC 8 August 2007.

At a later stage of this research project, the NCEP GFS global analysis Global Data Assimilation System (GDAS) final analysis (FNL) was added in order to examine PV and streamlines. To calculate the OW and SF parameters, the European Centre for Medium-Range Weather Forecasts (ECMWF) model data was used.

Vis5D supplements the GARP plots for more detailed analysis. Vis5D is a software system that can be used to visualize both gridded data and irregularly located data. Sources for these data can come from numerical weather models, surface observations and other similar sources. Vis5D can work on data in the form of a five-dimensional rectangle. That is, the data are real numbers at each point of a grid, which spans three space dimensions, one time dimension and a dimension for enumerating multiple physical variables. Of course, Vis5D works perfectly well on data sets with only one variable, one time step (i.e. no time dynamics) or one vertical level. However, the data grids should have at least two rows and columns. The Vis5D can also work with irregularly spaced data that are stored as records. Each record contains a geographic location, a time, and a set of variables that can contain either character or numerical data. A major advantage of Vis5D is that it readily supports intercomparison of multiple data sets. Data can be overlaid in the same 3-D display and/or viewed side-by-side spread sheet style. Data sets may be overlaid and aligned in space and time. In

the spreadsheet style, multiple displays can be linked. Once linked, the time steps from all data sets are merged and the controls of the linked displays are synchronized.

The University of Wisconsin - Cooperative Institute for Meteorological Satellite Studies (UW-CIMSS) and the National Oceanic and Atmospheric Administration - Hurricane Research Division (NOAA- HRD) products were also used to supplement the satellite data used here. This imagery was used as an overlay on the previous GARP generated GFS 0000-hour analysis fields of 850 hPa winds (knots) and 200 hPa winds (knots), and 850 hPa absolute vorticity (with values greater than  $10^{-5} s^{-1}$  shaded) from 0000 UTC 22 July through 1800 UTC 28 July. The imagery overlay helps contrast where the convective activity is located versus the analyzed generated absolute vorticity.

A smaller area within in the synoptic region was chosen and ingested inside the Vis5D software in order to simulate trajectories where the convection and vorticity was initiated. The streamlines were superimposed in the wave-centric perspective. The Vis5D analysis region was also used to obtain a sense of the area of deep convection in comparing the developing and non-developing circulation. Plots of the low-level convergence vs. cold cloud-top temperatures were constructed (Vis5D, 2005).

The Air Force Weather Agency's (AFWA's) Interactive Grid Analysis and Display System (IGrADS) visualization tool was also used to display the detailed graphics. The Center for Ocean-Land-Atmosphere Studies (COLA) IGrADS is available over the AFWA's webpage, Joint Air Force and Army Weather Information Network (JAAWIN) (<https://weather.afwa.af.mil>) and has been operational since early 2002. The interface enables forecasters to create varieties of visualized or alphanumeric products designed to meet their customers' needs. These products range from meteograms, skew-Ts, vertical cross-sections, forecast maps, and seven different types of alphanumeric meteorological output. Forecasters have the option of choosing from among

eight different numerical forecast models. The most extensive product lines are available for AFWA's MM5. IGrADS users can choose any display region they desire, can animate forecast data, and can bookmark frequently needed charts, and then recall them with current model data whenever required (COLA, 2004).

## **A. SATELLITE DATA PROCESSING**

### **1. MTSAT Infrared-Red Imagery**

Multi-Functional Transport Satellite (MTSAT) series fulfill two functions: a meteorological function by the Japan Meteorological Agency and an aviation control function by the Civil Aviation Bureau of the Ministry of Land, Infrastructure and Transport. The MTSAT series succeed the Geostationary Meteorological Satellite (GMS) series as the next generation satellite series covering the East Asia and the Western Pacific regions. Satellite images are available over the WNP region and over each of the tropical western Pacific sites. The Cloud-top temperatures defined from MTSAT imagery will be used with thresholds to distinguish between warmer lower level clouds (from -20°C to less than -70°C) and colder upper-level cloud tops.

The raw data are down-linked to the SeaSpace Corporation receiving station at the University of Hawaii. GMS-5 was launched in March 1995 into a geostationary orbit above 0° N, 140°E. It carries a Visible and Infrared Spin Scan Radiometer (VISSR) with four channels, one in the visible part of the spectrum and three in the infrared. The ground resolution at the sub satellite point is 1.25 km in the visible channel and 5 km in the infrared. A set of matching overlay files showing a latitude and longitude grid and the positions of the coastline are available for the WNP 5km resolution spatial coverage. The overlay files consist of an image of value one everywhere, except at the positions of the features (coastlines) in which case the pixel value is zero. Thus, the overlays can be written into the image by multiplying them together; the image data remain unchanged and the overlain pixels become zero.

## **2. Tropical Rainfall Measuring Mission (TRMM)**

Accurate measurement of the spatial and temporal variation of tropical rainfall around the globe remains one of the critical unsolved problems of tropical meteorology. TRMM, with its broad sampling footprint between 35°N and 35°S, is providing some of the first detailed and comprehensive dataset on the four dimensional distribution of rainfall and latent heating over vastly under sampled oceanic and tropical continental regions. Combined with concurrent measurement of the atmosphere's radiation budget, estimates of the total diabatic heating are being realized for the first time ever on a global scale. TRMM will fill many gaps in our understanding of rainfall properties and their variation. These includes frequency distributions of rainfall intensity and area coverage; the partitioning of rainfall into convective and Stratiform categories; the vertical distribution of hydrometeors (including the structure and intensity of the stratiform region bright band), and variation of the timing of heaviest rainfall. These are particularly relevant in the documentation of nocturnal intensification of large mesoscale convective systems over the oceans, and diurnal intensification of orographically and sea-breezed forced systems over land. TRMM will enable mapping of larger time and space variations of rainfall in quasi-periodic circulation anomalies, such as the Madden-Julian Oscillation (MJO) in the WNP and El Nino Southern Oscillation (ENSO) over the broader Pacific basin. Furthermore, the critical onset of large annual circulation regimes, such as the Asian summer monsoon, can be more thoroughly studied (TRMM 2008)

### **B. NUMERICAL MODEL FIELDS**

This case study utilizes a variety of numerical model fields from operational global models, and derived products to analyze the evolution of the non-developer and the SIs that became Typhoon Usagi during 22-28 July 2007.

## **1. GFS**

The NCEP GFS global analysis GDAS FNL, used as initial conditions for the GFS, will be used primarily. The GFS 0000, 0600, 1200, and 1800 UTC analysis fields were used to provide a 6-hour time snapshots. Only the 00-hour analyses will be used to avoid model forecast bias from entering the forecast plots. The 850 hPa and 200 hPa streamlines will be used to illustrate both the synoptic flow patterns at their respective levels. The 850 hPa absolute vorticity (with values greater than  $10^{-5}\text{s}^{-1}$  shaded) will be used to correlate with active areas of deep tropical convection. Finally, the distribution of PV within the levels of 850-500 hPa will be used to illustrate low-level circulation. The potential vorticity will be displayed in potential vorticity units (PVU), defined as  $10^{-6} \text{ m}^2 \text{ s}^{-1} \text{ K kg}^{-1}$  following Hoskins et al. (1985). The thresholds used in GARP are at a minimum of 0.3 and a max of  $0.7 \times 10^{-6} \text{ m}^2 \text{ s}^{-1} \text{ K kg}^{-1}$  with intervals of  $0.1 \times 10^{-6} \text{ m}^2 \text{ s}^{-1} \text{ K kg}^{-1}$ .

## **2. NOGAPS and UKMET**

The NOGAPS and UKMET model analysis fields provided by Naval Research Laboratory-Monterey (NRL-MRY) are used in this study at 0000 UTC and 1200 UTC to examine the baroclinic system, TC structure and dynamics as compared to IR, WV, and when available, microwave imagery. Because the 0600 UTC and 1800 UTC analyses were not available, the 6-h forecasts from the 0000 UTC and 1200 UTC model integrations respectively were substituted to provide a 6- hour time resolution. The 850 hPa and 200 hPa streamlines will be used to illustrate both the synoptic flow patterns at their respective levels. The 850 hPa absolute vorticity (with values greater than  $10^{-5}\text{s}^{-1}$  shaded) will be used to correlate with active areas of deep tropical convection through the whole TT period.

### **3. ECMWF**

The ECMWF forecasting system consists of five components: a general circulation model, an ocean wave model, and data assimilation. In 1998, a seasonal forecasting system started to operate and in 2002, a monthly forecasting system was introduced (ECMWF, 2007).

#### **C. LIMITATIONS**

The limitations of the data sets used are model resolution, data gaps, and the time of satellite imagery. The GFS model horizontal resolution is spectral triangular 254 (T254) with a Gaussian grid of 768 x 384, which is roughly equivalent to 0.5° x 0.5° latitude/longitude. The vertical domain is divided into 64 layers with enhanced resolution near the bottom and the top. For a system with a surface pressure of 1000 hPa, the lowest atmospheric level in the model would be at a pressure of about 997.3 hPa, 15 levels would be below 800 hPa, 24 levels would be above 100 hPa and the top level would be at about 0.27 hPa (NCEP, 2004). By contrast, the NOGAPS model is 0.75 degree horizontal resolution (spectral resolution = T159) and 24 levels in the vertical, from the Earth surface to 50 km. The model runs operationally on 12 processors with a sustained performance of five Gflops ( $5 \times 10^9$  Floating point Operations Per Second) (NRL, 2003).

### **III. ANALYSIS AND DISCUSSION**

The scope of this study will be from the inception of Cosme until the weakening of Usagi with focus on 22-28 July 2007. The spatial domain is from longitude 130°E to 179°W and latitude 30°N to 10°N. The study will demonstrate that the tip of the PV streamer, which is dominated by curvature vorticity, is the key factor leading to the TC formation.

The main objective of this study is to show the comparison between the non-developing and developing (Usagi) systems. A simple strategy is to compare the precursors of the two tropical systems by looking at the large-scale tropospheric environment of Usagi, lower tropospheric interactions within the non-developer (gyre) and developer (Usagi), by employing the OW and SF parameters.

The GFS initial model analysis was examined, using the VORTRACK system analysis (Figure 2-4) that identifies vorticity centers and tracks them. Examination of this model data led us to the initial hypothesis that the Usagi system resulted from the vortex merger of two distinct convective systems (Cosme and Usagi) of different origin. The interaction between the two systems was originally believed to have led to a warm-core system that eventually became typhoon (Usagi). The VORTRACK analyses suggest that as the two vortices approached each other, they start to undergo axisymmetrization and filamentation (Figure. 2-4). Initial analysis using the VORTRACK model led us believe that Usagi formed by the ingestion of like-sign PV anomalies (Montgomery and Enagonio 1998).

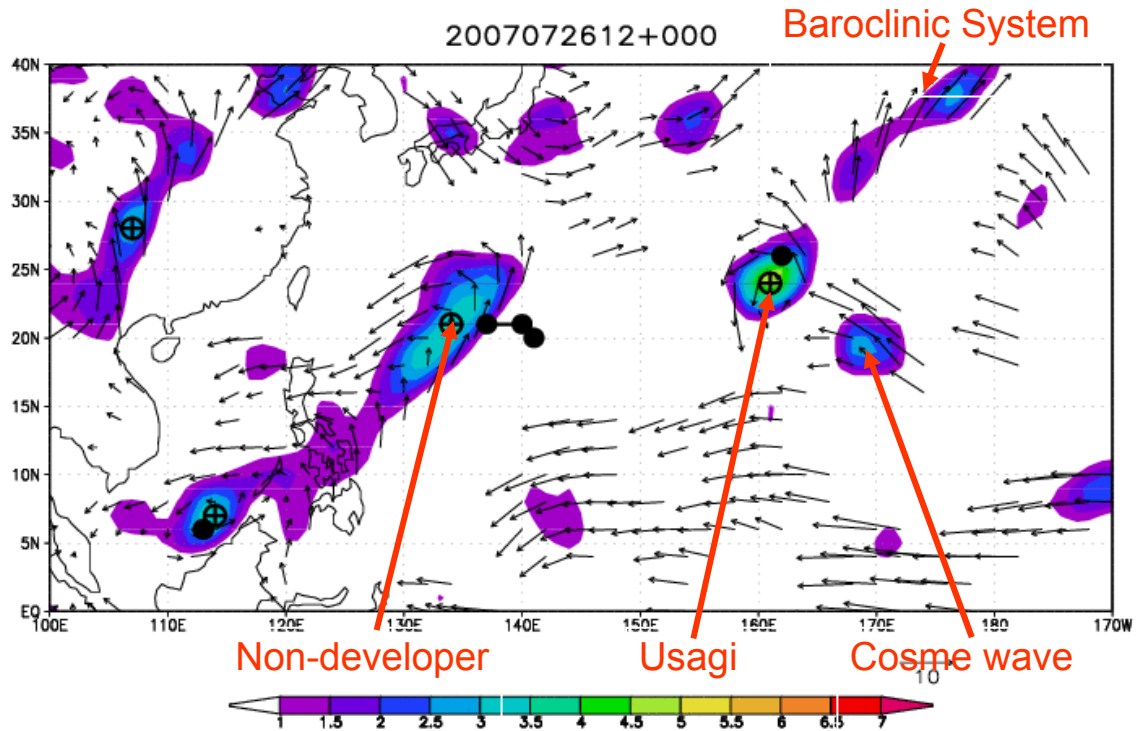


Figure 2. VORTTRACK analysis of Usagi and Cosme interaction on 1200 UTC 26 July 2007 48 hours before Usagi was named as TD 05W. Shadings are relative vorticity (unit:  $1 \times 10^{-5}$ ), winds @ 850 hPa plotted if relative vorticity is  $> 0$ , and black dots are track (12 hour steps) where relative vorticity is  $1.5$  (unit  $1.5 \times 10^{-5}$ ).

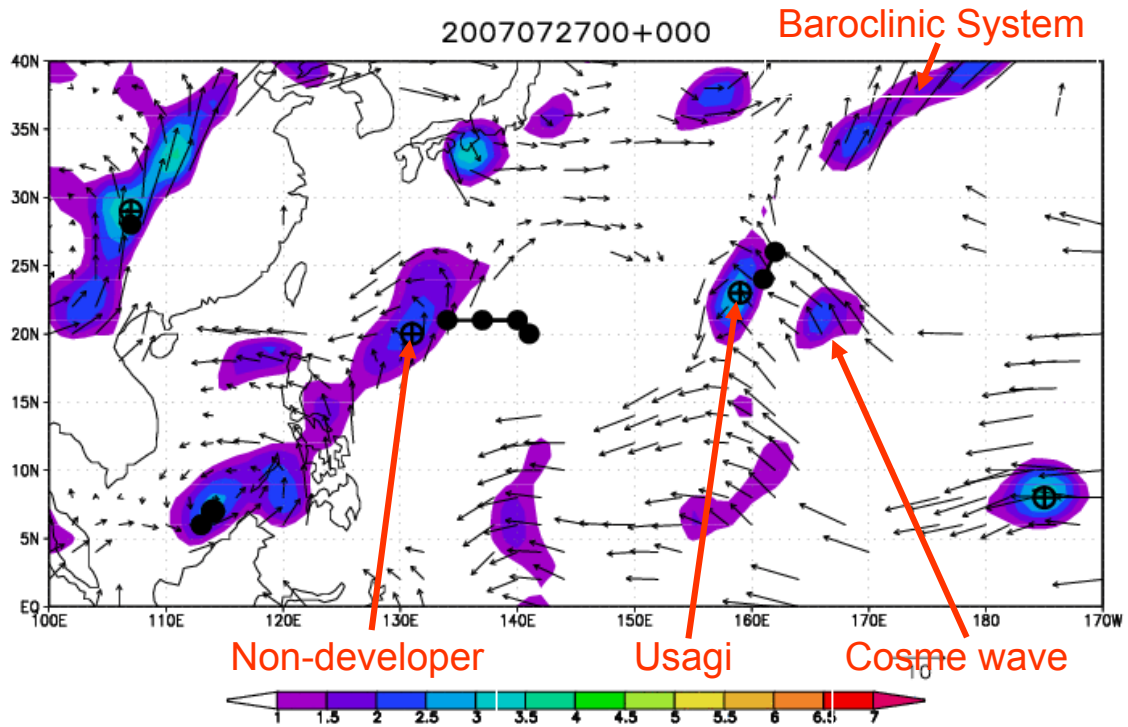


Figure 3. VORTTRACK analysis of Usagi and Cosme interaction on 0000 UTC 27 July 2007 36 hours before Usagi was named as TD 05W. Shadings are relative vorticity (unit:  $1 \times 10^{-5}$ ), winds @ 850 hPa plotted if relative vorticity is  $> 0$ , and black dots are track (12 hour steps) where relative vorticity is 1.5 (unit  $1.5 \times 10^{-5}$ ).

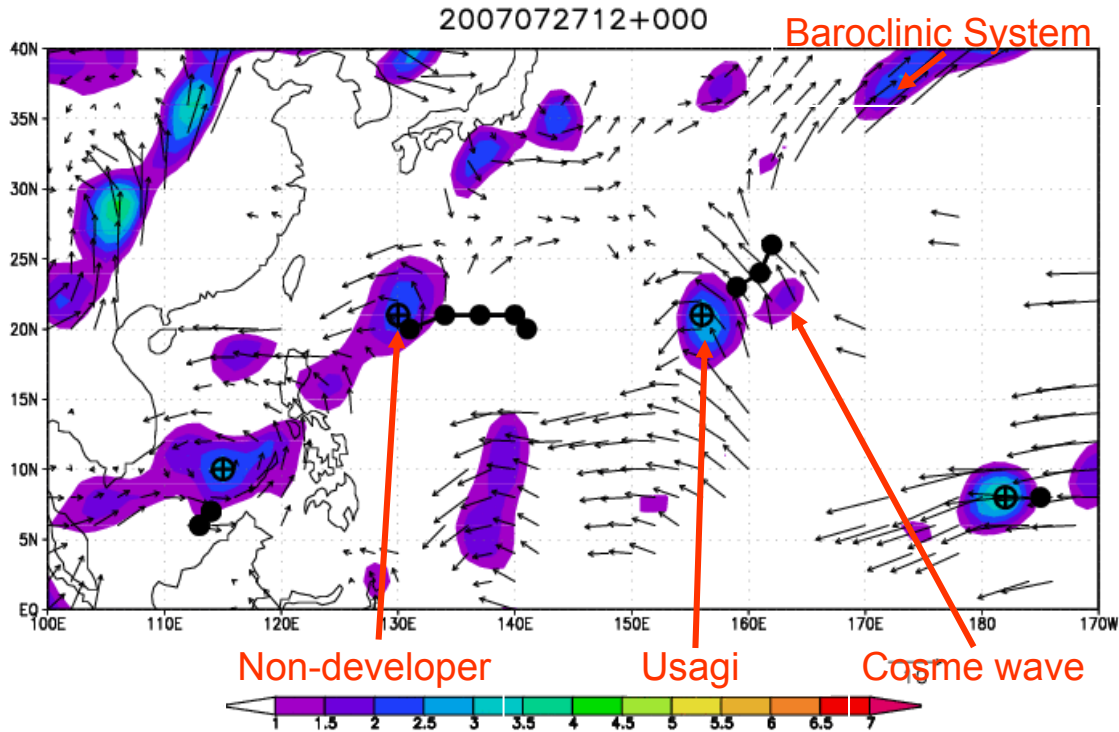


Figure 4. VORTTRACK analysis of Usagi and Cosme interaction on 1200 UTC 27 July 2007 24 hours before Usagi was named as TD 05W. Shadings are relative vorticity (unit:  $1 \times 10^{-5}$ ), winds @ 850 hPa plotted if relative vorticity is  $> 0$ , and black dots are track (12 hour steps) where relative vorticity is  $1.5$  (unit  $1.5 \times 10^{-5}$ ).

When the GFS FNL and ECMWF model analysis became available, a closer investigation of the high resolution analysis data using OW and SF parameters lead to a revision to the initial hypothesis and an explanation of the events leading to the Usagi TC formation as being fundamentally different from vortex merger, axisymmetrization, and filamentation. This study will document the difference of TT in the WNP.

## A. OVERVIEW OF INITIATING BAROCLINIC SYSTEM

### 1. The Large-Scale Lower Tropospheric Environment of Usagi

From 22-28 July 2007, two distinct areas of disturbed weather with SI emerged out of remnants of a decaying baroclinic system in the WNP. The initial system on 22 July becomes detached but never develops and the second

identified system on 25 July eventually became Typhoon Usagi. In the non-developing system, an area of weaker vorticity and a Tropical Upper Tropospheric Trough (TUTT) damped the convection. In the Usagi case, a strong line of low-level confluence and convection occurs along the line of confluent region. This region of convection will continue to intensify until the whole system develops as an organized center of deep convection.

The PV streamers are detached from the baroclinic system as the upper-level low is occluded. This formation precursor is still cold core since it is a reflection of an upper-level trough axis. As time progresses, this PV anomaly gets detached and is wrapped into the anticyclone. This baroclinic type of initiation process may not be seen in the Atlantic cyclone signatures from past research studies (DB04), which are induced by upper-level troughs. In this case, a large-scale anticyclone is to the west of the baroclinic system. In the lower levels, the vorticity anomaly becomes organized with enhanced low-level convergence from the existing instability from the low-level. This would be consistent with the bottom-up formation of a frontal system stagnating in the subtropics and transforming to warm-core characteristics.

The synoptic features indicate areas of strong enhanced convection had been local and mainly associated with tropical cyclones north of the Philippines. From 16 July to 1 August, the MJO signal remained weak (Figure 5). During these weeks, convective anomalies had generally been weak across the deep tropics, with slightly above average conditions across the eastern Indian Ocean and western Maritime Continent. The outgoing long-wave radiation anomalies during late July and early August confirmed the wet conditions over the Maritime Continent.

From mid-June into early August, weak to moderate MJO activity was observed as velocity potential anomalies propagated eastwards (Figure 6). Since mid-June, weak-moderate MJO activity had been observed as regions of suppressed and enhanced convection had shifted eastward from the Indian Ocean into the far western Pacific. Convection had become near average across

much of the equatorial tropics with dry conditions only evident just west of the date line. The 850 hPa zonal wind easterly anomalies increased during mid-July over the Maritime continent and western Pacific and shifted eastward during mid-late July. The MJO index is defined by Wheeler and Hendon (2004) based on the first two Empirical Orthogonal Functions (EOFs) of the combined fields of near-equatorially-averaged 850 hPa zonal wind, 200 hPa zonal wind, and satellite-observed outgoing long-wave radiation (OLR) data. Projection of the daily-observed data onto such multiple-variable EOFs, with the annual cycle and components of inter-annual variability removed, yields principal component (PC) time series that vary mostly on the intra-seasonal time scale of the MJO only. This projection thus serves as an effective filter for the MJO without the need for time filtering, making the PC time series an effective index for real time use. For the observations, the OLR data are measured by the NOAA polar-orbiting satellites and is used by Wheeler and Hendon, while the NCEP/NCAR Reanalysis and the Global Assimilation Prediction (GASP) analyses provide wind fields. The index is usually available in near real time about 12 hours after the end of each Greenwich day (Wheeler and Hendon, 2004).

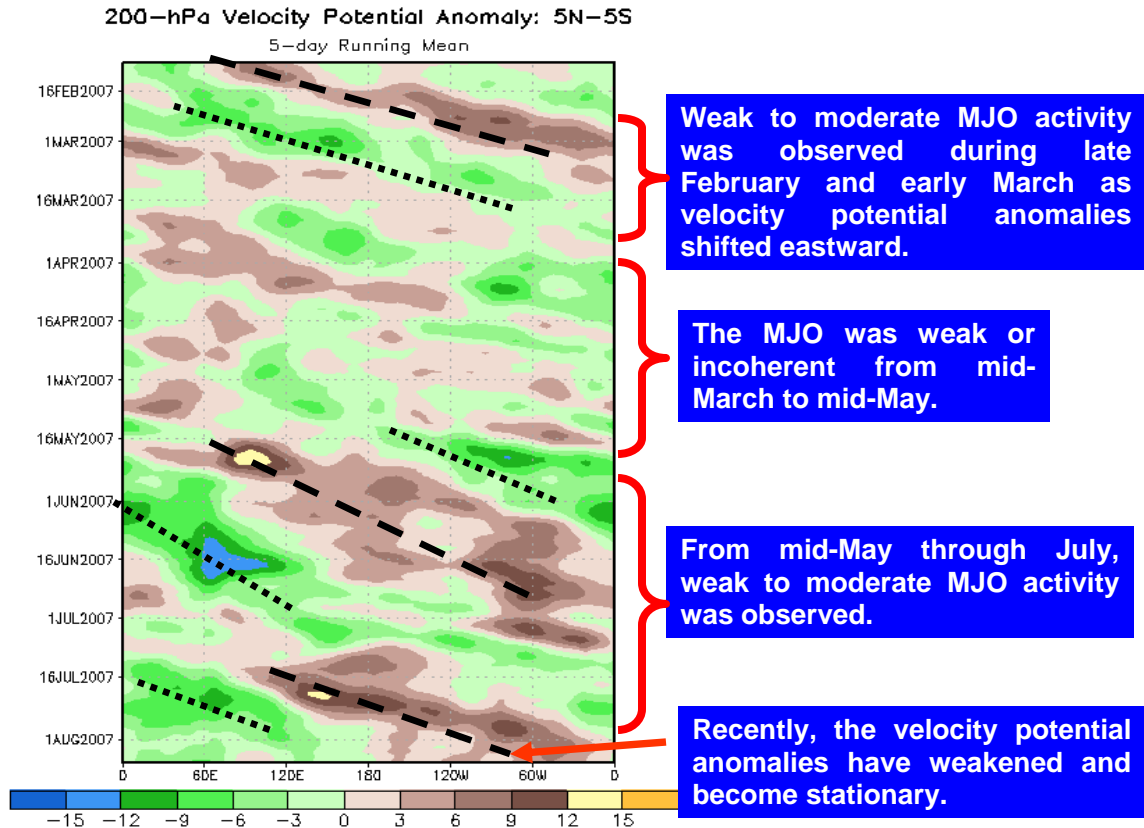


Figure 5. From mid-May into early August, weak to moderate Madden-Julian Oscillation (MJO) activity was observed as velocity potential anomalies propagated eastwards. .

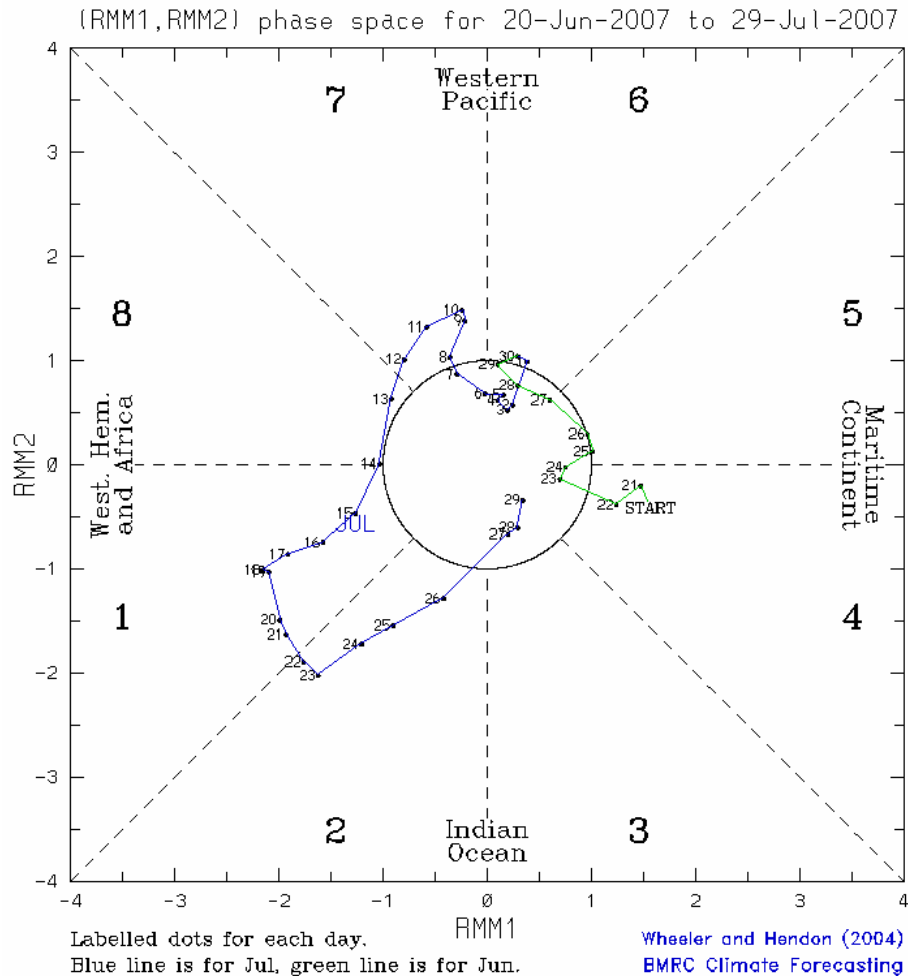


Figure 6. The MJO index indicates that the MJO signal has weakened rapidly. July is indicated in blue and June in green. Courtesy of <http://www.bom.gov.au/bmrc/clfor/cfstaff/matw/maproom/RMM/index.htm> 1 December 2007.

## 2. The Local Environment of Usagi

Deep convection in the developing system may already have started the transition to becoming a warm-core barotropic system even before 25 July (next section) due to hot towers excavating the negative vorticity and importing positive vorticity that then undergoes filamentation in the tail end of the baroclinic system.

A key process is the horizontal shearing of such vorticity patches by the incipient vortex with an upgradient transport of vorticity into the vortex and a

downgradient transport into surrounding vorticity filaments. As the dynamics of vortex Rossby waves have been referenced to usefully characterize the wave mean flow interaction for the PV anomaly amplitudes considered here, it would also be of interest to observe wavelike features in the PV field that are consistent with their local dispersion relation derived in Montgomery and Kallenbach (1997).

The filamentation, which is a consequence of the differential velocity field (i.e., shear, strain rate) due to one vortex acting on another that increases rapidly as the vortex separation distance diminishes (McWilliams, 2006). This filament area of high PV gradient adds to the filamentation area. The filamentation increases in the spiral bands, which helps to increase the circulation inside the intensity of the storm. The cyclogenesis of the Usagi event in the western North Pacific is not consistent given the scenario of TTs in the Atlantic and Gulf of Mexico region. In the Usagi case, aside from the broad area of anticyclone there was a streamer of PV anomalies pulling away from the main low depository from the baroclinic system.

However, the biggest difference in the Usagi case is that the PV streamers detaches first from the main PV reservoir in the baroclinic system before undergoing cyclogenesis. The traditional paradigm for tropical cyclone formation in the Atlantic and southwest Pacific states “that a baroclinic disturbance in the mid-latitudes undergoing transformation of disturbances of sub-tropical or extratropical origin into tropical cyclones are often synonymous with a transition from a cold-core disturbance to a warm-core disturbance” (Elsberry, 2007). Can this occurrence happen in the western North Pacific? The Usagi transformation occurred while the system is already warm core as it is already below an area of the large anticyclone west of the decaying baroclinic system. In addition, this study will provide new insights into the genesis sequences of the WNP basin.

### 3. Lower Tropospheric Interactions within the Non-Developer (Gyre) and Developer (Usagi)

This non-developer (gyre) initial area of convection is closely analyzed in the following sections and will be compared to the developer (Usagi) case. The 850 hPa streamlines overlaid with the MTSAT imagery will highlight areas of convection zones of confluence. When compared with the following sections, you will see that the vorticity and convection difference between the two will be consistent with the OW and SF analysis in Section C. The investigation will show that the SF values in the non-developer are far less than that of the Usagi case as can be seen on Figure 42 and 43. The difference between the non-developer and the Usagi case is shown as a strong line of confluence and convection right along the line of confluent region in Usagi.

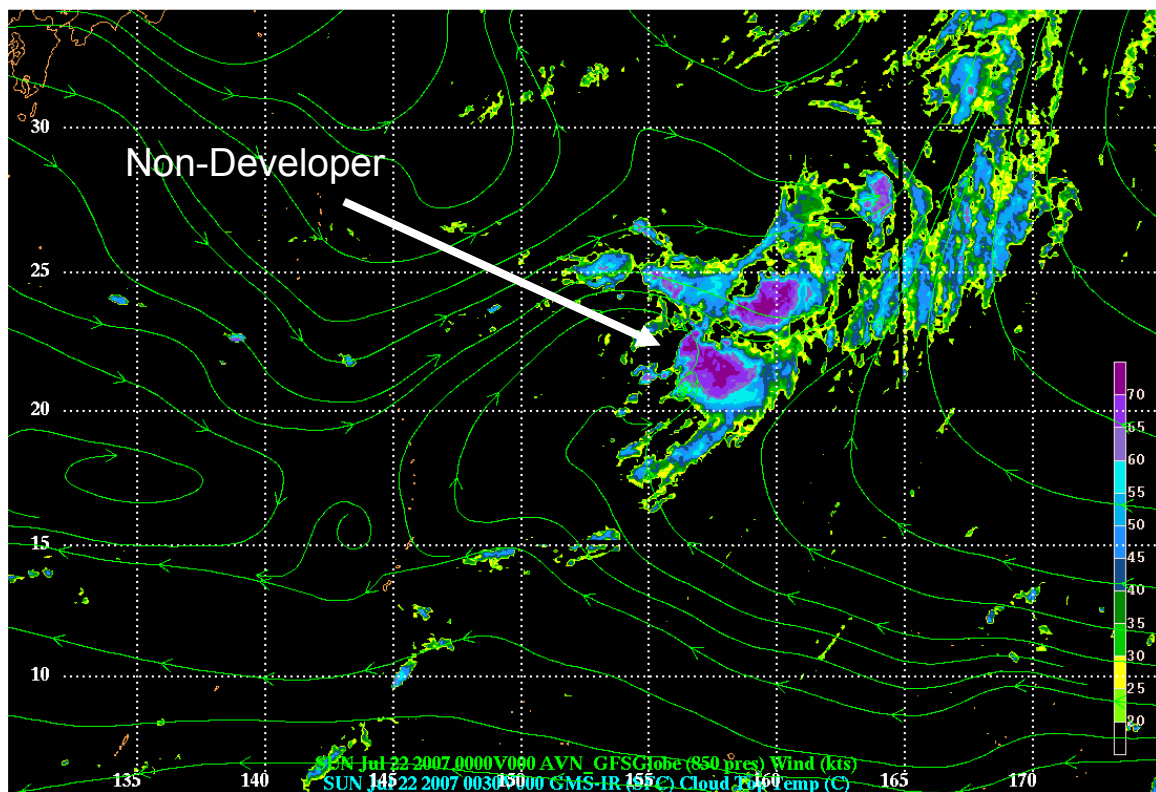


Figure 7. Streamlines of horizontal flow at 850 hPa and MTSAT satellite for 0000 UTC 22 July. Shadings are temperature values from -20°C to less than -70°C.

At 0000 UTC 22 July, the initial non-developing system begins to detach the decaying baroclinic system as the anticyclone spins along behind the system

and stretches the convection (Figures 7). There is an area of weaker vorticity, moisture, and a mid-level trough sheared and damped the convection as shown (Figure 7).

At 0600 UTC 22 July (not shown), the area of persistent convection is still being detached from the main baroclinic system. However, as the convection detaches a trough develops behind the anticyclone (Figure 7) This feature would soon damp the convection all the way thru the life cycle of this initial system.

At 1200 UTC 22 July (not shown), the initial system completely detaches the baroclinic system and undergoes persistent convection. However, the large mid-level trough behind the developing convection is still persistent and will eventually shear the convection.

By 1800 UTC 23 July (Figure 8), the initial system goes through the diurnal cycle and does not change in intensity as can be seen on the satellite animation. The system is completely detached and farther from the baroclinic system. As the persistent convection moves farther away from the baroclinic source region, the anticyclone never aligns above the convection and the mid-level trough axis clearly seen on Figure 8 will shear convection.

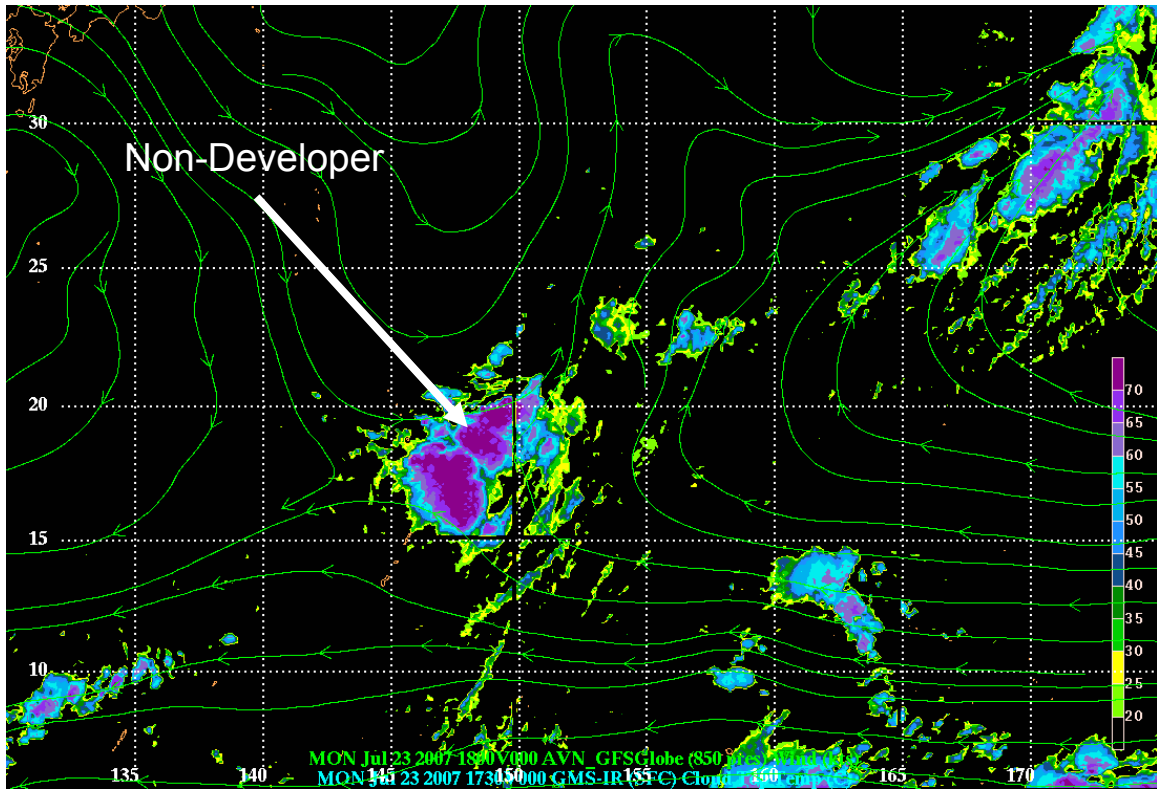


Figure 8. Streamlines of horizontal flow at 850 hPa and MTSAT satellite for 1800 UTC 23 July. Shadings are temperature values from  $-20^{\circ}\text{C}$  to less than  $-70^{\circ}\text{C}$ .

At 1200 UTC 24 July, a short wave trough (Figure 9) begins to emerge from the northwest and interact with the initial system (non-developer). At 1800 UTC 24 July thru 1800 UTC 25 July, the initial system and the short wave trough interact and eventually enhance deep convection. The anticyclone never aligns to enhance upper level exhaust mechanism. There is significant increase in moisture as the two systems combines and move farther south into an area of higher SSTs, high ocean heat content, and little to no wind shear (not shown). This initial system is further studied in the next two sections, as to why it never develops.

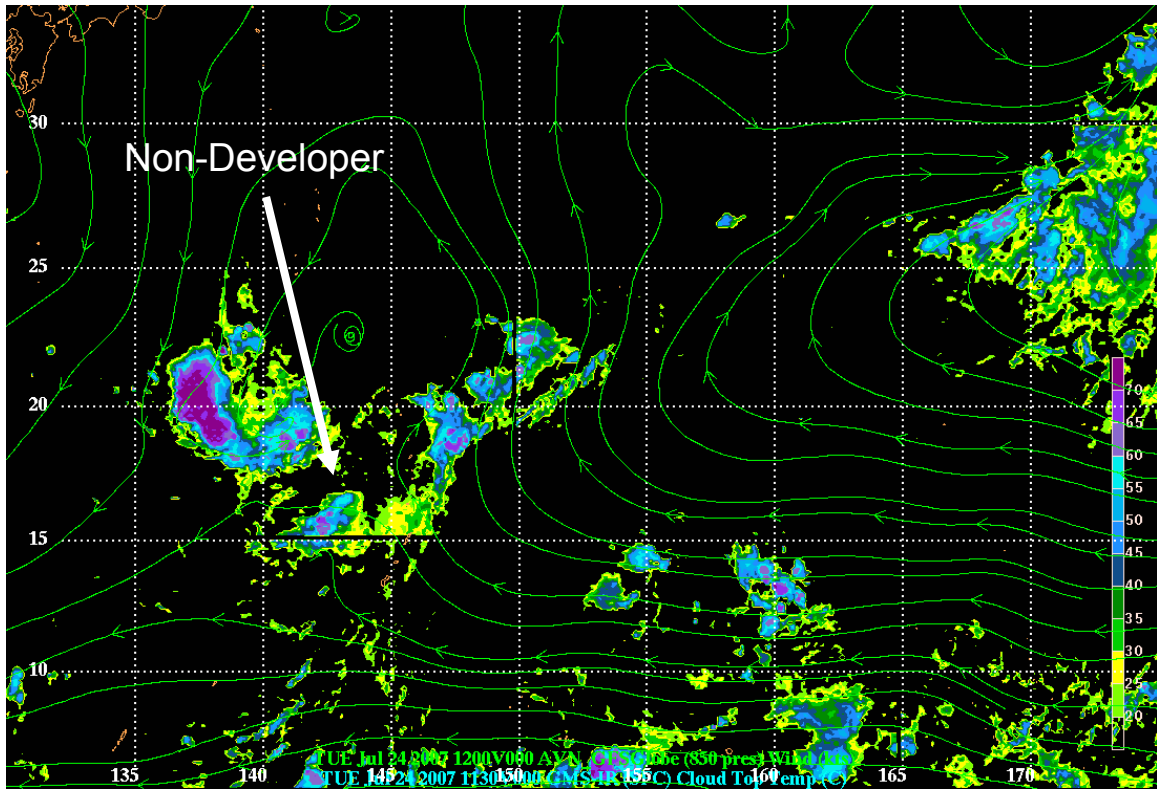


Figure 9. Streamlines of horizontal flow at 850 hPa and MTSAT satellite for 1200 UTC 24 July. Shadings are temperature values from -20°C to less than -70°C.

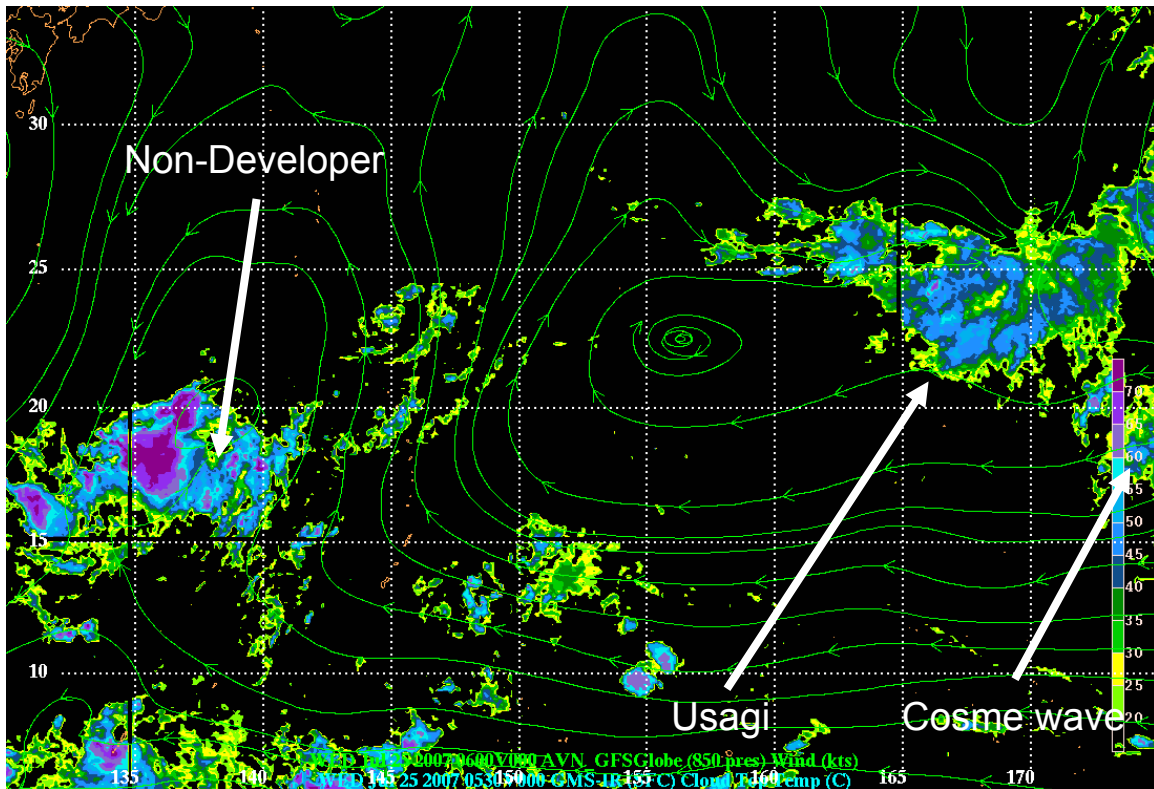


Figure 10. Streamlines of horizontal flow at 850 hPa and MTSAT satellite for 0600 UTC 25 July. Shadings are temperature values from  $-20^{\circ}\text{C}$  to less than  $-70^{\circ}\text{C}$ .

At 0600 UTC 25 July (Figure 10), the remnant of Cosme is visible to the east and continues to move east-northeast to be 680 nautical mile east-southeast of Wake Islands. Banding convection has continued to organize over the last 6-hours. The 850 hPa streamline at continues to indicate moderate, westerly vertical wind shear and this remains the primary limiting factor for development. Maximum sustained winds are estimated at 15 to 20 knots. Minimum sea-level pressure is estimated to be near 1006 hPa. With the forming of an area of persistent convection, the incipient (Usagi) begins to detach from the decaying baroclinic system. The subtropical ridge and a decaying baroclinic system to the north that propagates southeastward from the mid-latitudes of Asia dominated the synoptic pattern. This baroclinic system eventually weakened the subtropical ridge enough to allow the westward movement of the persistent area of convection (Usagi). A large anticyclonic circulation dominated the circulation over the eastern North Pacific over the upper mid-latitudes.

The animated infrared satellite depicts degraded deep convection and more disorganized low-level circulation center (LLCC). This weakening disturbance has occurred over the past 6 hours due to moderate to high amount of vertical wind shear as indicated by strong winds in the 850 hPa streamline and satellite. Although the system is moving to an area of high ocean heat content (not shown), the vertical wind shear is unfavorable for development at this time (Gray, 1968)

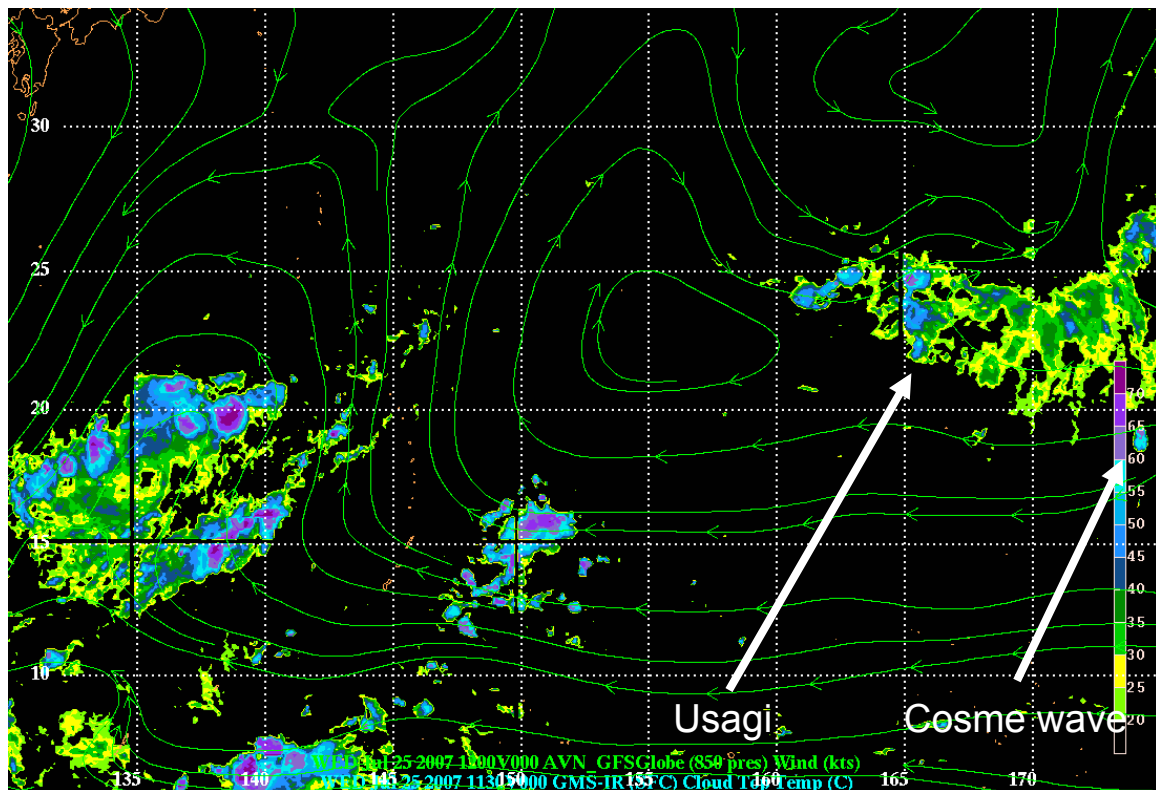


Figure 11. Streamlines of horizontal flow at 850 hPa and MTSAT satellite for 1200 UTC 25 July. Shadings are temperature values from  $-20^{\circ}\text{C}$  to less than  $-70^{\circ}\text{C}$ .

At 1200 UTC 25 July (Figure 11), the tail end of the baroclinic system is still part of a frontal boundary and the remnant of Cosme slowly moving eastward roughly along  $20^{\circ}\text{N}$  as it crosses longitude  $170^{\circ}\text{E}$ . A connection between the outflow of Usagi and the local jet maximum associated with the mid-tropospheric cyclones to the northeast is not evident. The persistent area of convection (Usagi) continued to propagate to the southwest as the subtropical ridge continued to be weakened by the cyclonic circulation moving to the east. The

strong and large anticyclonic ridge over the mid-latitudes had advanced to be east of the Sea of Japan. As the persistent area of convection (Usagi) convection detaches from the source baroclinic system, it undergoes fluctuations during the diurnal cycle. This eventually limits the mechanism for deep convection and allows strong dry air entrainment that slows cyclone development.

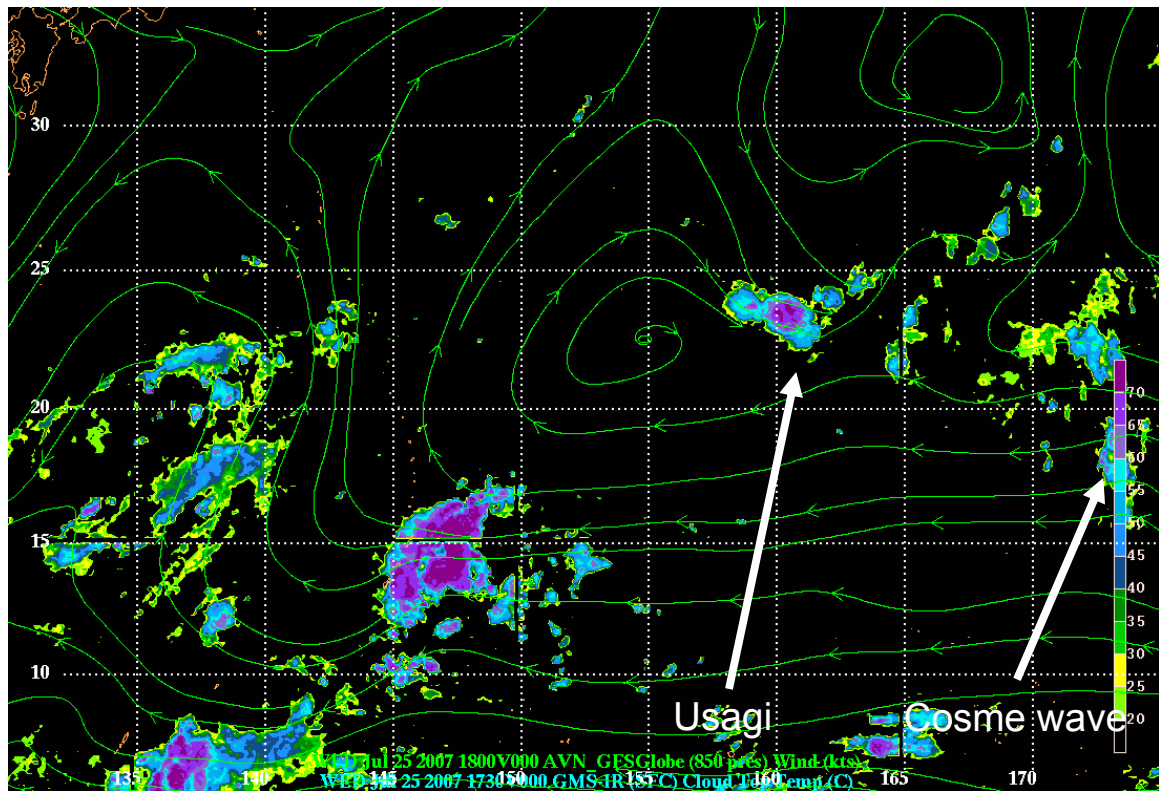


Figure 12. Streamlines of horizontal flow at 850 hPa and MTSAT satellite for 1800 UTC 25 July. Shadings are temperature values from  $-20^{\circ}\text{C}$  to less than  $-70^{\circ}\text{C}$ .

At 1800 UTC 25 July (Figure 12), the interaction between the outflow from the persistent area of convection (Usagi) and the remnants of Cosme is not evident. The outflow from the persistent area of convection (Usagi) has a pronounced anticyclonic curvature as it extends toward the mid-tropospheric low to the east. The pronounced anticyclonically curved outflow from the persistent area of convection (Usagi) associated with the mid-tropospheric low to the east coincides with a northward extension of the subtropical ridge. However, satellite reveals a diurnal variation from the previous satellite images. Tropical convective

systems, especially those at sea, undergo large diurnal variations because of the differences in the shortwave and long-wave radiation budgets of clear and cloudy regions (McBride and Gray, 1980).

The diurnal variability of satellite-observed cloudiness has been described for the western North Pacific (Zehr, 1992). The times of maximum and minimum cloud area in a satellite image depend upon the cloud type and therefore the range of IR brightness temperatures ( $T_b$ ) being considered:

1. The strongest diurnal variation is in very cold temperature brightness ( $T_b < -65^\circ\text{C}$ ) clouds associated with deep convection. The maximum area of such cold cloud occurs between 0300-0600 Local Solar Time (LST) and the minimum between 1200-1800 LST.

2. The area covered by cirrus clouds ( $-15^\circ\text{C} < T_b < -45^\circ\text{C}$ ) also follows a strong diurnal cycle but with an area maximum around 1800 LST, at the time of the minimum in deep convective cloud area.

3. The diurnal cycle in total cloudiness ( $T_b < -15^\circ\text{C}$ ) is weaker and follows that of cirrus, with a late afternoon (1800 LST) maximum.

4. Heavy rain follows the same diurnal cycle as convection. The maximum occurs between local midnight and dawn over the ocean, but can be anytime over land, especially when orographic effects dominate.

Tropical cyclone structure changes, on the other hand, show little substantiated diurnal preference. Because many forecasting methods use trends in satellite imagery, it is critical that forecasters be aware that cloudiness, and therefore the satellite signatures of tropical systems, also show a marked diurnal variation unrelated to structural changes. Short-term trends in satellite imagery can be very misleading and cause major forecast errors (BOM 2008).

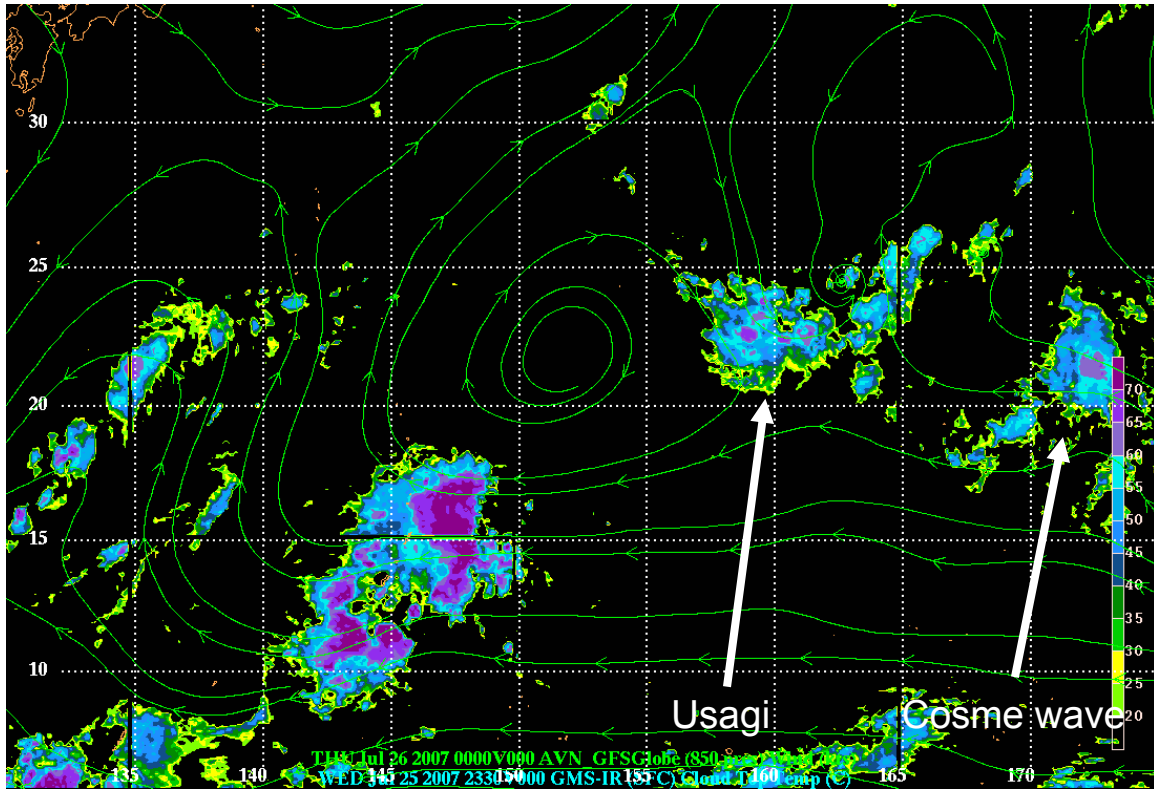


Figure 13. Streamlines of horizontal flow at 850 hPa and MTSAT satellite for 0000 UTC 26 July. Shadings are temperature values from -20°C to less than -70°C.

At 0000 UTC 26 July (Figure 13), the subtropical ridge weakened enough to allow Usagi to begin recurvature to the southwest. The trough (old baroclinic system) to the northeast of Usagi became nearly fully aligned with the tropical cyclone. The continued southwestward motion of Usagi initiates the merger between the outflow from the tropical cyclone and the mid-latitude anticyclone to the north. The outflow region of the persistent area of convection (Usagi) continues to exhibit pronounced anticyclonic curvature in association with the mid-tropospheric baroclinic system to the northeast.

The outflow of the persistent area of convection (Usagi) and the anticyclone to the northwest have combined to form a single wind maximum exceeding  $50 \text{ ms}^{-1}$  north of the tropical cyclone. However, the downstream outflow continues to curve anticyclonically toward the mid-tropospheric cyclone, while the mid-latitude flow maintains a meridional orientation. Furthermore, the subtropical ridge continues to build northward between the persistent area of convection (Usagi) and the 850-hPa low associated with baroclinic system to the east.

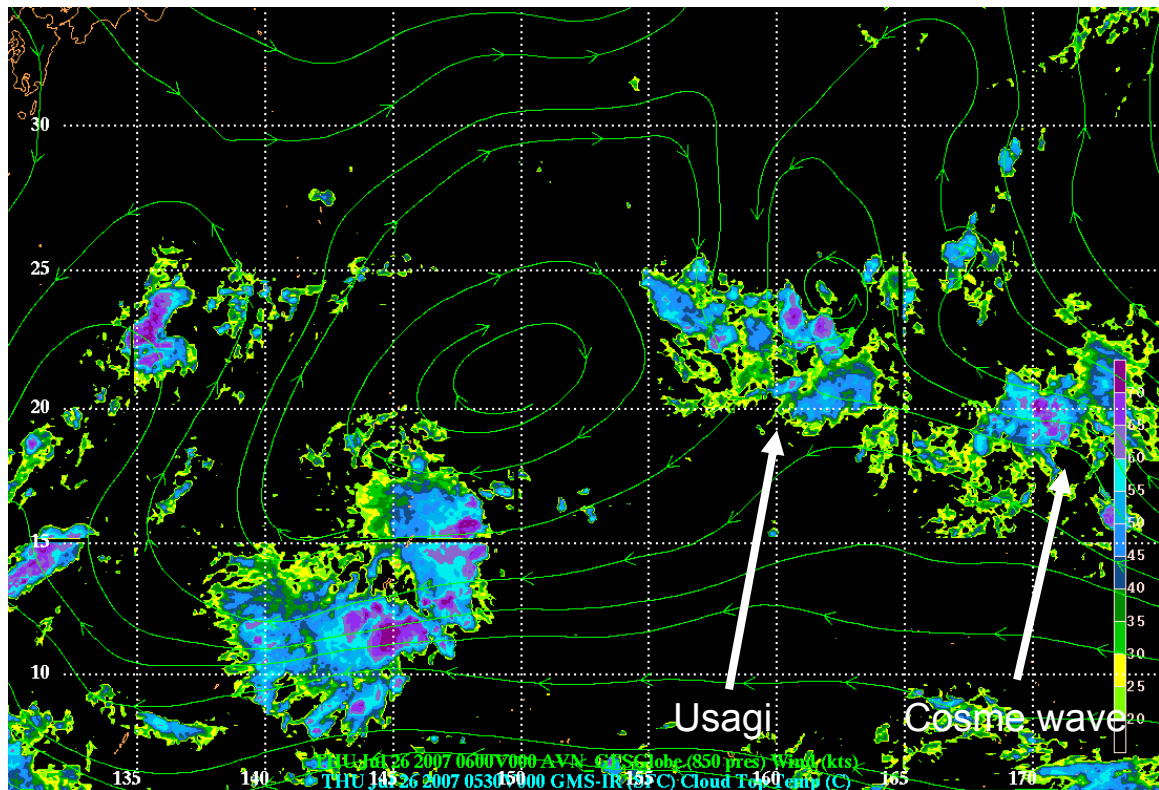


Figure 14. Streamlines of horizontal flow at 850 hPa and MTSAT satellite for 0600 UTC 26 July. Shadings are temperature values from  $-20^{\circ}\text{C}$  to less than  $-70^{\circ}\text{C}$ .

At 0600 UTC 26 July (Figure 14), the persistent area of convection (Usagi) and Cosme have become close enough that if there would be interaction this would be the time. However, as analysis suggest they are still at least  $10^\circ$  apart and too far to form interaction as mentioned earlier. The northward advection of warm air is defined as the anomalously warm regions (not shown) to the west of the storm center. At low levels, warm anomalies to the east (not shown) are associated with the warm-air advection. A mid-level warm anomaly is found over the center in association with the developing tropical cyclone (not shown).

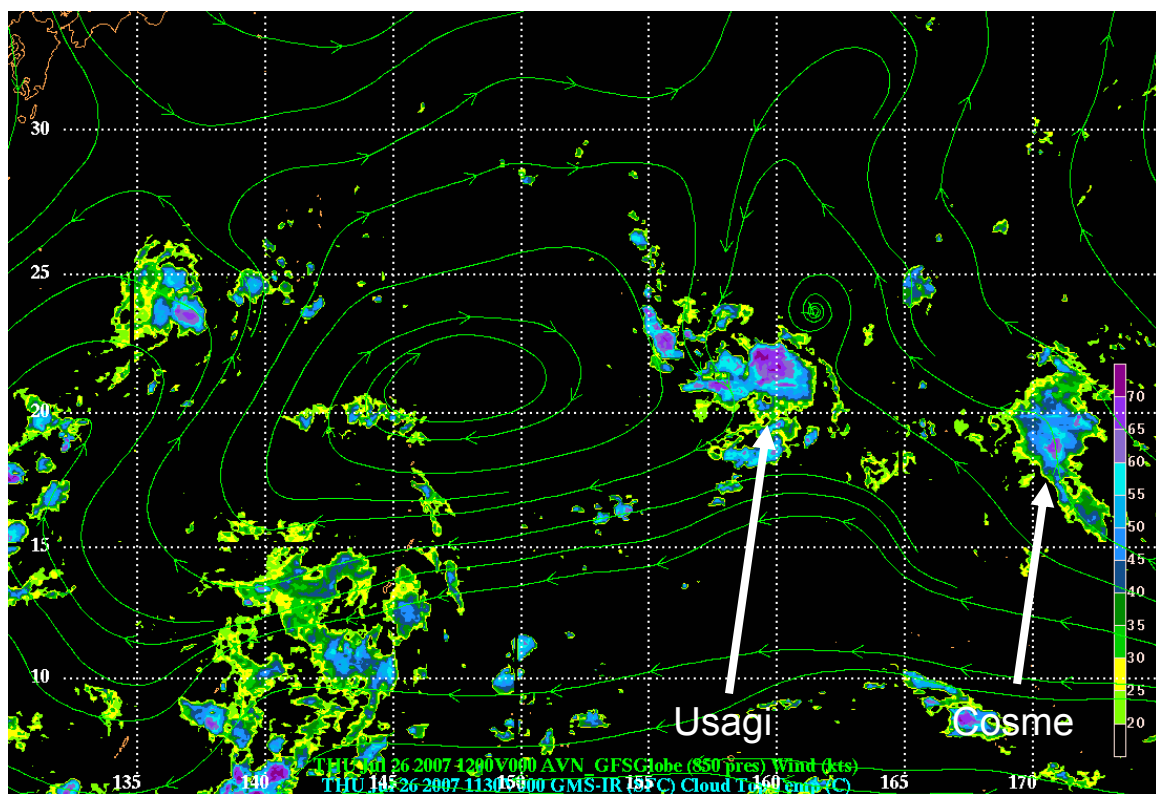


Figure 15. Streamlines of horizontal flow at 850 hPa and MTSAT satellite for 1200 UTC 26 July. Shadings are temperature values from  $-20^\circ\text{C}$  to less than  $-70^\circ\text{C}$ .

At 1200 UTC 26 July (Figure 15), the persistent area of convection (Usagi) continued to recurve and became fully imbedded in the anticyclonic ridge propagating off the mid-latitudes. The relative positioning of the tropical and mid-latitude circulations was indicative of the start of the formation stage of SI.

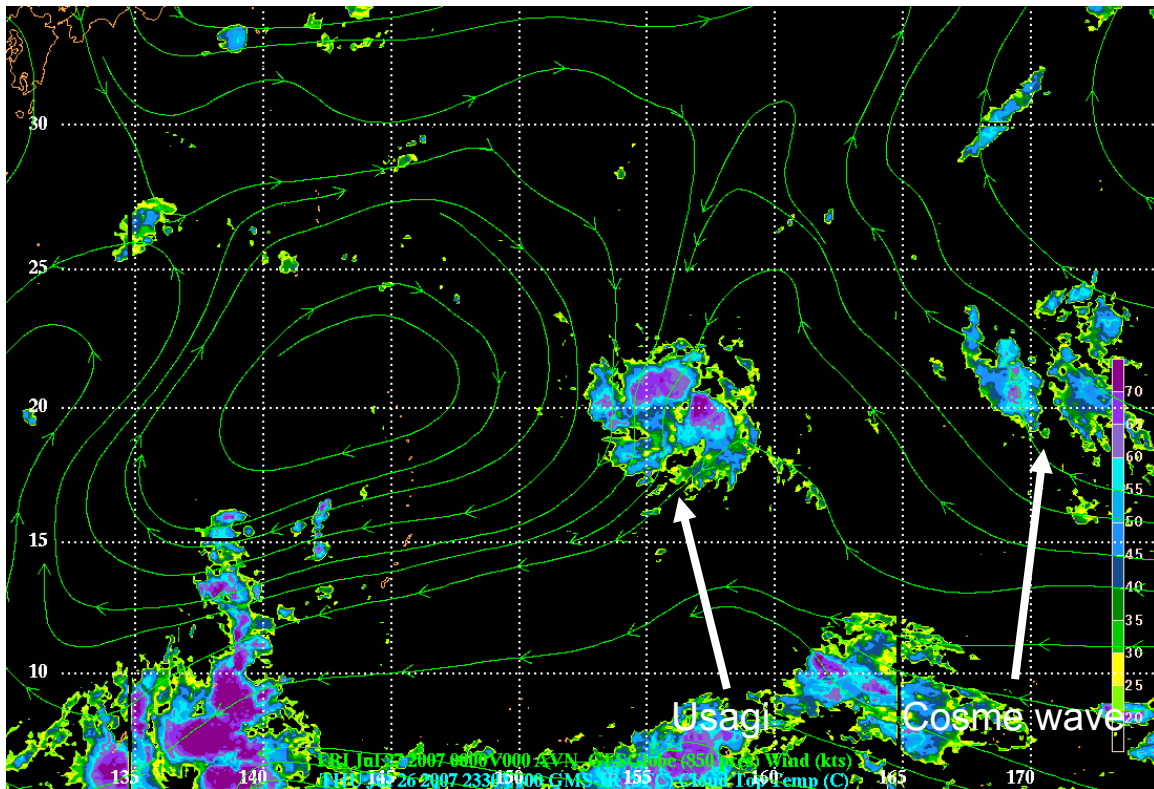


Figure 16. Streamlines of horizontal flow at 850 hPa and MTSAT satellite for 0000 UTC 27 July. Shadings are temperature values from -20°C to less than -70°C.

At 0000 UTC 27 July (Figure 16), the persistent area of convection (Usagi) outflow and anticyclone to the northwest have closely merged. The decaying baroclinic system is now fully washed out to the east in conjunction with the forcing of vertical motion north of the persistent area of convection (Usagi). This vortex interaction as seen on VORTTRACK (Figure 2-4) could have started about this time. However, the weaker vortex that is the remnants of Cosme being advected poleward from the stronger baroclinic vortex, which is the tail end of the baroclinic system.

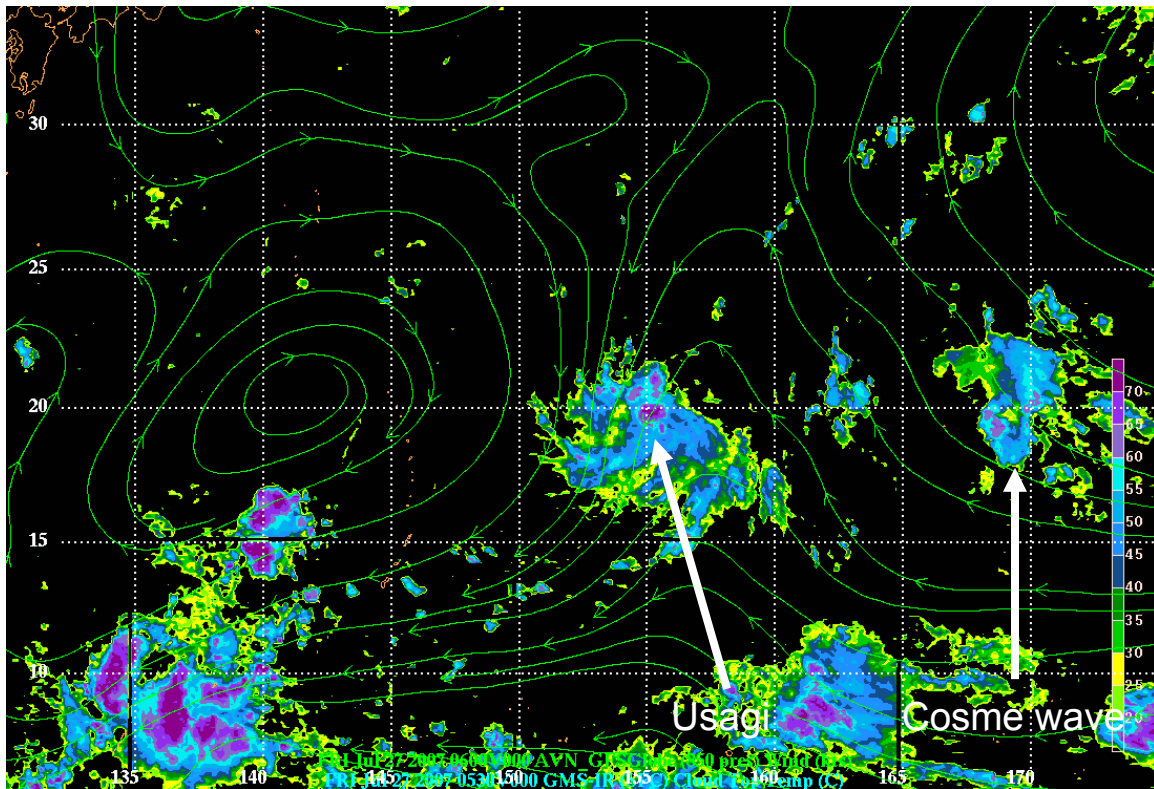


Figure 17. Streamlines of horizontal flow at 850 hPa and MTSAT satellite for 0600 UTC 27 July. Shadings are temperature values from -20°C to less than -70°C.

At 0600 UTC 27 July (Figure 17), the area of persistent deep convection (Usagi) is becoming consistent near 19°N 155°E. This is approximately 570 nautical miles east northeast of Saipan. The animated infrared imagery indicates a rapidly consolidating LLCC with deep convection. The disturbance is imbedded in a tail end of a baroclinic system over the central Pacific. The 850 streamline analysis suggest a large anticyclone west of the decaying baroclinic system that will enhance equator ward flow and low vertical wind shear ideal for deep convection and will move this area of deep convection to a favorable environment for cyclogenesis. This rapid consolidation of LLCC and favorable region for convection enhances this tropical seedling to develop and form a significant tropical cyclone.

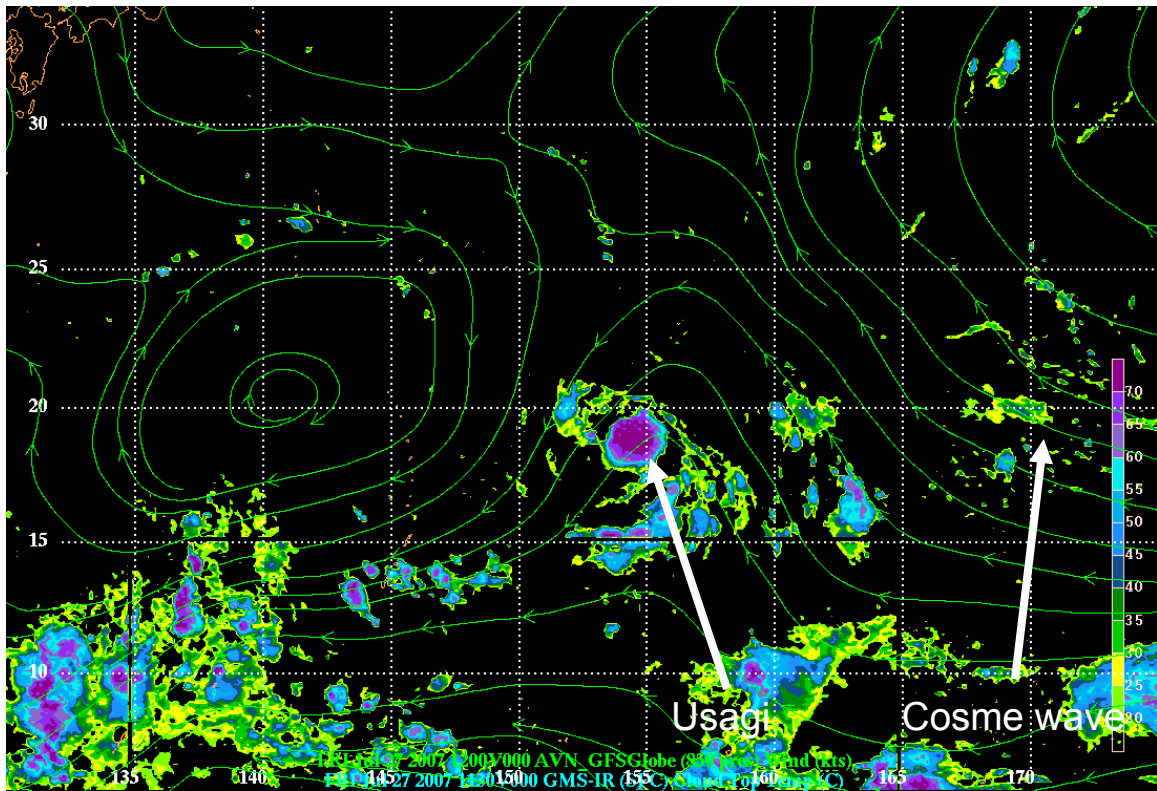


Figure 18. Streamlines of horizontal flow at 850 hPa and MTSAT satellite for 1200 UTC 27 July. Shadings are temperature values from  $-20^{\circ}\text{C}$  to less than  $-70^{\circ}\text{C}$ .

At 1200 UTC 27 July (Figure 18), the deep convection results in a strong cyclonic curvature toward the mid-tropospheric anticyclone to the east of Usagi. The cyclonic curvature is maintained as the persistent area of convection (Usagi) moves northward and the mid-tropospheric cyclone to the east digs southward at 1800 UTC 27 July (Figure 19).

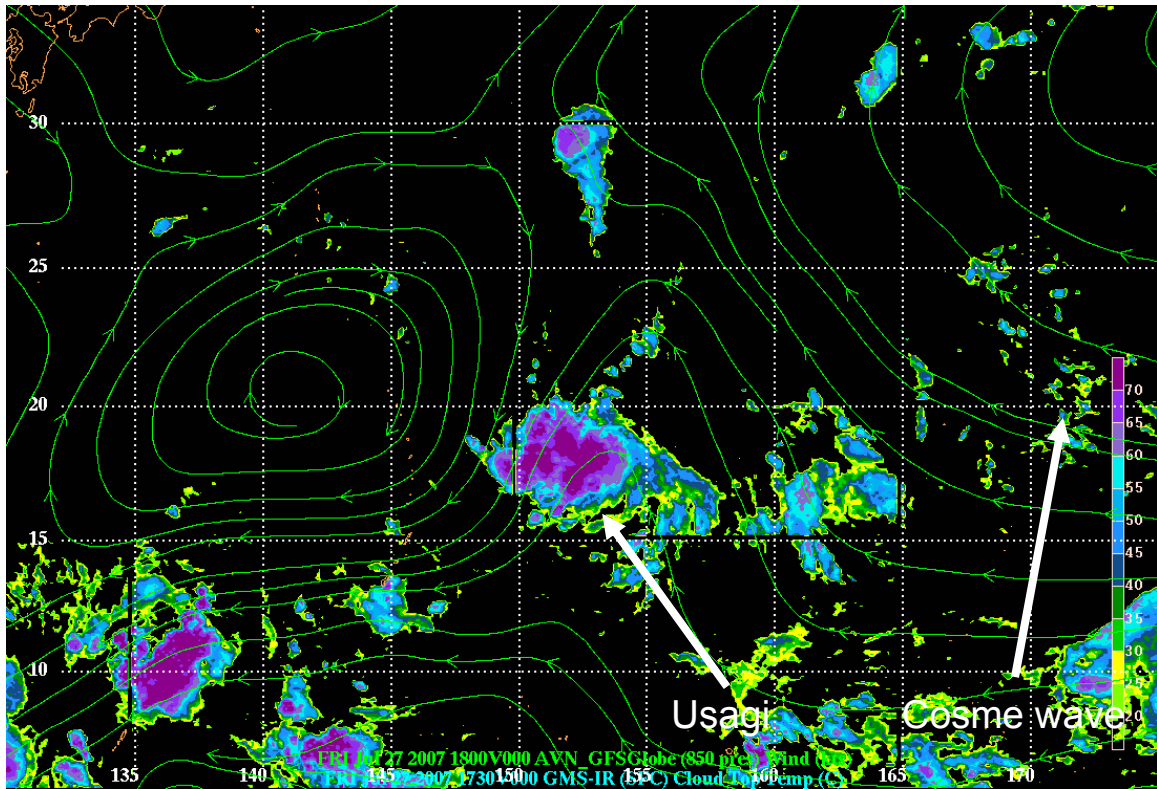


Figure 19. Streamlines of horizontal flow at 850 hPa and MTSAT satellite for 1800 UTC 27 July. Shadings are temperature values from -20°C to less than -70°C.

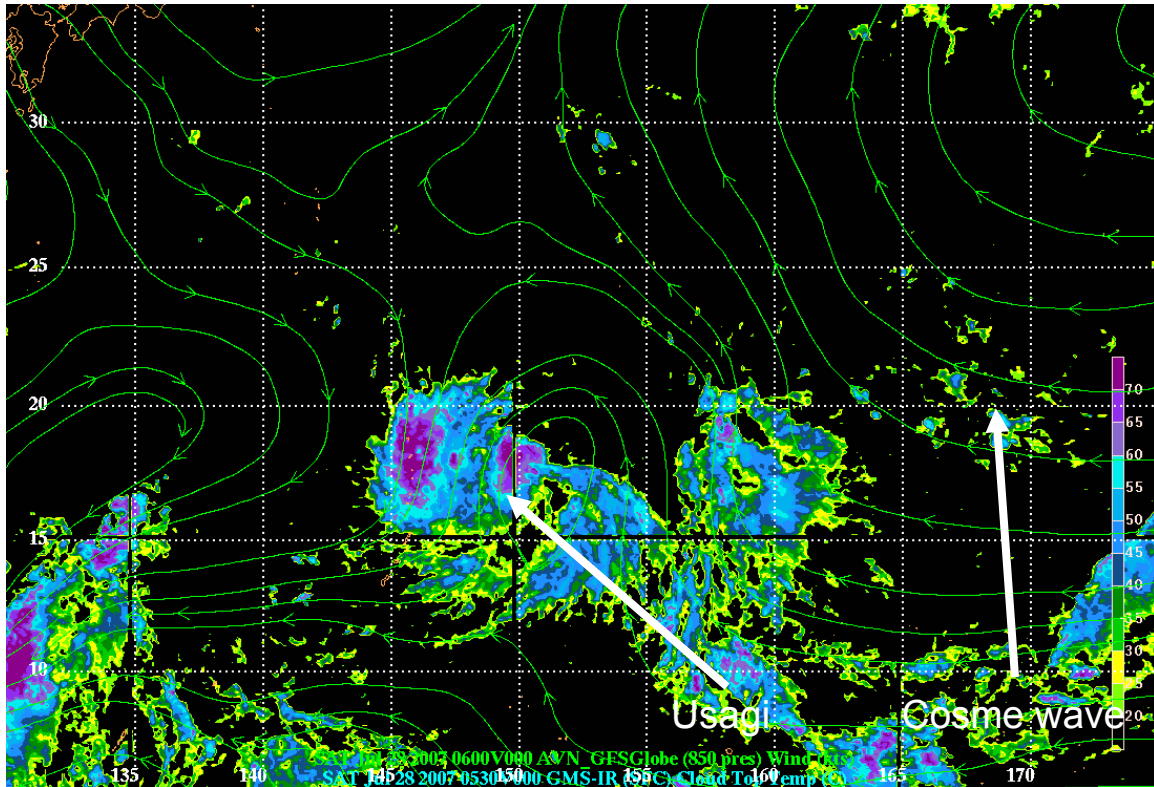


Figure 20. Streamlines of horizontal flow at 850 hPa and MTSAT satellite for 0600 UTC 28 July. Shadings are temperature values from  $-20^{\circ}\text{C}$  to less than  $-70^{\circ}\text{C}$ .

At 0600 UTC on 28 July (Figure 20), the SI has begun by increased moisture and increased cyclonic circulation of the system. The system also has moved farther south into an area of higher SSTs, high ocean heat content, and little to no wind shear. Thus, the remnants of the tail end of the baroclinic system eventually became Typhoon Usagi. Usagi initially moved southward in response to an anticyclone to its northwest, and then northwestward toward Japan after having as it moved around the southern periphery of the ridge.

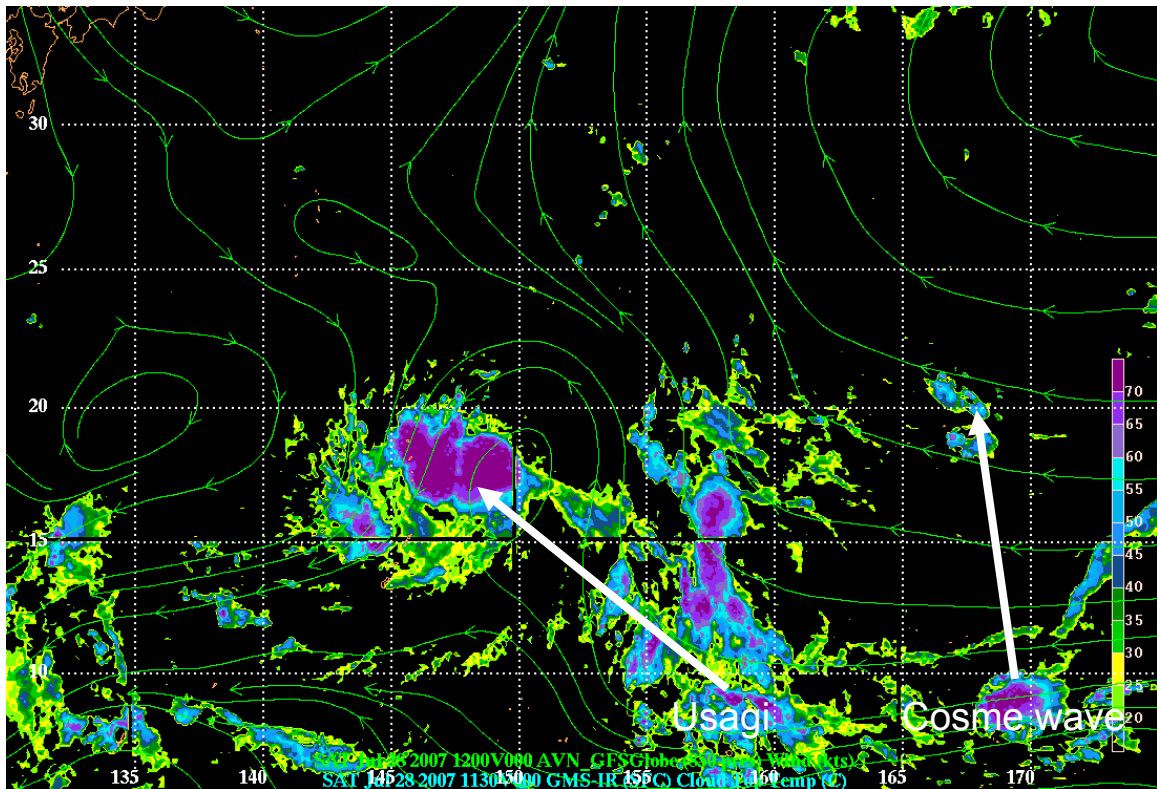


Figure 21. Streamlines of horizontal flow at 850 hPa and MTSAT satellite for 1200 UTC 28 July. Shadings are temperature values from -20°C to less than -70°C.

At 1200 UTC on 28 July (Figure 21), as TD 5W (Usagi) entered the formation stage of SI a clear interaction occurred between the outflow of the decaying baroclinic wave circulation and a mid-tropospheric anticyclone to the west. The outflow first curved anticyclonically toward the cyclone to the east. The curvature became pronounced as Usagi moved northward and the cyclonic circulation drifted southward. This interaction coincided with a pronounced northward extension of the subtropical ridge. In this case, TD 5W (Usagi) was classified as a tropical depression 05W at 1200 UTC 28 July, which defines 36-h duration for the transformation stage (JTWC, 2007).

At 0000 UTC on 29 July (not shown), TS Usagi (5W) entered its strongest stage to date as an area of deep convection where the upper anticyclone is aligned for the much-needed exhaust of deep convection. At this time of SI, a clear interaction occurred between the outflow of the decaying baroclinic wave circulation and a mid-tropospheric anticyclone to the west.

At 0000 UTC on 30 July (not shown), Usagi was named as Typhoon Usagi (5W) and is now 315 nautical miles south-southeast of Iwo-Jima, tracked northwestward at 11 knots. Maximum sustained winds were estimated at 65kt gusting to 80kt (JTWC, 2007).

## **B. DYNAMIC AND THERMODYNAMIC EVOLUTION OF USAGI**

This section will investigate high-resolution analysis of the GFS FNL model to show that the PV of Cosme is too far away from the baroclinic system and did not play any essential role in the development of Usagi. The analysis will show how Cosme could have aided the development of Usagi via an indirect factor. As mentioned in the previous section, the apparent vortex merger starts about 0000 UTC on 27 July as shown in figure 2, and with each passing chart, the weaker vortex that is the remnants of Cosme are being advected to the stronger baroclinic vortex, which is the tail end of the baroclinic system and eventually became Usagi. The PV from the baroclinic disturbance could have become close enough to wrap around the filaments from Cosme into the disturbance that eventually became Usagi.

Potential vorticity is defined on constant potential temperature isobaric surfaces in layer average between 500 and 850 hPa (Holton, 2004) as follows:

$$\overline{PV} = -g \left[ \zeta + f + (k * \frac{dV}{d\theta}) \right] \frac{\partial \theta}{\partial p} \quad (2.1)$$

where

g is the gravitational acceleration,

$\zeta$  is the relative vorticity on a pressure surface,

$f$  is the Coriolis parameter,

$V$  is the layer-average vector wind at 500 and 850 hPa,

$\theta$  is potential temperature,

and  $p$  is pressure.

The PV anomaly is defined by the deviation from the zonal average PV. For adiabatic motions potential vorticity is a materially conserved quantity. It is not materially conserved when moist processes are active. Using synoptic-scale gridded fields, the computation of the diabatic influences can be difficult to compute. However, the total derivative of PV can be used to define a proxy for diabatic processes as:

$$\frac{d(\overline{PV})}{dt} = \frac{1}{\rho} (\zeta \bullet \nabla \dot{\theta}) \quad (2.2)$$

where

$\rho$  is the density,

$\dot{\theta}$  is the diabatic heating,

and the overbar represents the layer average.

A tropical cyclone is represented by a large deep vertically upright region of positive PV. As the seeding PV anomaly undergoes SI, warm advection begins in the eastern quadrants of the storm, while cold advection occurs in the western quadrants. The warm, moist air that is advected around the western side of the storm is associated with rising motion. The warm advection and upward vertical motion and associated release of latent heat will contribute to an increase in thickness to the east of the southward-moving tropical cyclone. In terms of the distribution of PV, the mid-tropospheric heating maximum on the western side of

the decaying baroclinic cyclone will contribute to a positive change in the lower-

level PV ( $\frac{d(\overline{PV})}{dt} > 0$ ), and a negative change in the upper-level PV ( $\frac{d(\overline{PV})}{dt} < 0$ ).

At the same time, the warm advection occurring on the eastern side of the storm brings warm, moist air into the storm, which enhances the convection and eventually the eye wall convection. This enhancement eventually causes the storm to take on the more symmetric appearance of a tropical cyclone. To diagnose the dynamic evolution of the PV distribution, plan-view diagrams of the PV, PV anomaly, the time derivative of the potential vorticity, relative humidity and vertical motion ( $\omega$ ) are constructed from the gridded analyzed fields.

The time tendency of the PV distribution is used to diagnose areas where diabatic heating is influencing the PV distribution at upper and lower levels (Vancas 2007).

Relative humidity (SF) and vertical motion (OW) are used to indicate the potential for sustained deep convection.

Tropical cyclone formation brings regions of anomalously warm temperatures, particularly in the lower atmosphere, poleward. For a baroclinic system undergoing decay, warm anomalies typically have an upright structure similar to that of the PV distribution discussed above. The peak warm anomaly in this case occurs in the lower atmosphere. The amount of the anomalous warming may be related to the intensity of the tropical cyclone, with stronger storms having higher peak anomaly temperatures (Krishnamurti et. al. 1987).

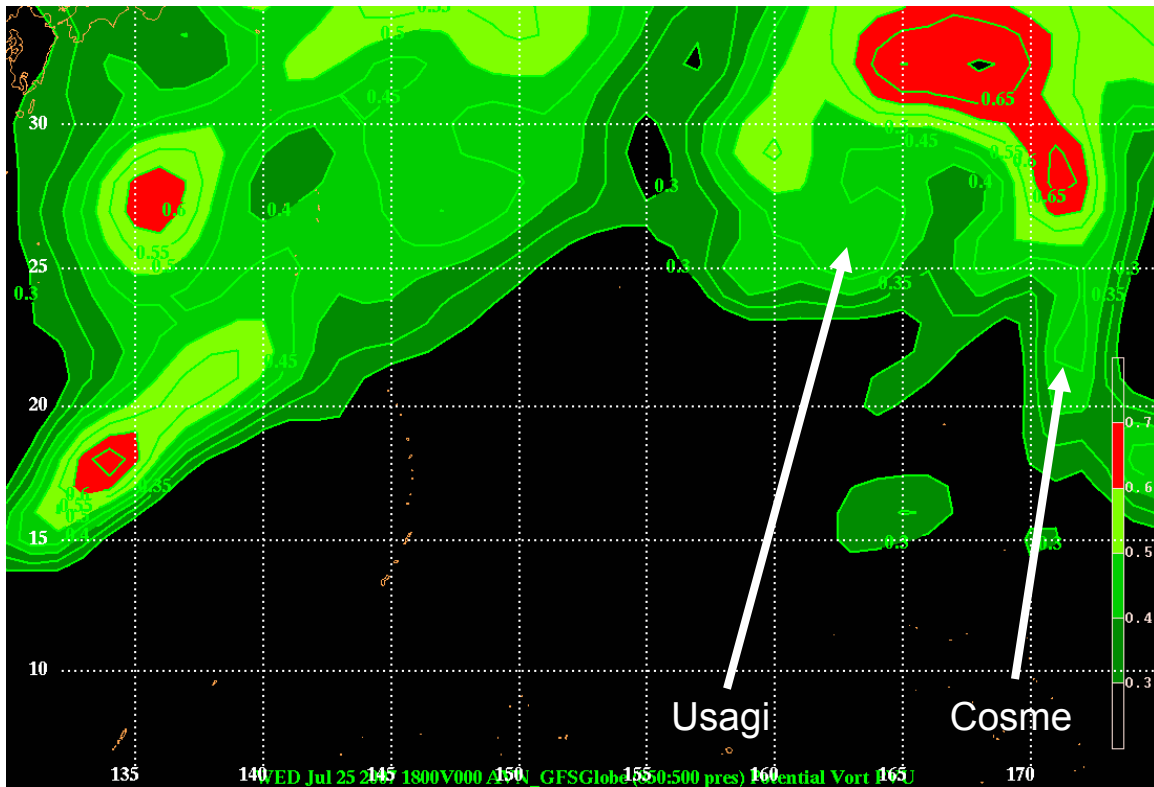


Figure 22. Potential vorticity in units of PVU at 850-500 hPa overlay for 1800 UTC 25 July

By 1800 UTC 25 July (Figure 22), the distribution of PV is becoming evident as a the persistent area of convection (Usagi) and the approaching remnants of Cosme. However, regions of positive and negative PV tendency (not shown) are beginning to appear centered near 850-500 hPa to the east and west of Usagi.

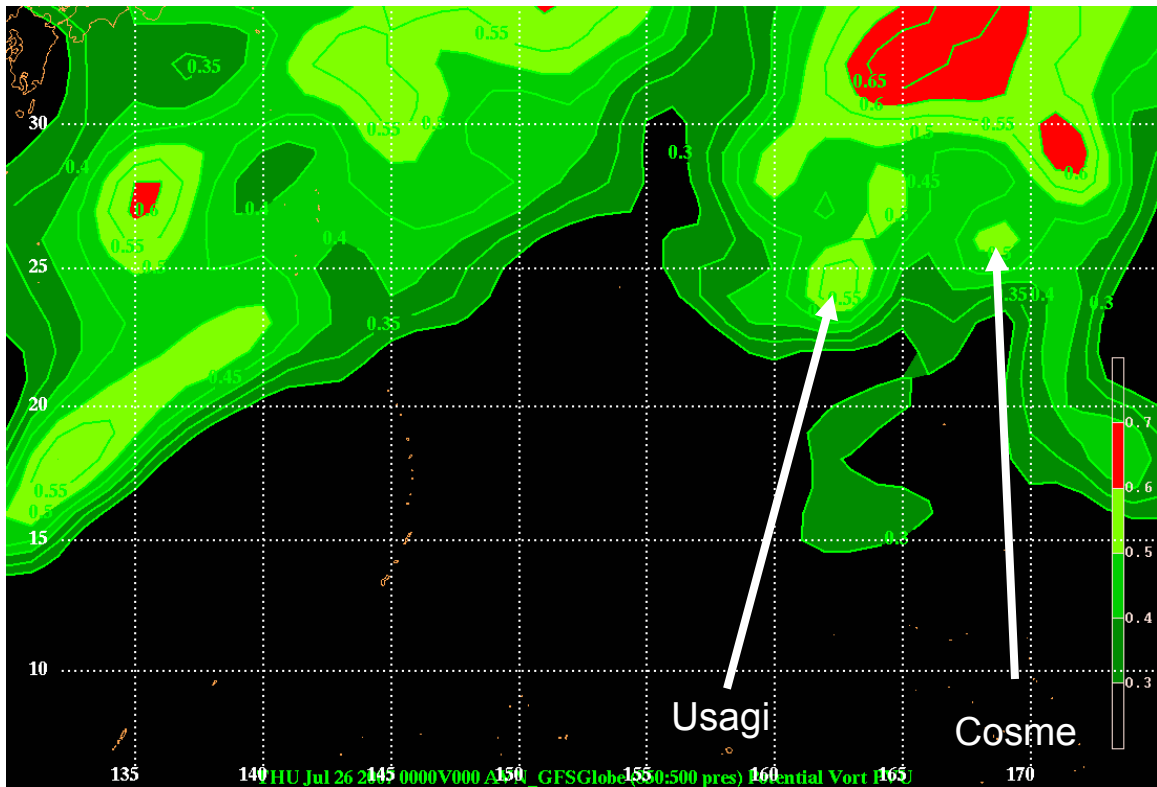


Figure 23. Potential vorticity in units of PVU at 850-500 hPa overlay for 0000 UTC 26 July

By 0000 UTC 26 July (Figure 23), the region of positive PV had increased in the mid-troposphere on the persistent area of convection (Usagi). The distribution of OW values becomes stronger than it was 6-hour earlier (Appendix A).

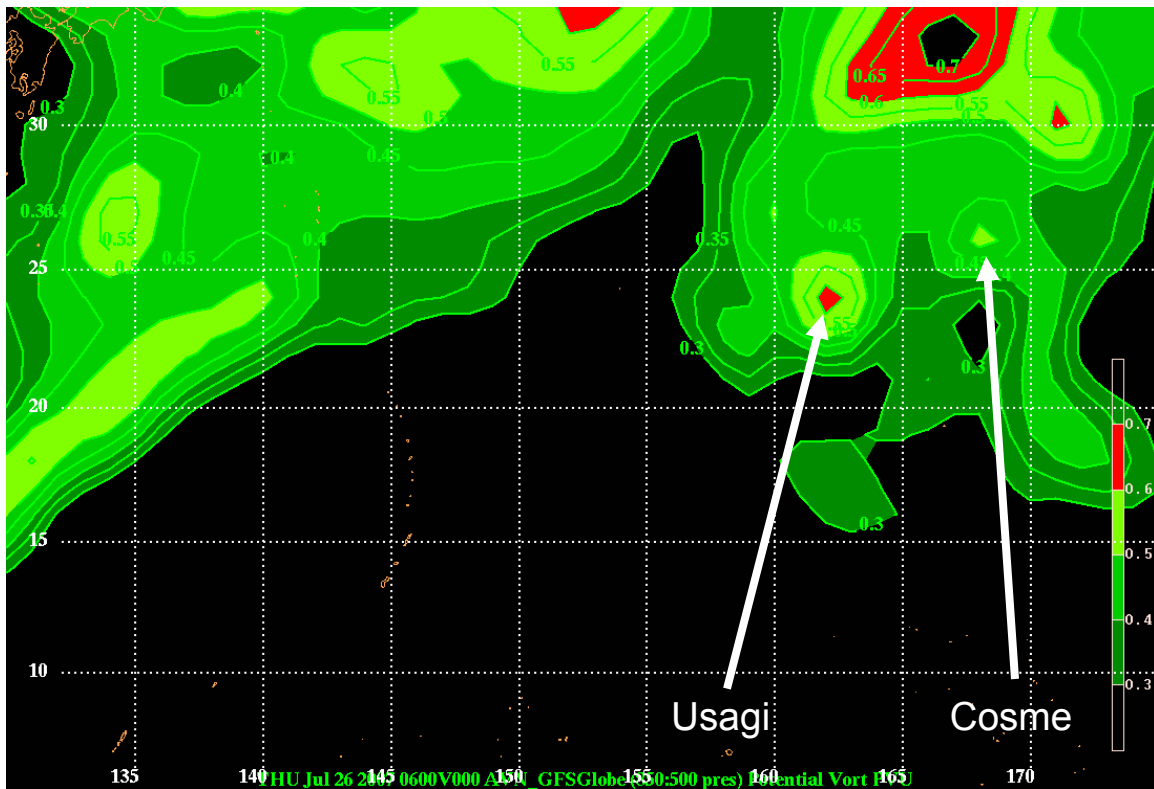


Figure 24. Potential vorticity in units of PVU at 850-500 hPa overlay for 0600 UTC 26 July

By at 0600 UTC 26 July (Figure 24), the PV has become concentrated over the storm center at low levels. The vertical distribution of upward vertical motion has changed dramatically. Sinking motion is found west and east near the center of Usagi. Therefore, between 1800 UTC 25 July and 0000 UTC 26 July the circulation of Usagi seems to have become better defined. This may be in response to a period of reduced vertical wind shear. Strong vorticity at the tip of the PV streamer favors deep convection, which will enhance the low-level vorticity and moisten the mid level, while the remnants of the Cosme wave may act to enlarge the wave “pouch” and help protect the moisture in the middle levels from outside influences. In this sense, the Cosme wave may have played a role in the development of the persistent area of convection (Usagi) even though it did not directly interact with the baroclinic system and Usagi. At this time, the region between Usagi and Cosme also reveals a small area of clearing between the two consistent areas of convection.

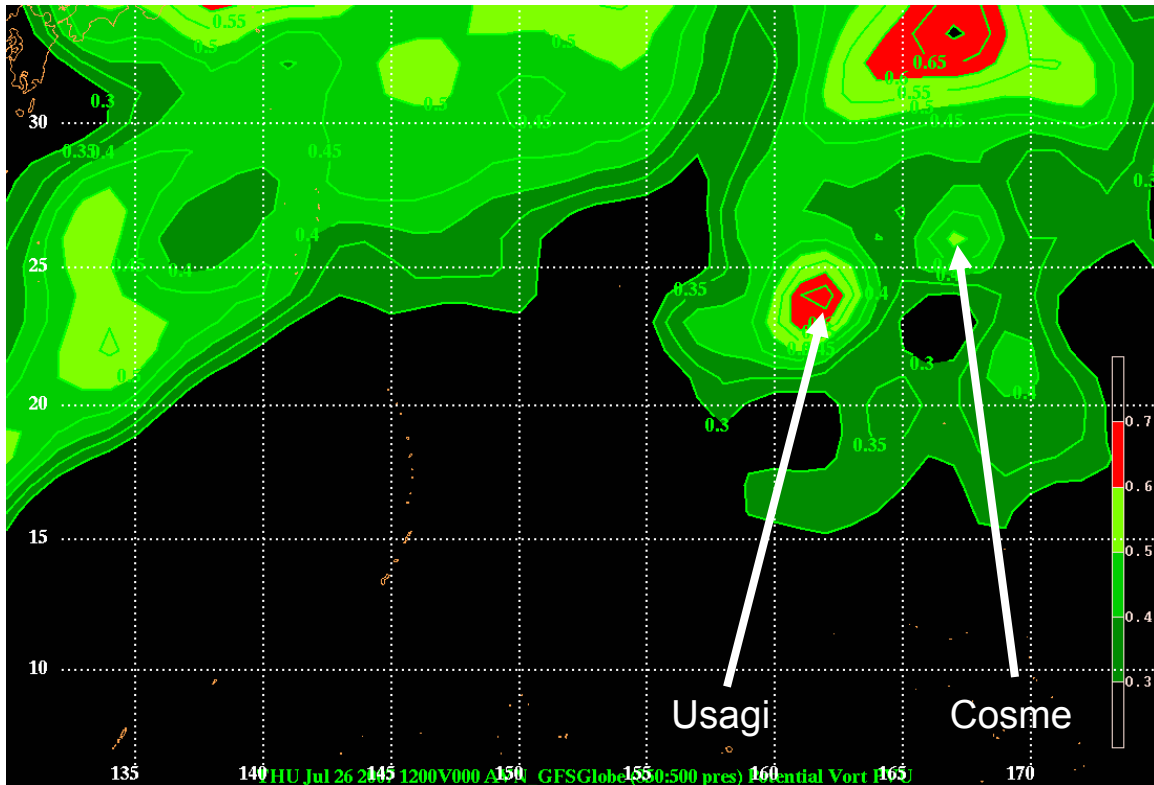


Figure 25. Potential vorticity in units of PVU at 850-500 hPa overlay for 1200 UTC 26 July

By 1200 UTC 26 July (Figure 25), several important features can be noted. It is from this time in the SI event that a more detailed description will be given in the following sections when we review the OW and SF analysis. The anticyclone is evident behind the baroclinic system to the west of Usagi (as seen in the previous section) as a lobe of low PV and an area clearing behind it. Furthermore, an area of positive at low levels just to the west of the storm center is associated with the anticyclone that is a broad region of subsiding air to the west of the center of Usagi. Because the lower troposphere warm anomaly (not shown) remains over the storm center, there is also a southern extension of low level warming. In the lower levels, the vorticity anomaly becomes organized with enhanced low-level convergence from the existing instability from the low-level. This would be consistent with the bottom-up formation of a frontal system stagnating in the subtropics and transforming to warm-core characteristics (DMW 2008).

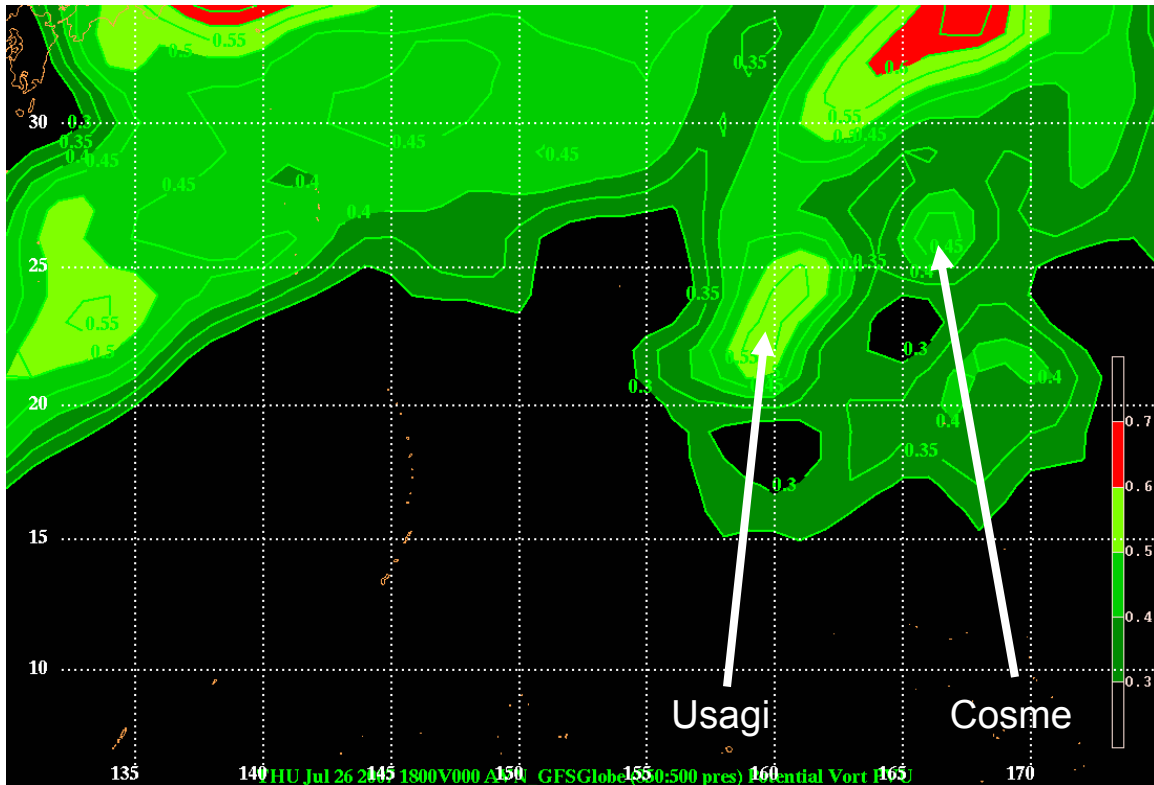


Figure 26. Potential vorticity in units of PVU at 850-500 hPa overlay for 1800 UTC 26 July

By 1800 UTC 26 July (Figure 26), the area of low-level positive PV to the center Usagi extends to the mid-troposphere as the mid-latitude anticyclone approaches the forming storm (Usagi). A large area of dry air (not shown) exists to the west of the storm center with some subsidence. However, the warm anomaly through the entire troposphere has been shifted to the east of the center of Usagi. Significant changes in the distribution of PV, time tendency of PV, and temperature distribution now occur in the 6 hour between 1800 UTC 26 July and 0000 UTC 27 July. As the large anticyclone approaches Usagi from the west seen the previous section, the region of positive PV time tendency (not shown) is nearly adjacent to Usagi, and the distribution of PV in the mid-troposphere has begun to extend into Usagi. The area of stronger PV of Cosme moves to cooler waters and eventually dissipates.

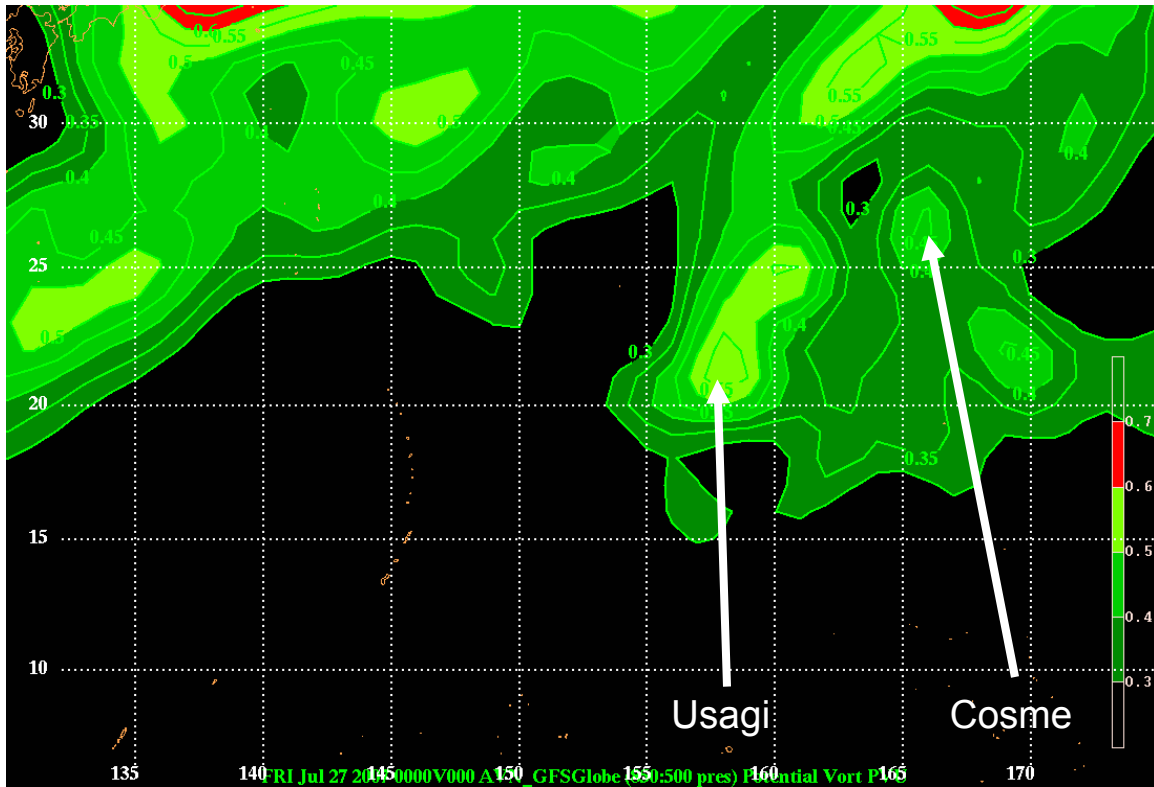


Figure 27. Potential vorticity in units of PVU at 850-500 hPa overlay for 0000 UTC 27 July

By 0000 UTC 27 July (Figure 27), at low-levels the distribution of vertical motion is distinctly over to the center of Usagi. Cosme has decreased in the strength at this time, as its PV gets weaker and smaller in horizontal scale, the low-level maximum PV anomalies of Usagi are shifted southerly.

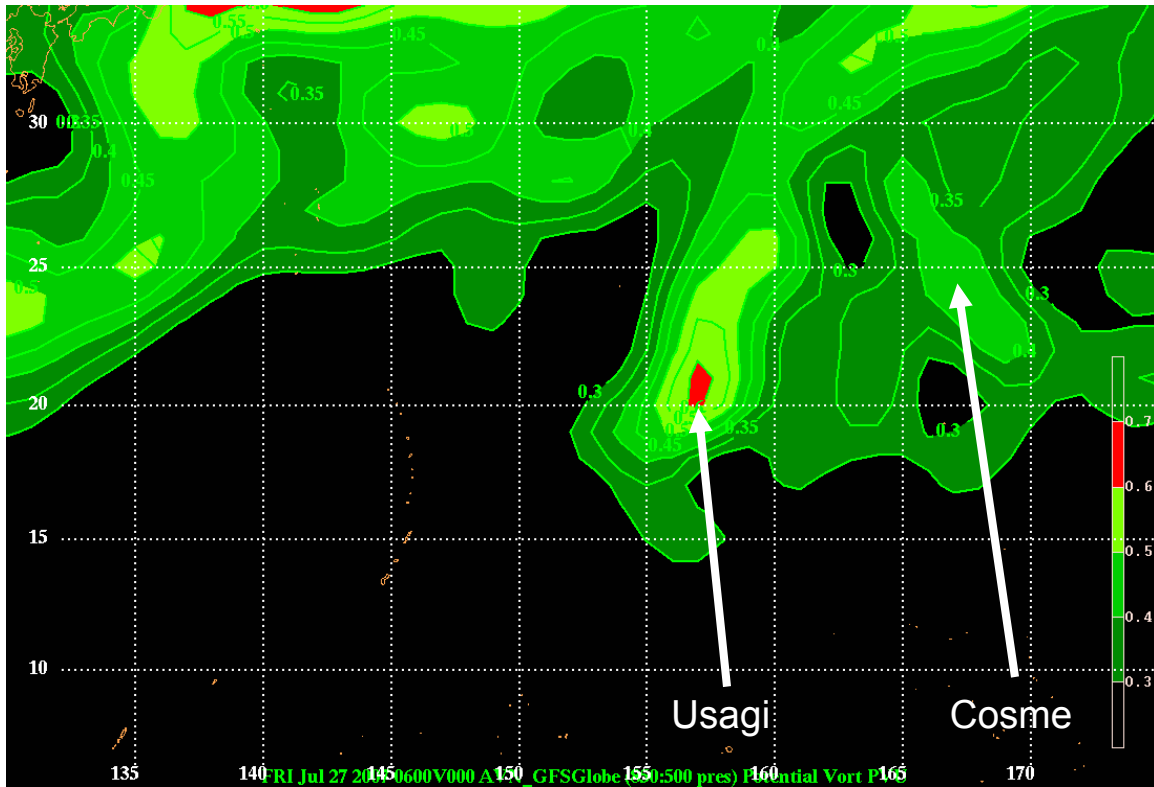


Figure 28. Potential vorticity in units of PVU at 850-500 hPa overlay for 0600 UTC 27 July

By 0600 through 1200 UTC 27 July (Figure 28 and 29), the area of persistent convection (Usagi) has taken on characteristics of the formation stage of SI. The maximum positive PV region in the low-levels has moved over the center of the storm as the developing circulation of the convection (Usagi) moves to an area of higher SSTs and weak vertical wind shear favorable for TC formation.

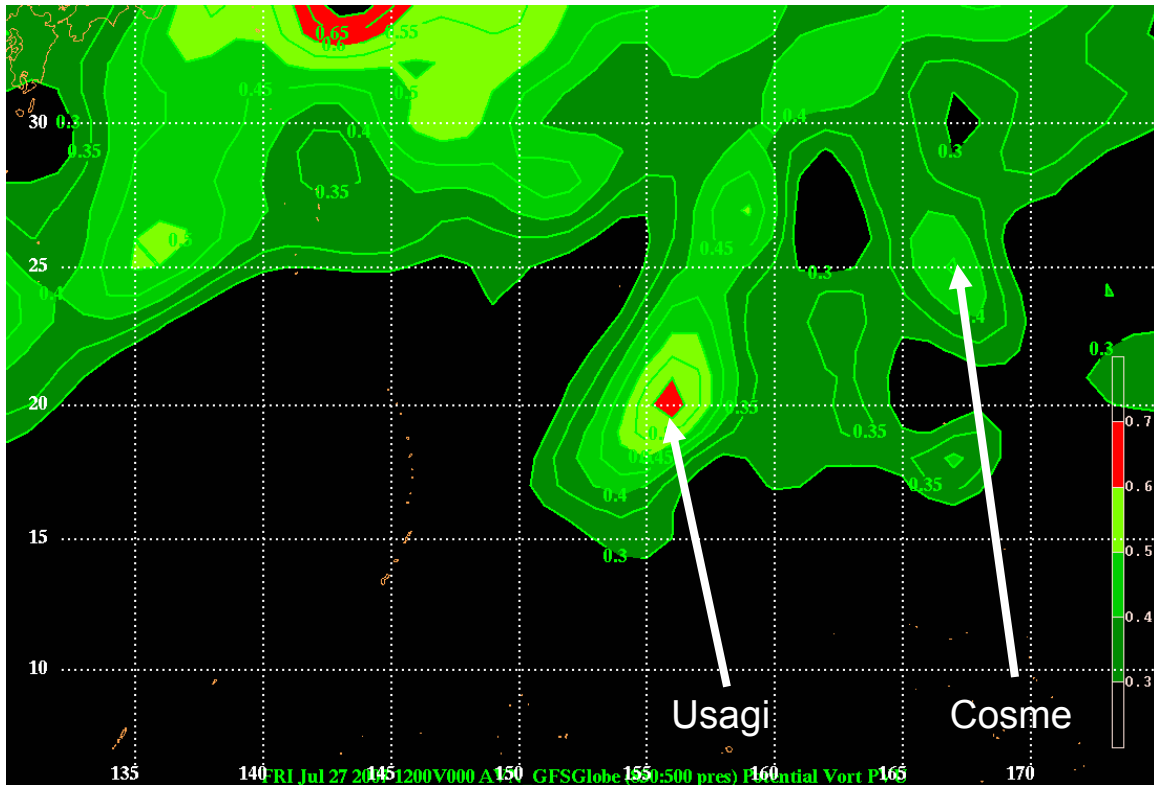


Figure 29. Potential vorticity in units of PVU at 850-500 hPa overlay for 1200 UTC 27 July

As Usagi entered the low latitudes, it underwent several important dynamic and thermodynamic changes. The distribution of upward vertical motion underwent dramatic changes under the influence of the mid-latitude circulations. As the SI stage was completed, a strong region of upward vertical motion developed farther to the east associated with the remnants of the cyclonic circulation of the lower tropospheric baroclinic system. A secondary upward vertical motion region centered east and over the decaying baroclinic system was associated with the system moving off the mid-latitudes.

The temperature distribution also underwent complex changes as seen in the MTSAT data. As expected for a developing tropical cyclone with such baroclinic origin, the temperature distribution initially had the maximum warm anomaly in the lower troposphere centered over the storm. Under the influence of the mid-latitude circulations, the low-level warm anomaly first shifted to the east and north of the storm center. To examine the processes associated with

the southward extension of the baroclinic system, the detachment of the PV anomaly and the lower-level wind field is now examined.

The original hypothesis that Cosme was essential in the development of Usagi and this study was at first motivated by this hypothesis, the analysis shows that there is no vorticity connection between the two systems. there an area of subsidence between the baroclinic system and the remnants of Cosme on 0600 UTC 26 July when both are close proximity to each other ( $10^\circ$  apart). If indeed Cosme aided the formation of Usagi it may have been through another means rather than direct vorticity transfer between ex-hurricane Cosme and pre-Usagi. The analysis suggests that the Cosme wave may have played an important indirect role in the formation of Usagi by enlarging the wave pouch and helping protecting the proto-vortex from hostile outside influences. Further evaluation of this theory will be shown in the next section by comparing OW, relative humidity, and SF fields. This is confirmed using VIS-5D simulations (Figures 30-32). The VIS-5D illustrated that there is no vorticity or trajectory connection between the two systems. One method to further explore the direct influence of ex-Cosme would be to remove the Cosme circulation from the initial condition of a model and compare the predictions with and without Cosme circulation; however such an experiment is beyond the scope of this study.

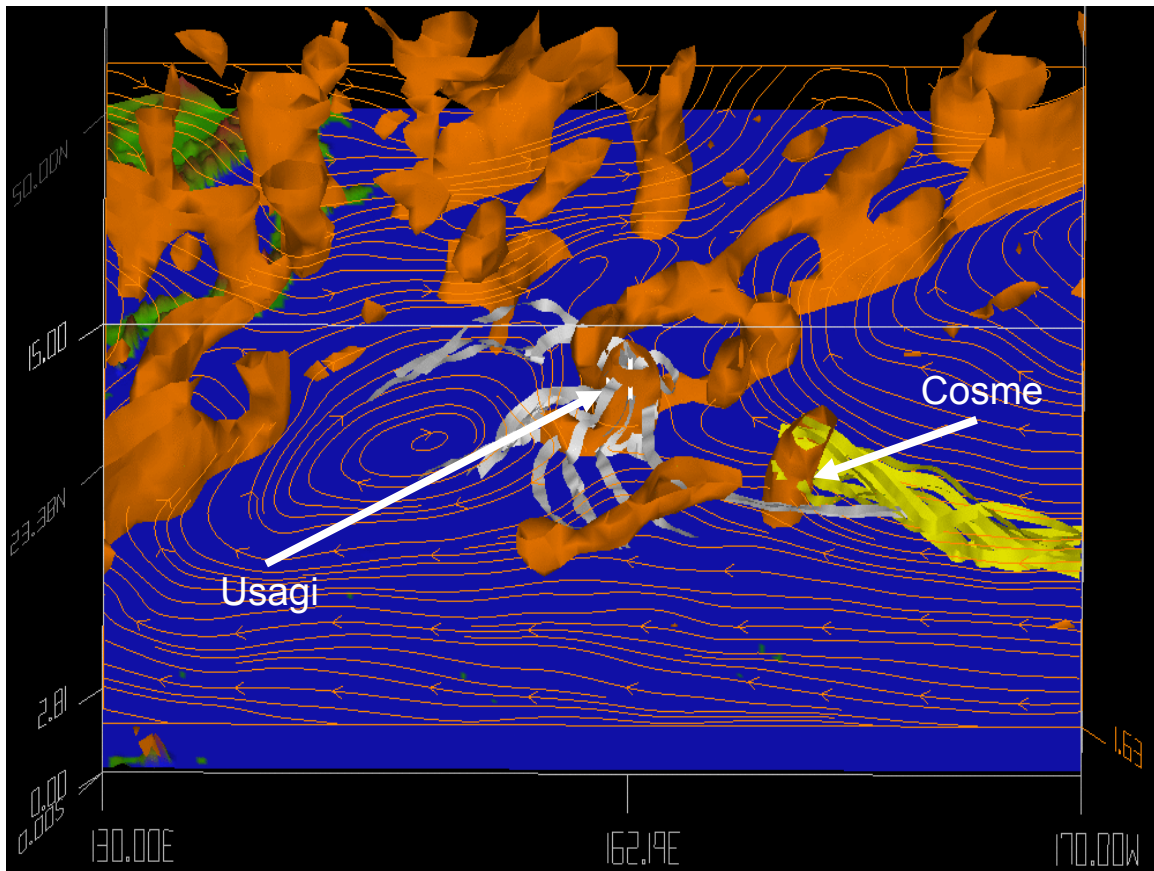


Figure 30. Vis5D trajectories between Usagi and Cosme during 0600 UTC 26 July. Streamlines are 850 hPa. The orange figures are absolute vorticity ( $10^{-4} \text{S}^{-1}$ ). The white strips are trajectories with Usagi and the yellow are trajectories associated with Cosme from the last 72 hours.

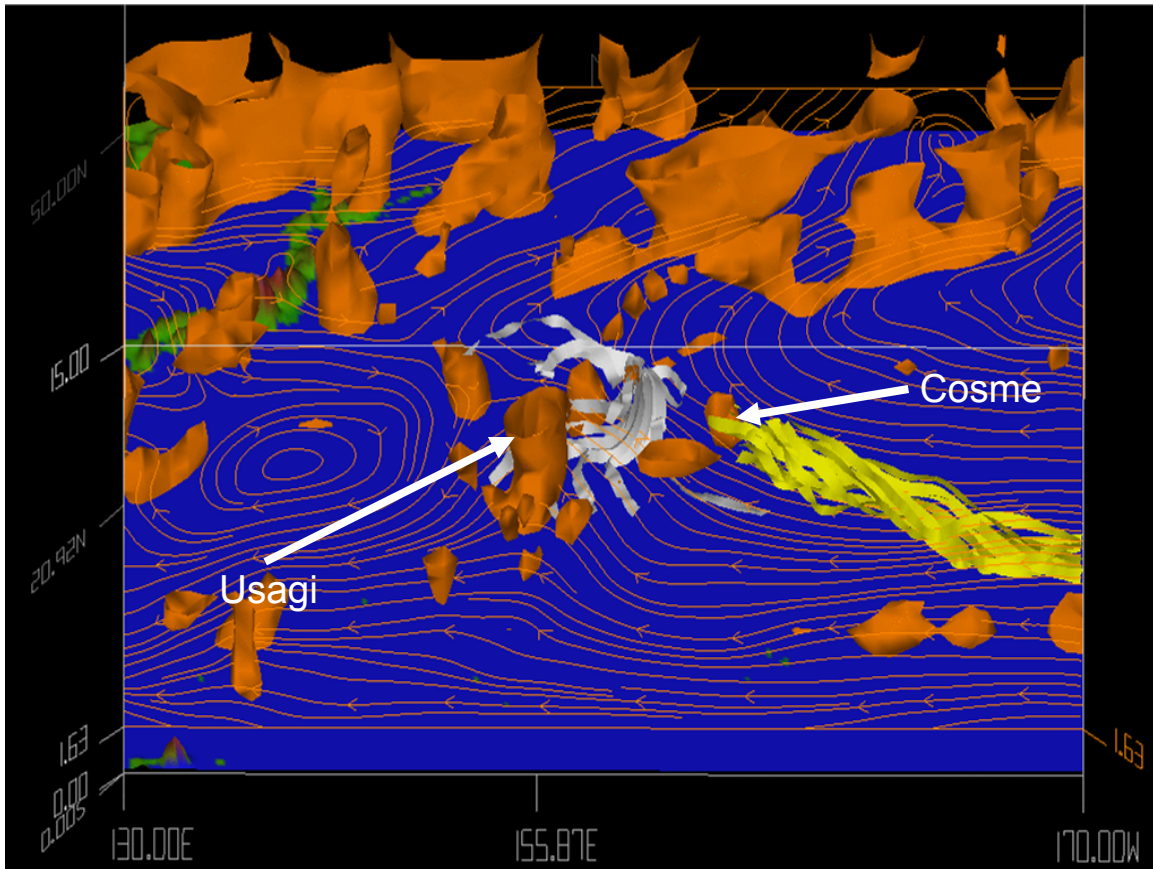


Figure 31. Vis5D trajectories between Usagi and Cosme during 1200 UTC 27 July. Streamlines are 850 hPa. The orange figures are absolute vorticity ( $10^{-4} \text{S}^{-1}$ ). The white strips are trajectories with Usagi and the yellow are trajectories associated with Cosme from the last 72 hours.

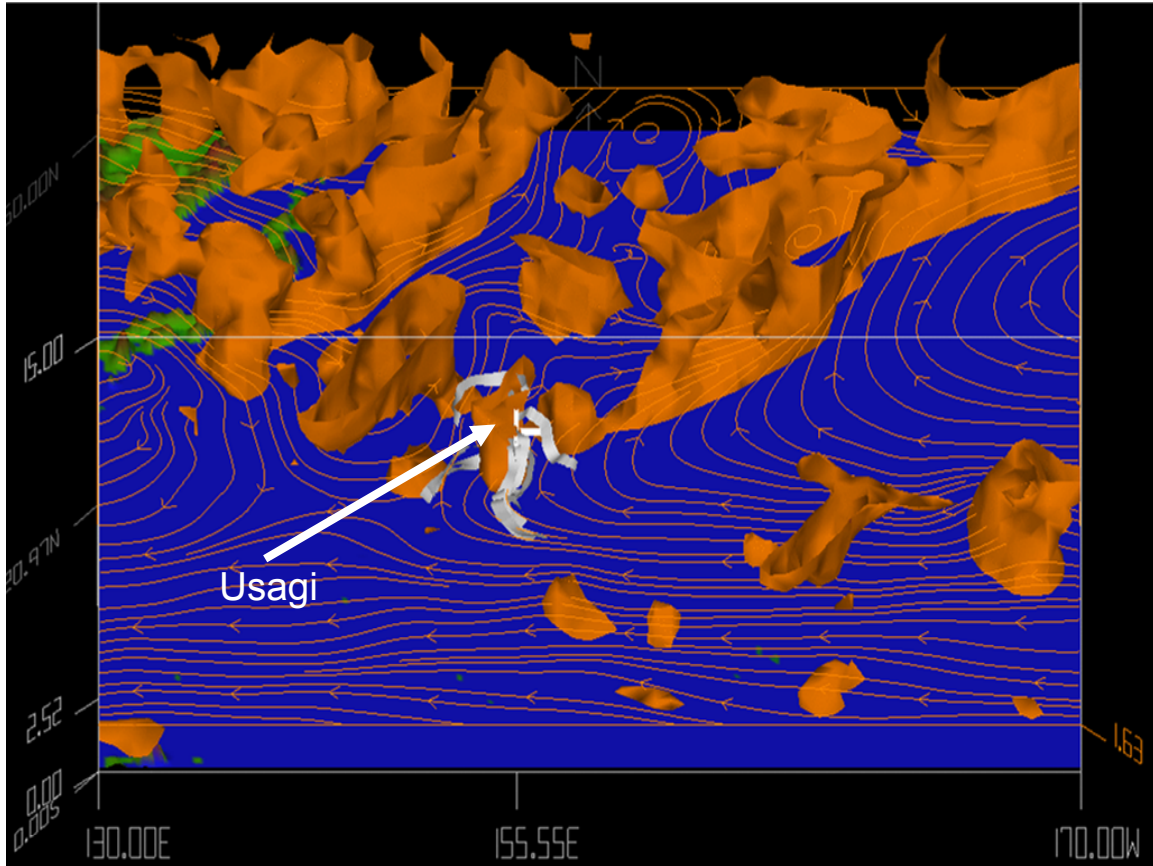


Figure 32. Vis5D trajectories of Usagi during 1800 UTC 28 July. Streamlines are 850 hPa. The orange figures are absolute vorticity ( $10^{-4}\text{S}^{-1}$ ). The white strips are trajectories with Usagi and the yellow are trajectories associated with Cosme from the last 72 hours.

### C. OW CRITERION AND SF PARAMETERS TO DISTINGUISH THE NON DEVELOPER (GYRE) AND DEVELOPER (USAGI)

In Chapter I, the relative vorticity and OW criterion are discussed as they are used to distinguish curvature vorticity from shear vorticity. The large positive value of OW parameter suggests regions where curvature vorticity is dominant. The moving frame of reference is optimal to display the Lagrangian flow and the evolution of the storm vortex. Isolating these parameters, you can see true Lagrangian parcel motions that are affecting the dynamics and thermodynamics of the transformation process in the ground based frame of reference. Here, we use the criterion based on the OW parameter to extract the vortex statistics from the full vorticity field.

This section will test the hypothesis that the tip of the PV streamer, which is dominated by curvature vorticity, is the key factor leading to the TC formation. Strong vorticity may be sufficient to initiate deep convection, which will then in turn enhance the low-level vorticity and moisten the middle level.

The distributions of vertical motion (PV) and moist air (SF) suggest that the relationship of the thermodynamics along the tip of the decaying baroclinic system contributes to a mid-troposphere moist anomaly that will be confirmed by TRMM data. The relative humidity SF parameter steadily increases (in percent) beginning at 1200 UTC 25 July and reaches its strongest value (most moist) at 0000 UTC 27 July.

The dynamic and thermodynamic processes discussed in Chapter III.B are compared with the relative vorticity, OW, and SF findings, respectively, and appear to be important precursors associated with the SI the non-developer and Usagi. The dynamic and thermodynamic forcing of these parameters evidence noticeable changes in the middle and lower-troposphere are noticeable in changes in OW, SF and PV anomaly magnitude.

### **1. OW Parameter Comparison**

By comparing the two disturbances, using previous finding from PV, relative vorticity and OW values, the following interesting features distinguished the non-developer from the developer.

The PV streamer within the baroclinic system has a positive value of OW at its tip, which suggests that vorticity is dominant in that area. This became detached from the PV streamer and subsequently formed the non-developer and Usagi (Figures 33 and 34). At 1800 UTC 23 July, the initial system detaches from the decaying baroclinic system as anticyclone spins along behind the system and stretches the convection. This persistent convection starts to interact with an existing trough axis behind the baroclinic system. This area of convection will become persistent as it moves thru a region favorable for TC

formation. However, as the persistent area of convection detaches from the main baroclinic region, a mid to upper-level trough behind the anticyclone begins to develop (Figure 33). This feature would soon shear and damp the convection all the way thru the life cycle of this initial system. Unfortunately, as the persistent convection of the initial system moves farther away from the baroclinic source region, the anticyclone never aligns above the initial system as the impeding trough axis damps the cyclogenesis process. Thus, this initial system never develops. There is significant increase in moisture as the two system combines and move farther south into an area of higher SSTs (not shown), high ocean heat content (not shown), and little to no wind shear (not shown). However, with the necessary and ideal component for deep convection, this initial system never develops into a tropical cyclone.

In contrast with the non-developing system, the Usagi case exhibits a different scenario. As the Usagi persistent area of convection detaches the main baroclinic source region, the PV streamers within the baroclinic system is as strong as the initial system and has a positive value of OW at its tip, which suggests that vorticity again is dominant in that area as can be seen in the four-panel evolution of Usagi (Figure 34). As it moves towards southeast, an area favorable for deep convection, the baroclinic system is already stronger near surface and the approaching remnants of wave Cosme is stronger at 600 and 850 hPa. During 1200 UTC 27 July, at 600 and 850 hPa (Figures 34 and 36) in the frame of reference moving with the baroclinic system, a big pouch formed as Cosme approached the baroclinic system and two sub-gyres (Usagi and Cosme) formed within the mother pouch. The one in the west (Usagi), which is directly related to the baroclinic system later became TD 5W on 1200 UTC 28 July. Although the baroclinic system is stronger near the surface at 850 hPa, there was no closed circulation in the moving frame of reference until 6 hours before genesis at 1200 UTC 27 July as can be seen at 600 hPa.

By comparing the non-developer (gyre) and developer (Usagi) based on the four panel 600 and 850 hPa OW and relative vorticity analysis (Figure 33-40),

the non-developer has almost the same values of vorticity compared to the developer. However, the non-developer encountered environmental limitations such as a mid to upper-level trough axis interaction and lack of protection from outside elements that eventually limit the internal mechanisms for deep convection, allowing for strong dry air entrainment that inhibits cyclone development.. These processes inhibits deep convection needed for TC formation, thus the initial invest region never develops. Whereas, the Usagi system had environmental protection in the critical level needed for deep convection persistent enough for TC formation as it moves to a favorable region of cyclogenesis. As introduced in Chapter I, the marsupial paradigm discusses the proto-vortex cyclonic eddies instrumental in TC formation are intimately associated with parent wave's critical latitude in the lower-troposphere. This structure forms a critical layer because of the wave's finite amplitude interaction with its own critical latitude, is a region of cyclonic rotation and weak strain/shearing deformation in which synoptic and mesoscale anomalies move together and amplify on a nearly zero relative mean flow. This multi-scale interaction provides dynamically pathway to bottom-up development of the proto vortex from below. The critical layer of the parent wave provides a set of closed material contours inside of which air is repeatedly moistened by convection. The wave is protected to some degree from lateral intrusion of dry air impinging vertical shear, and able to keep in pace with the parent wave until the proto-vortex has strengthened into a self-maintaining entity and begins control its own destiny. By correlating the marsupial analogy for TC formation in this study, we can verify in theory that the remnants of Cosme acted as a protective proto vortex associated with the parent's wave (Usagi) critical latitude at 600 hPa as can be clearly seen on Figure 34 panel 2 as a closed streamline of protected area.

The findings above would be consistent with the hypothesis that Cosme may not be essential in the development of Usagi, but have just probably widened the area of the “pouch” of vorticity anomalies. This anomaly can be

seen at 600 hPa on 1200 UTC 27 July (Figure 34 panel 2). This area of strong vorticity at the tip of the PV streamer favors deep convection, which will enhance the low-level vorticity and moisten the mid level, while the Cosme wave enlarges the wave pouch and helps to preserve moisture in the middle level of Usagi convection. In this sense, the Cosme wave played an important role although it did not directly interact with the baroclinic system.

The relative vorticity Hovmöller diagram as seen on Figure 41 suggest a consistent vorticity motion of  $-7 \text{ ms}^{-1}$  from 1000 thru 500 hPa. This is consistent that vorticity is all the way down in the low-levels. The Usagi storm propagation is nearly parallel to the trough propagation.

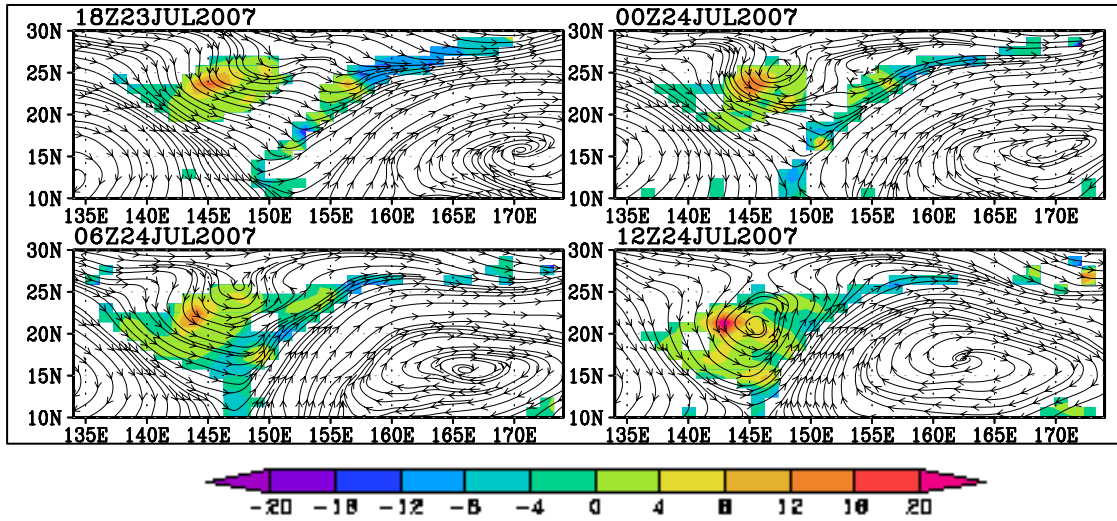


Figure 33. Streamlines of horizontal flow at 600 hPa for the genesis sequence of the non-developer from 1800 UTC 23 July to 1200 UTC 24 July. The shadings indicate high values of OW parameter (units:  $10^{-10} \text{ s}^{-2}$ ) as defined in Eq. (1.1). This quantity, like vorticity, is invariant with respect to translation, therefore identical in translating and moving frames. Red areas are strong values and blue values areas are weak.

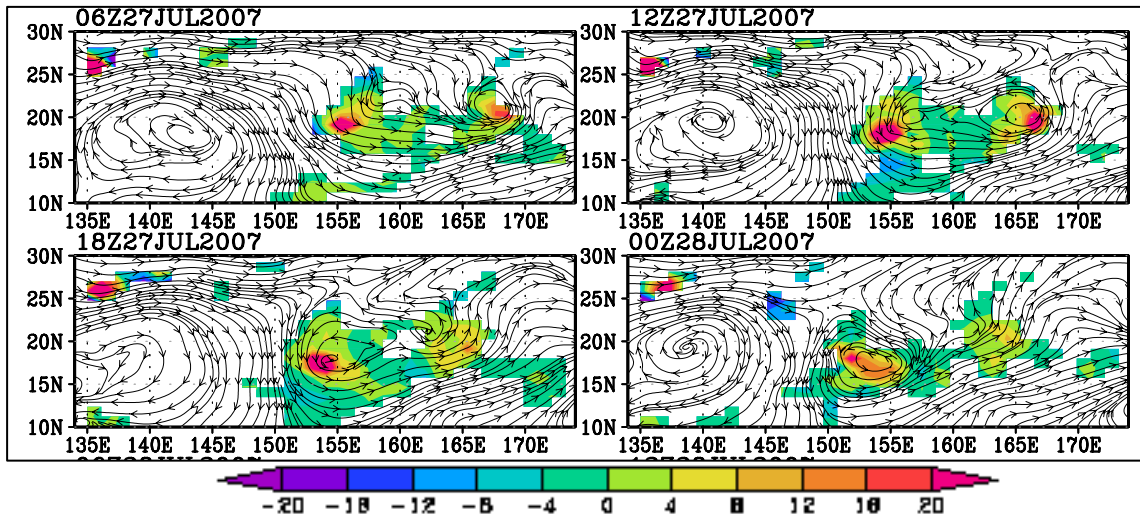


Figure 34. Streamlines of horizontal flow at 600 hPa for the genesis sequence of the Usagi system from 0600 UTC 27 July to 0000 UTC 28 July. The shadings indicate high values of OW parameter (units:  $10^{-10} \text{ s}^{-2}$ ) as defined in Eq. (1.1). This quantity, like vorticity, is invariant with respect to translation, therefore identical in translating and moving frames. Red areas are strong values and blue values areas are weak.

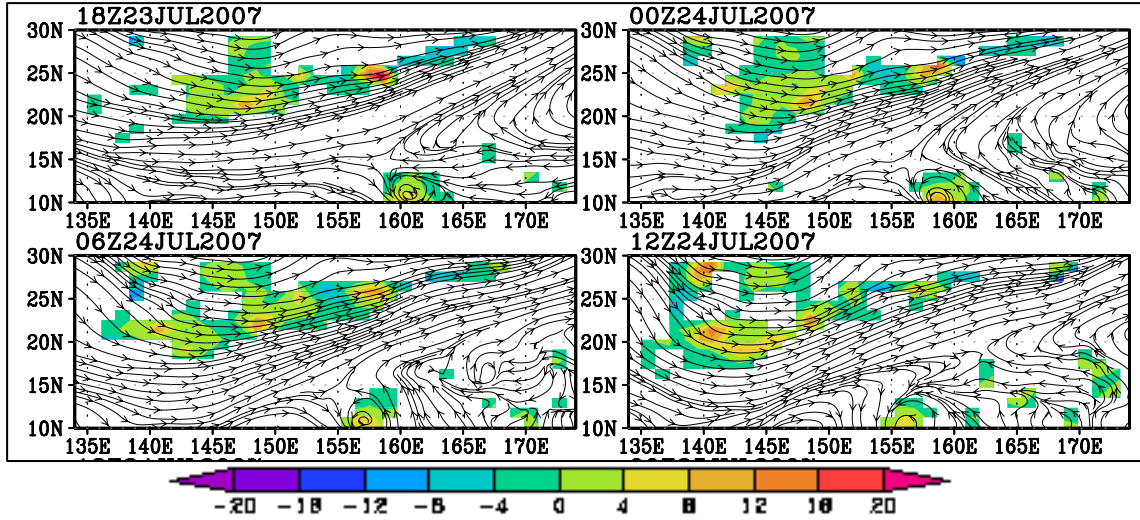


Figure 35. Streamlines of horizontal flow at 850 hPa for the genesis sequence of the non-developer from 1800 UTC 23 July to 1200 UTC 24 July. The shadings indicate high values of OW parameter (units:  $10^{-10} \text{ s}^{-2}$ ) as defined in Eq. (1.1). This quantity, like vorticity, is invariant with respect to translation, therefore identical in translating and moving frames. Red areas are strong values and blue values areas are weak.

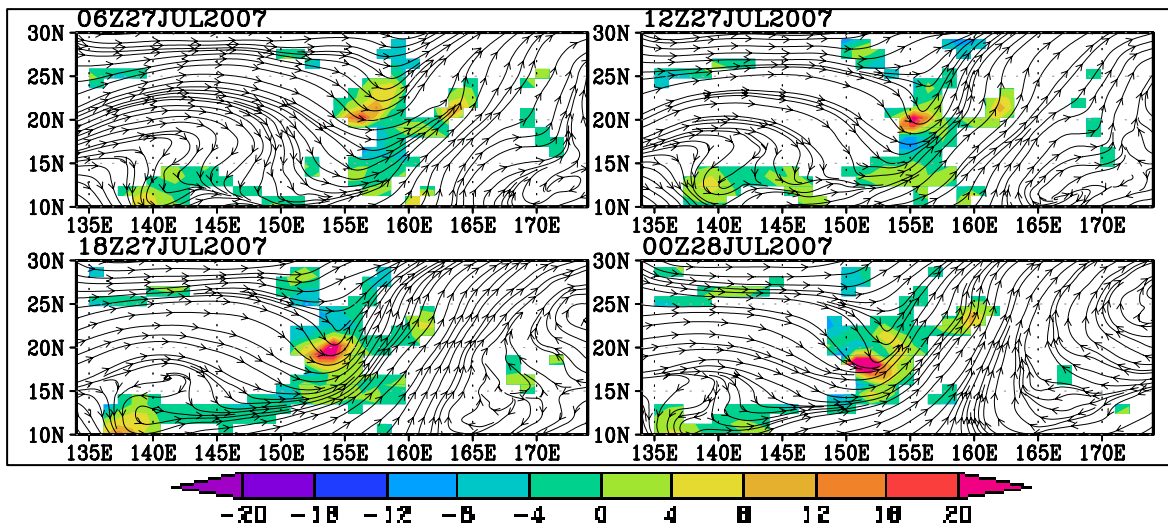


Figure 36. Streamlines of horizontal flow at 850 hPa for the genesis sequence of the Usagi system from 0600 UTC 27 July to 0000 UTC 28 July. The shadings indicate high values of OW parameter (units:  $10^{-10} \text{ s}^{-2}$ ) as defined in Eq. (1.1). This quantity, like vorticity, is invariant with respect to translation, therefore identical in translating and moving frames. Red areas are strong values and blue values areas are weak.

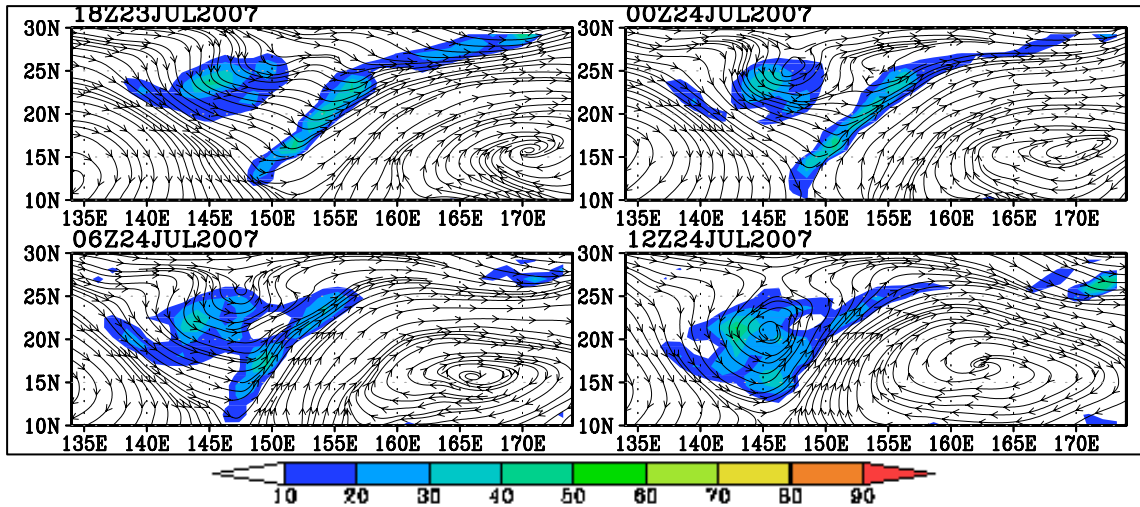


Figure 37. Streamlines of horizontal (rotational + divergent) flow and Zeta at 600 hPa of the non-developer from 1800 UTC 23 July to 1200 UTC 24 July. Shading indicates relative vorticity (units:  $10^{-5} \text{ s}^{-2}$ ).

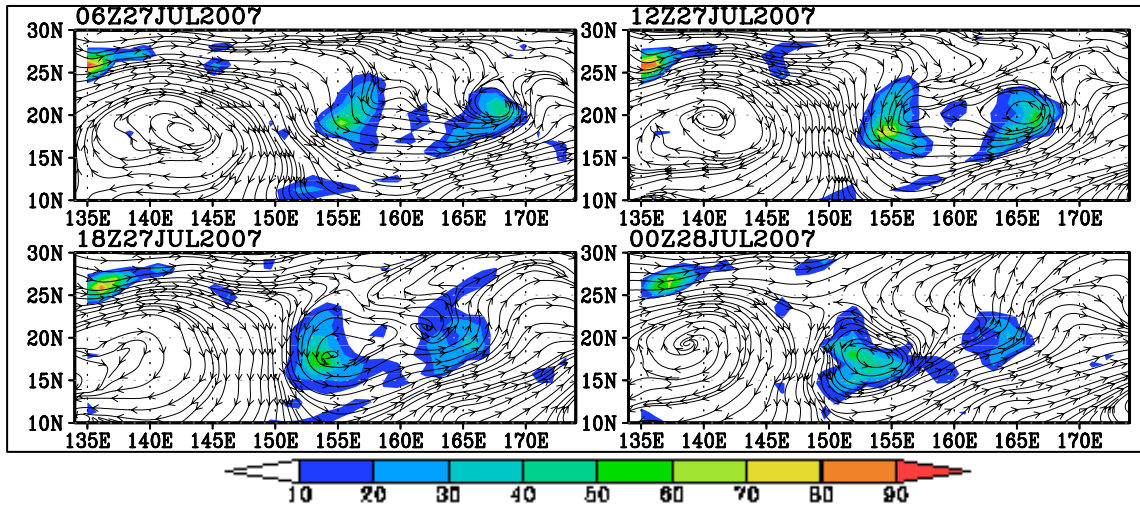


Figure 38. Streamlines of horizontal (rotational + divergent) flow and Zeta at 600 hPa of the Usagi system from 0600 UTC 27 July to 0000 UTC 27 July. Shading indicates relative vorticity (units:  $10^{-5} \text{ s}^{-2}$ ).

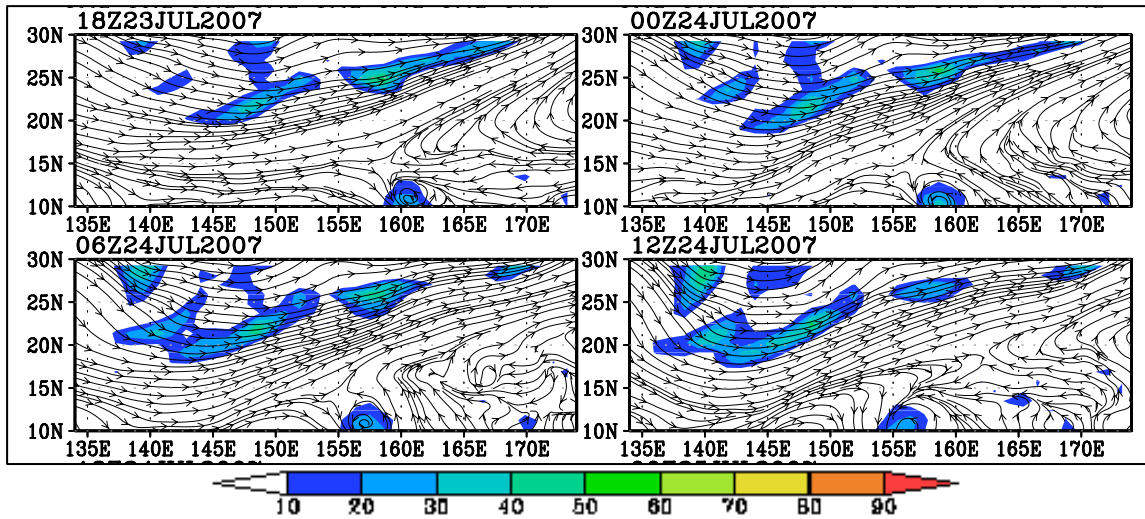


Figure 39. Streamlines of horizontal (rotational+divergent) flow and Zeta at 850 hPa of the non-developer from 1800 UTC 23 July to 1200 UTC 24 July. Shading indicates relative vorticity (units:  $10^{-5} \text{ s}^{-2}$ ).

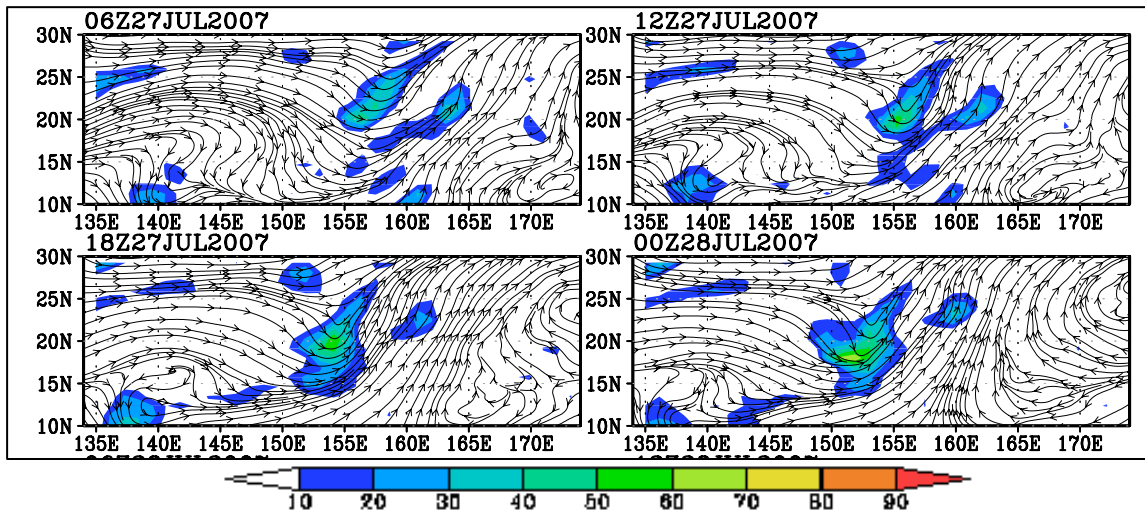


Figure 40. Streamlines of horizontal (rotational+divergent) flow and Zeta at 850 hPa of the Usagi System from 0600 UTC 27 July to 0000 UTC 28 July. Shading indicates relative vorticity (units:  $10^{-5} \text{ s}^{-2}$ ).

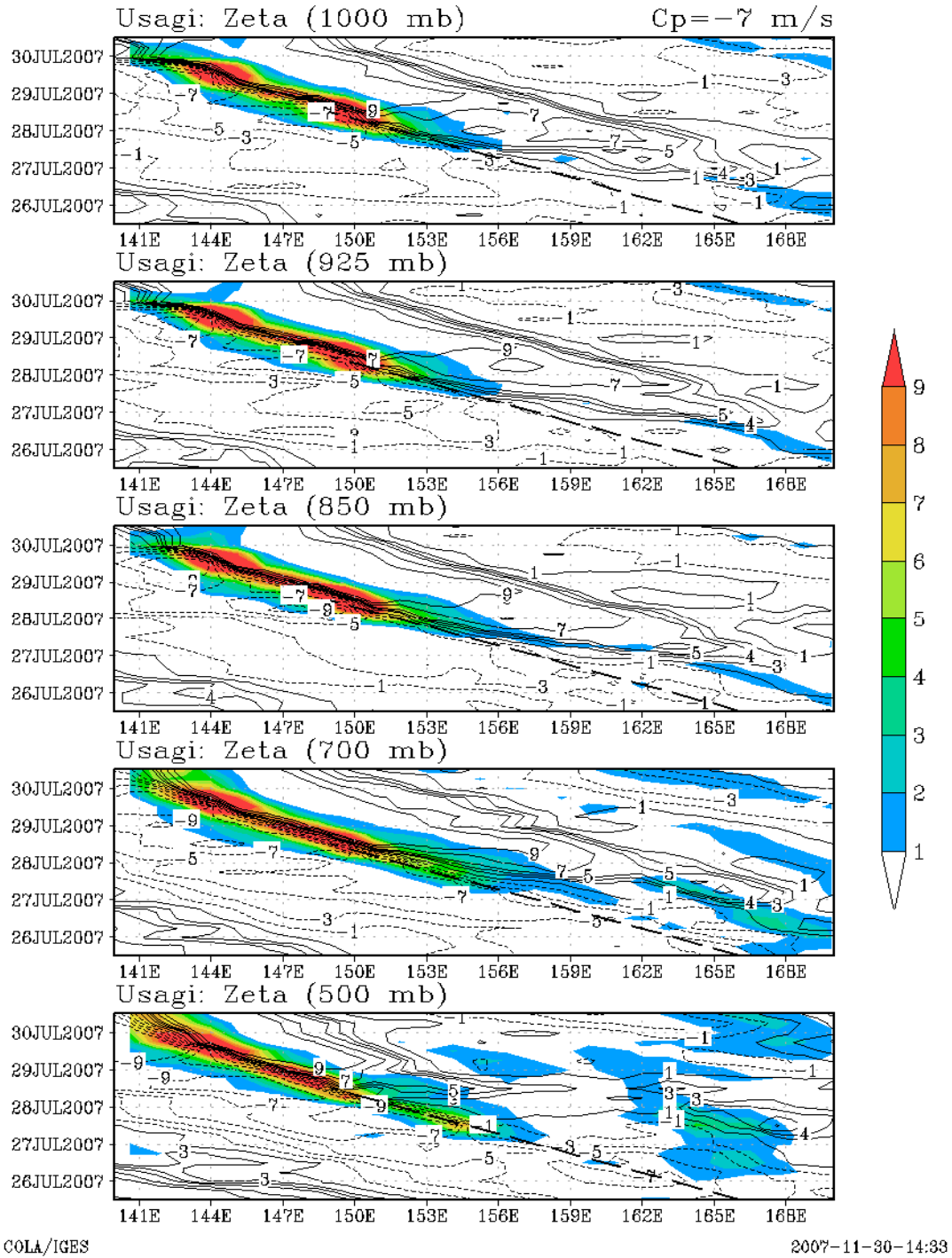


Figure 41. Relative vorticity Hovmöller diagram 3 days before development of Usagi from 26 -30 July.

## **2. SF Comparison**

The time evolution of SF and RH at 600 hPa (Figure 42 and 43 in the moving frame of reference of the baroclinic system) was examined and the two disturbances, the non-developer and developer were compared. As mentioned in Chapter 1, the SF of the lower troposphere, defined as the ratio of precipitable water to saturated precipitable water.

By comparing the two disturbances using SF values, the non-developer over the developer, it is suggested that the non-developer had less precipitable water (lower SF) than the developer (Usagi). As discussed in the previous section, the non-developer also became detached from the source baroclinic system, it undergoes fluctuations as it gets under the influence of a mid-level trough (can be seen on Figure 42 as an area of lower SF values west of the non-developing system) as it moves southeastward through the lower latitudes. The non-developer is moving to an area of low vertical wind shear that is ideal for deep convection and moves into an area that is a favorable environment for cyclogenesis area of deep convection. In comparison, using the precipitation distribution it is evident that the TRMM distribution (Figures 44 and 45) is consistent with SF analysis. The low SF values eventually limit the mechanism for deep convection, allows strong dry air entrainment that slows cyclone development to weaken, and then the system becomes disorganized (Elsberry 2007).

In contrast with the non-developer, major changes in the thermodynamic structures of the developer (Usagi) began at 1200 UTC 26 July due to the influence of the low-level anticyclone to the west and the high distributions of temperature (SST), moisture (SF), and large values of OW. The maximum OW anomaly and SF parameters in the 600-hPa is consistent with the TRMM that occurs in a round-shaped region over the northern half of the circulation with a maximum to the west of the storm center (SF compared to TRMM four panel). The upward vertical motion seen as vorticity (OW) to the storm center coincides

with a broad, low-level PV anomaly seen in the entire PV figure in the past section. A relative moist anomaly occurs to the storm center at 600 hPa is consistent with the SF values (Figure 42 and 43). The SF evolution and translating streamlines in the development of Usagi is shown in Figure 43 at 600 hPa. The closed streamlines of directional flow are formed near the trough axis, delineating a recirculating gyre of finite width. Strong cyclonic/rotational vorticity, high SF and weak vertical wind shear simultaneously coincide within the gyre and provide a favorable sub-synoptic scale environment for TS formation. The vertical signature of the Cosme wave and diabatic vortex prior to Usagi formation is clearly consistent with TRMM data suggesting that convective activity is present near the critical latitude 24 hours prior official TD 5W (Usagi) formation in 1200 UTC 28 July (JTWC 2007). Near the critical latitude, the convective activity near pre-Usagi becomes sustained and more focused, while the Cosme wave moves northeastward away from the critical latitude and dies out, consistent with the conclusions of DMW08.

Compared to the non-developing intrusion, the stronger Usagi has consistently high values of SF as it detaches from the baroclinic system, approaches the remnants of Cosme, and protrudes into the lower latitudes. The pre-Usagi system is stronger near the surface. The Cosme wave has become less moist (<50%) as it gets near with Usagi by 0600 UTC 27 July (Figure 43 Panel 2). However, at 600 hPa in the frame of reference moving with the baroclinic system, a pouch formed as Cosme approached the baroclinic system and two sub-gyres formed within the parent pouch. This area of high SF values favors deep convection, which will enhance the low-level vorticity and moisten the mid level, while the Cosme wave appears to enlarge the wave pouch and helps moisten the middle levels. In this sense, again a hypothesis, Cosme wave played an important role although it did not directly interact with the baroclinic system. The convective activity that is Usagi becomes sustained and more focused, while the Cosme wave moves northeastward away from the critical latitude and dies out.

The Usagi system formed in relatively moist, precipitating environment with large values of vorticity as seen with the PV and OW parameter. This is true for a gyre and local averages alike, but the local average contains some exceptionally large values of precipitation and OW parameter, suggesting that the TRMM satellite has observed enhanced precipitation associated with the developing storm, concentrated at the best track location rather than distributed around the gyre. The ECMWF analysis have generally pinpointed the location of the developing vortex within the gyre (Figure 42 Panel 2) and identified its vorticity as predominantly rotational rather deformational, i.e. not deformed by strain or shear. The persistence of precipitation defined in TRMM imagery preceding formation is evident. The formation of closed streamlines implies that air with the closed space is protected, to some degree, from lateral entrainment of dry air. This containment is important in allowing a convective type of heating profile to dominate the closed region with relatively smaller contributions from stratiform precipitation that are otherwise common in mesoscale convective systems (Tory and Montgomery, 2006).

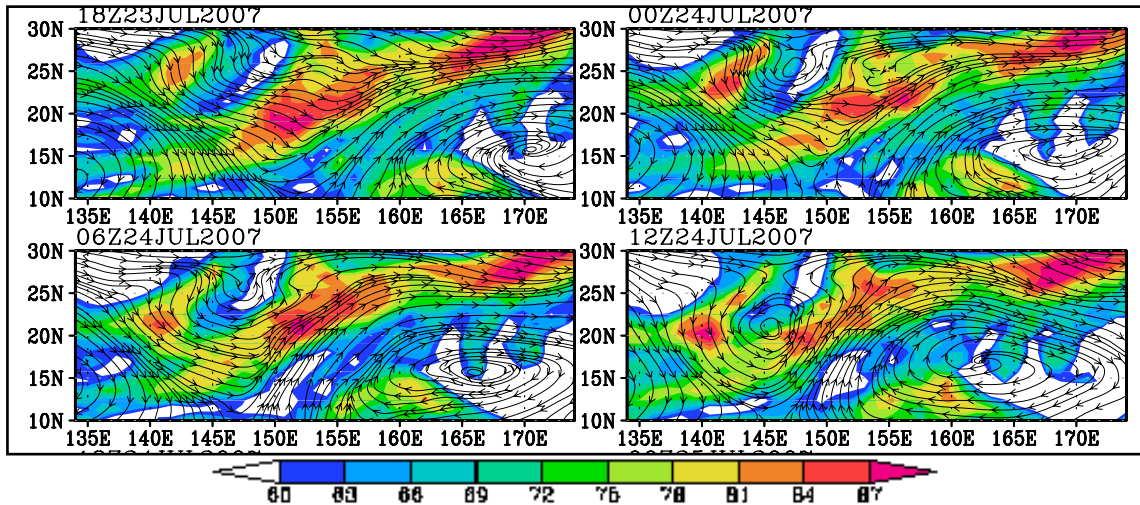


Figure 42. Streamlines of horizontal flow 600 hPa for the genesis sequence of the non-developer, with high values of saturation fraction from 1800 UTC 23 July to 1200 UTC 24 July. Red areas are strong values and white areas are weak values of SF.

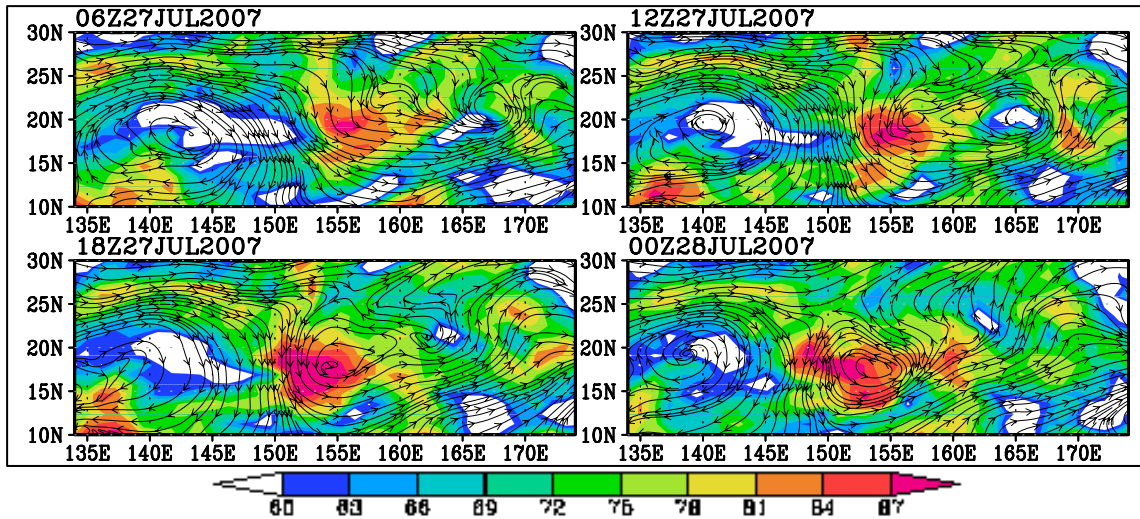


Figure 43. Streamlines of horizontal flow 600 hPa for the genesis sequence of the Usagi system, with high values of saturation fraction from 0600 UTC 27 July to 0000 UTC 28 July. Red areas are strong values and white areas are weak values of SF.

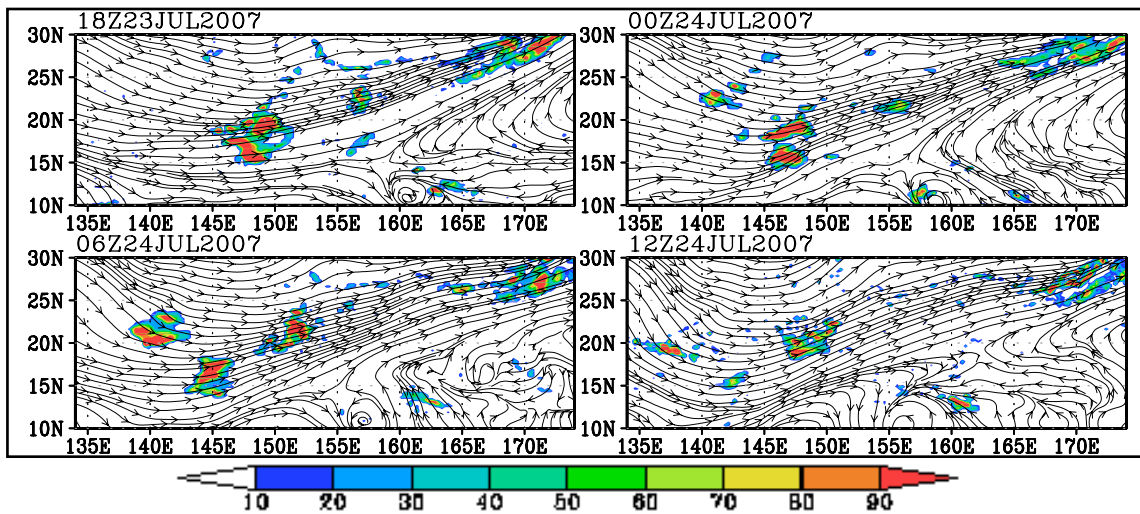


Figure 44. Streamlines of horizontal flow 850 hPa for the genesis sequence of the non-developer, with high values of TRMM 3-hour accumulated precipitation indicated by shading from 1800 UTC 23 July to 1200 UTC 24 July. Red areas are strong values and white areas are weak values of precipitation.

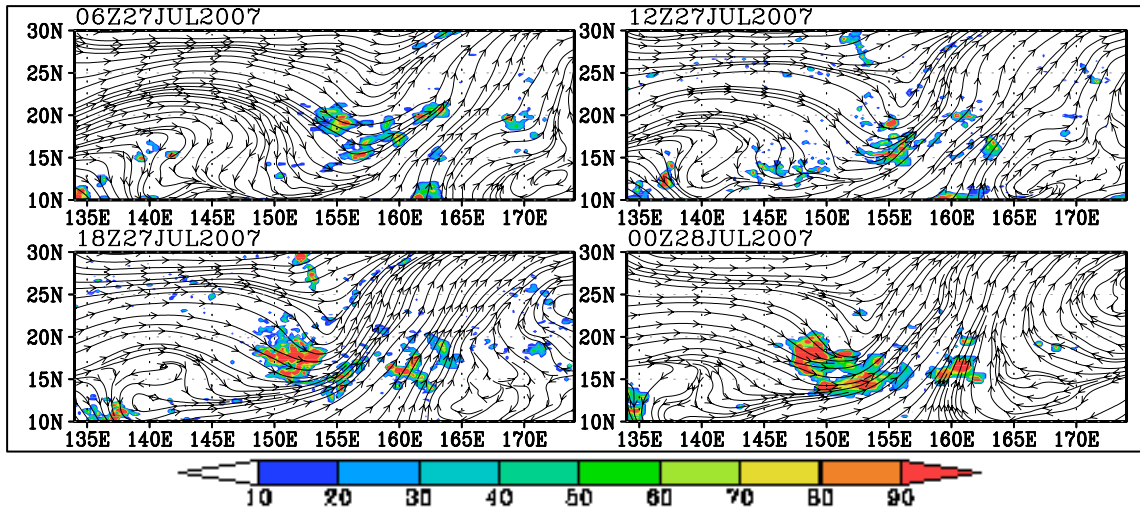


Figure 45. Streamlines of horizontal flow 850 hPa for the genesis sequence of the Usagi system, with high values of TRMM 3-hour accumulated precipitation indicated by shading from 0600 UTC 27 July to 0000 UTC 28 July. Red areas are strong values and white areas are weak values of precipitation.

### 3. Time Series Analysis

Time series analysis was constructed to show the relationship between the two systems. This experiment will be used to summarize the relationships between saturation fraction distribution area averages. The RH values at 700 hPa were averaged at each synoptic time from 0000 UTC 22 July until 1200 UTC 25 July in a 10 deg. lat. by 10 deg region centered eight deg. lat. of the storm for the non-developer and from 0000 UTC 26 July until 0000 UTC 29 July for Usagi. The selection of this region allowed the detection of the parameters as the storm progressed southwestward. By using GARP MTSAT overlay and Vis5D absolute vorticity parameters, the convection calculation is as follows:.

$$\text{Average RH} = (\text{RH max} + \text{RH min})/2$$

The saturation fraction (RH) was averaged over a moving frame between 15°-30°N and from 140°-165°E, which was the region directly on track of Usagi and the non-developer. For the Cosme wave, the SF is almost less than 60% as it interacts with the baroclinic system on 1200 UTC 27 Jul (not shown). The

Usagi case on the other hand has constant high values of SF at more than 85% all throughout formation time compared to Cosme and the non-developer (Figure 46 and 47).

The convective available potential energy (CAPE) time-series values associated with the non-developer and Usagi were calculated over the same time and moving frame of reference with the RH, which was the region directly on track of the persistent area of convection. By comparison, the non-developer has increasing values up to 2300 J/Kg then suddenly decreased while the Usagi case had increasing values up to 2700 J/Kg (Figure 48-49). A more complete estimate of buoyant energy can be computed by determining the temperature difference between the ascent path and the environment at all levels from the level of free convection up through the equilibrium level. This area provides a measure of the integrated effects of the potential temperature differences between the rising parcel and its environment. The quantitative measure of this positive area is CAPE. CAPE is measured in units of joules per kilogram (J/kg). This layer represents the average heat and moisture conditions fueling deep convection. The environmental CAPE ideal for deep convection and modulate convection is often in the range of 1000-2000 J/kg (METED, 2007).

Detailed time lines and figures of OW, Zeta, TRMM, and SF of the non-developer (Gyre) and developer (Usagi) are located in the Appendix.

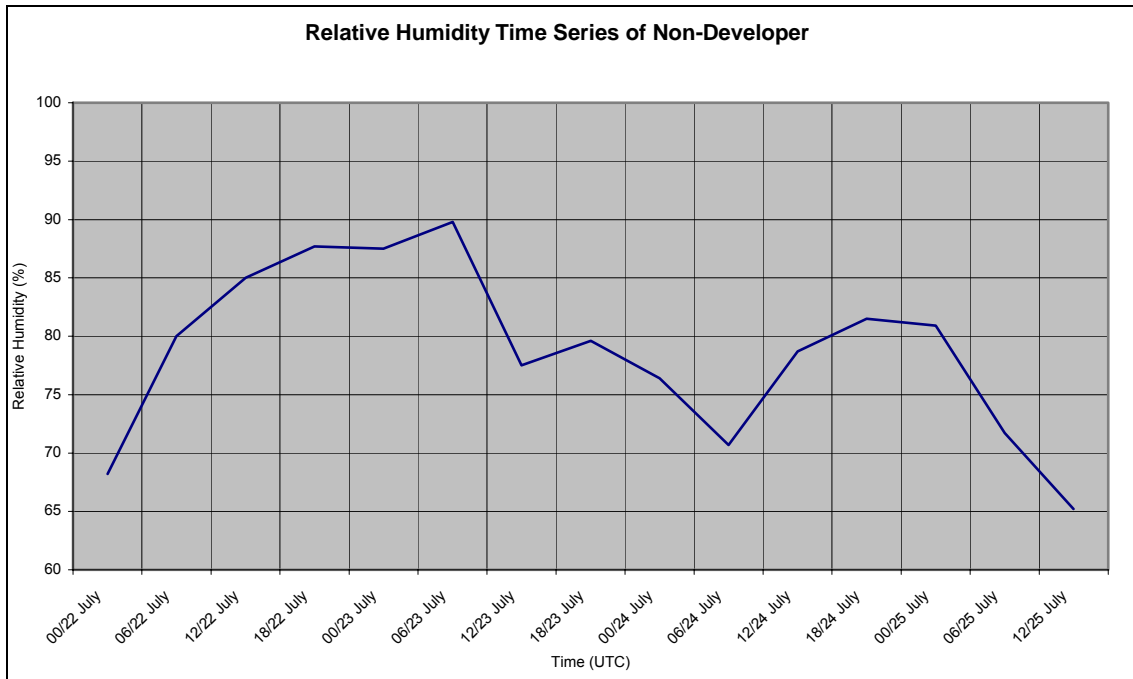


Figure 46. Relative humidity time series diagram of non-developer from 22 -25 July.

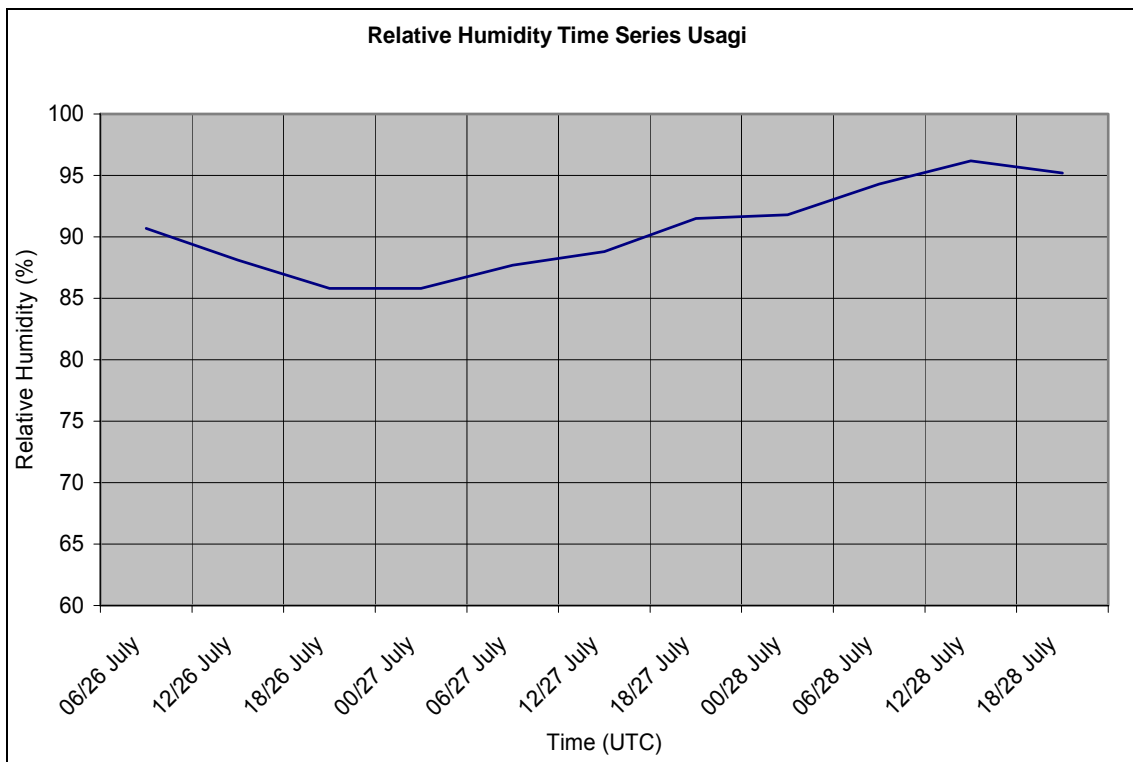


Figure 47. Relative humidity time series diagram of Usagi from 26 -28 July.

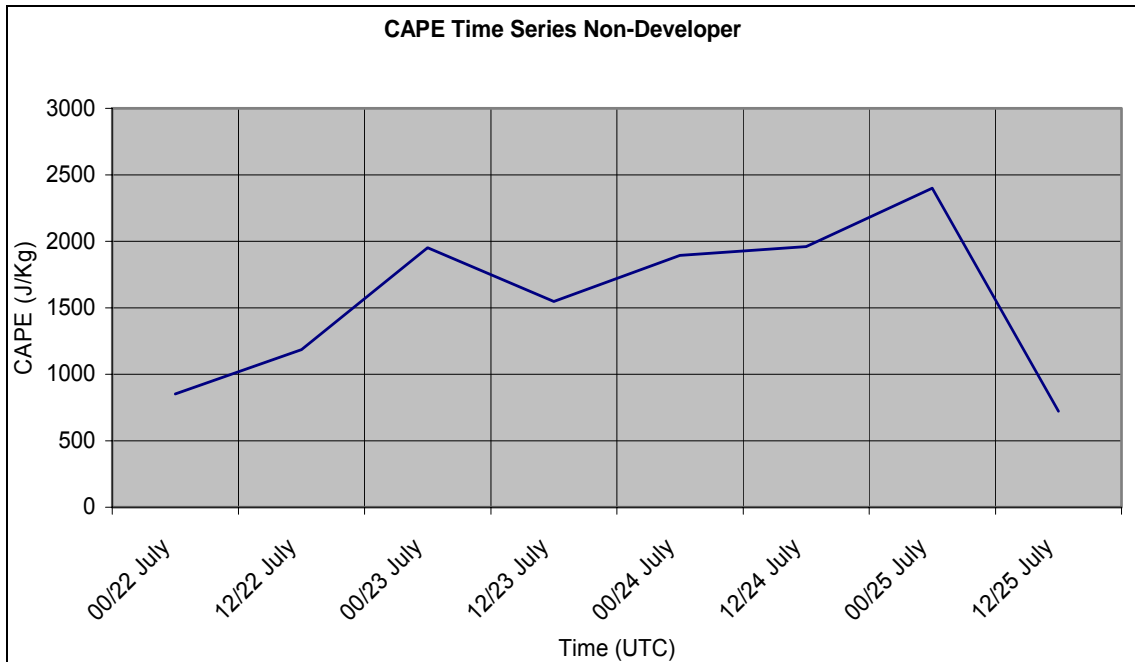


Figure 48. CAPE time series diagram of non-developer from 22 -25 July.

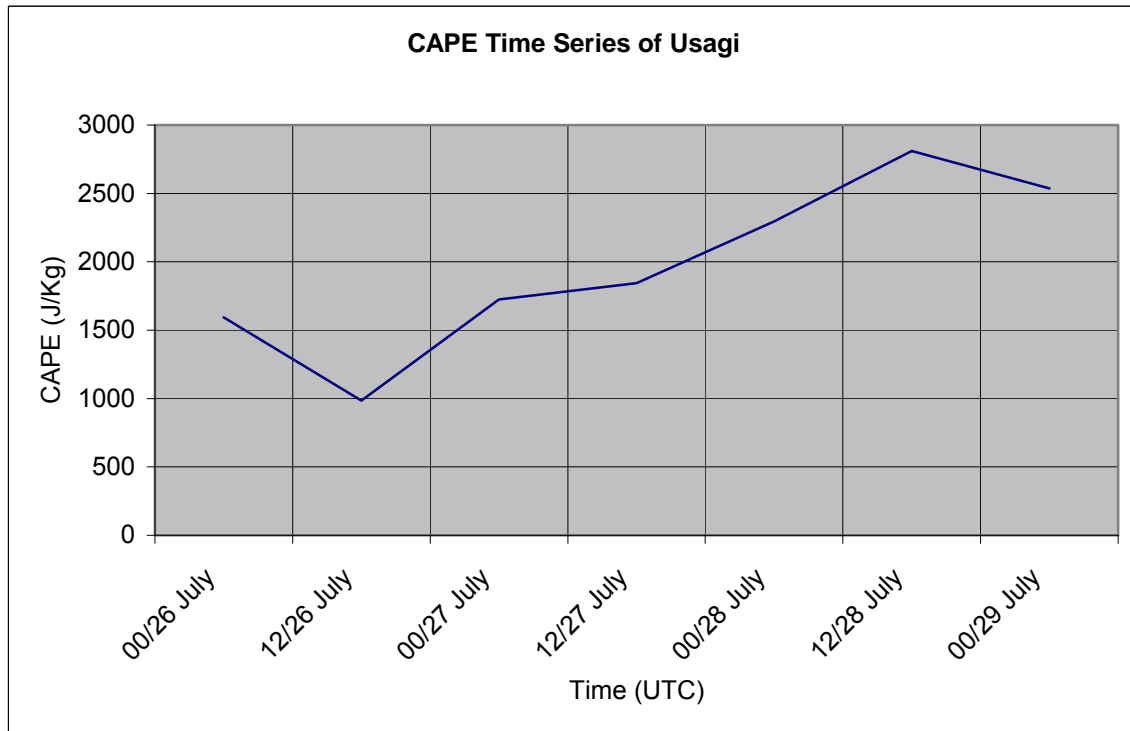


Figure 49. CAPE time series diagram of Usagi from 26 -29 July.

## **IV. SUMMARY AND RECOMMENDATION**

### **A. SUMMARY**

During July 2007, two distinct areas of disturbed weather with SIs emerged out of remnants of a decaying baroclinic system in the WNP. The initial invest system became detached but never developed and the second identified system eventually became Typhoon Usagi (5W). The decaying baroclinic system with a trailing cold front pushed through the WNP and the associated cyclogenesis occurred along the trailing edge of the cold front. (This was illustrated with the areas of concentrated 850 hPa PV and relative vorticity moving down the front.) The second persistent area of convection (Usagi) was already near the surface and was rather strong, so it did not take much to convert this cold core system into a tropical system given the fact it was moving south into warm SSTs, low vertical wind shear..

The keys to events that led to the non-development of the initial invest area and the developments of Usagi were investigated. Fields from the NCEP GFS final analyses and ECMWF model analysis of OW and SF each in 6-hour intervals suggested the development of two distinct areas of disturbed weather with sub-tropical cyclogenesis. The Vis5D was a valuable tool for visualizing both gridded data and irregularly located data. Sources for these data included numerical weather prediction models output, surface observations, and other similar sources. The high-resolution model analysis was used and we concluded that the events leading to the Usagi TC formation is not vortex merger and axisymmetrization of the ex-hurricane Cosme, as initially hypothesized.

By comparing the two sub-tropical intrusions, using regions where curvature vorticity is dominant (OW) and the ratio of precipitable water to saturated precipitable water (SF) is significantly above environmental values, it is found that the non-developer (gyre) has significantly less concentration and organization of OW and SF than the developing disturbance (Usagi). The non-

developer become detached from the source baroclinic system, and undergoes fluctuations as it interacts with a mid to upper-level pressure trough (an area of low SF values ( $< 50\%$ ) west of the non-developing system. In comparison to the Usagi system, the non-developer has less precipitable water and moves to lower latitudes due to environmental factors as it get detached and develops away from the source baroclinic system. The disorganized area of OW and low SF values are hypothesized to eventually limit the internal mechanisms for deep convection, allowing for strong dry air entrainment that inhibits cyclone development.

The Usagi system became detached from the baroclinic system and continued to move southwest between the two subtropical highs before finally moving west under the subtropical ridge and then northwest towards Japan. This system quickly strengthened as it approached the Mariana Islands, and the JTWC upgraded it to TS Usagi on 0000 UTC 29 July eventually becoming Typhoon Usagi 24 hours later. The JTWC advisories did not mention the possibility of SI from a decaying baroclinic system or the interaction with the remnants of Cosme. The first mention by JTWC of the seedling system was on 27 July as a system was already undergoing SI. We believe that the prediction of this tropical cyclogenesis could have been anticipated farther in advance, if forecasters had more knowledge on SIs in the WNP. This case study, along with future work on others in the WNP will lead to a better understanding of this challenging area of tropical cyclone forecasting.

The analysis suggest that the Usagi formation was the result of a SI from a strong baroclinic system in the mid-to-lower troposphere as it undergoes decay as it moved into an area of higher sea surface temperatures, weak low-level vertical wind shear, and persistent area of convection. As the PV anomalies were stretched and detached from the baroclinic source region, they were wrapped around a strong tropospheric anticyclone in the subtropics. This constitutes a different type of baroclinic initiation process than has been previously identified in Atlantic cyclone formation events associated with TT, which are induced by upper-level troughs.

The marsupial paradigm provides a convenient and self-consistent framework for the coupled dynamical/thermodynamical processes that are essential to tropical cyclogenesis. The study has highlighted the role curvature vorticity and moisture in the formation of Usagi through the analysis of the OW and SF parameters as done in DMW, 2008. We emphasized the formation of a closed gyre at the tip of the PV streamer from the baroclinic system, and confirmed that translated streamlines can be used as a good approximation of parcel trajectories to study the Lagrangian nature of the storm formation..

## **B. FURTHER STUDIES**

Further research is recommended on SI cases to better understand this type of tropical cyclone formation in the WNP, and thus contribute improved tropical cyclogenesis forecast.

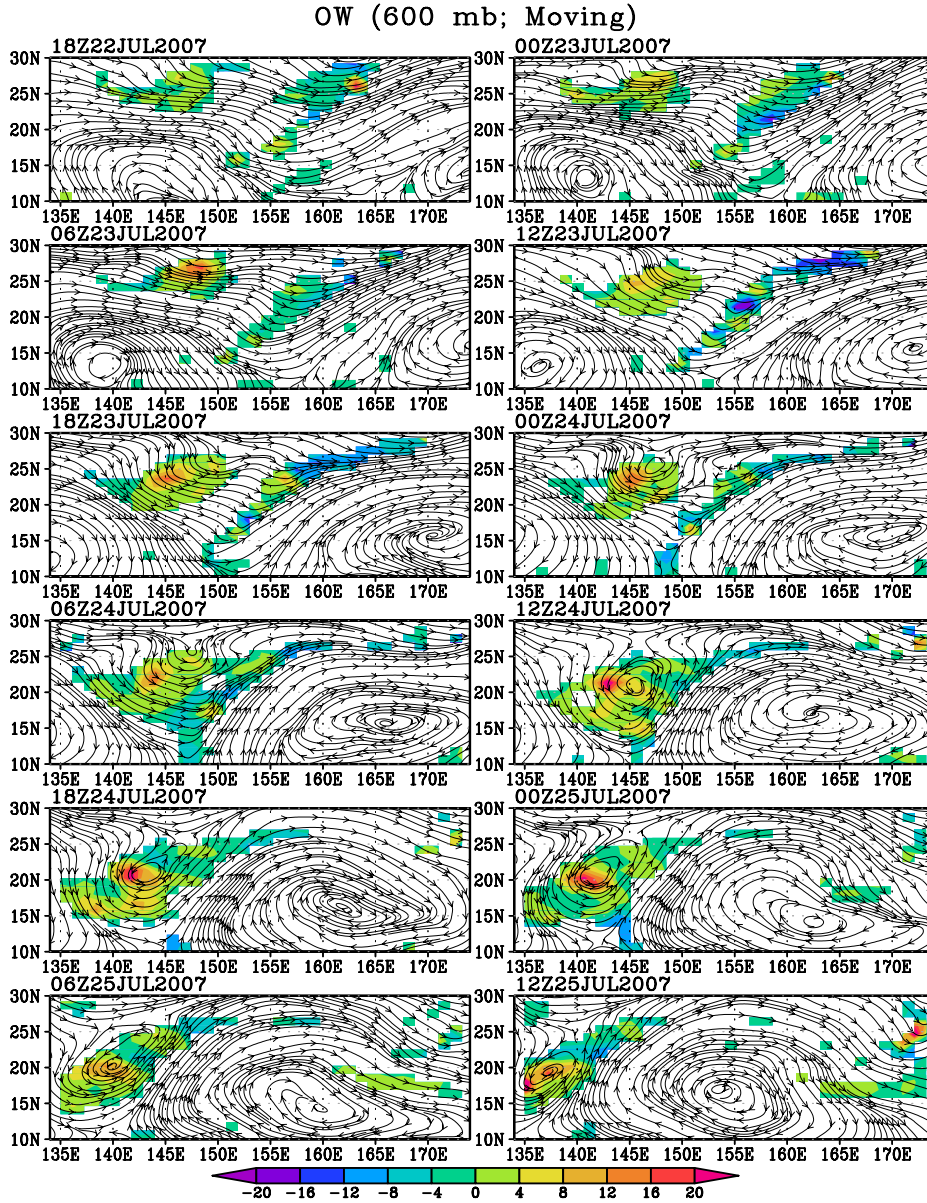
Future studies may include model studies that execute “vortex surgery” that remove Cosme and to examine whether or not Usagi would have eventually developed even in the absence of Cosme. This approach would allow a quantitative determination of the role of this circulation in the baroclinic system and the development of Usagi.

It is hoped that this study will aid Tropical Cyclone Structure’ 08 (TCS’08) and THORPEX (THE Observing system Research and Predictability EXperiment) Pacific-Asia Regional Campaign (PARC) in identifying the role of remnants of tropical cyclones in influencing the downstream flow. Do other storms completing SI like Usagi have similar anomaly patterns? Can these anomaly patterns be determined objectively and in a timely manner to be of use to the forecaster? These questions will be difficult to answer until a more robust data set is developed.

Further investigation and more qualitative documentation are desired to increase JTWC forecast capability and such synoptic patterns or anomalies

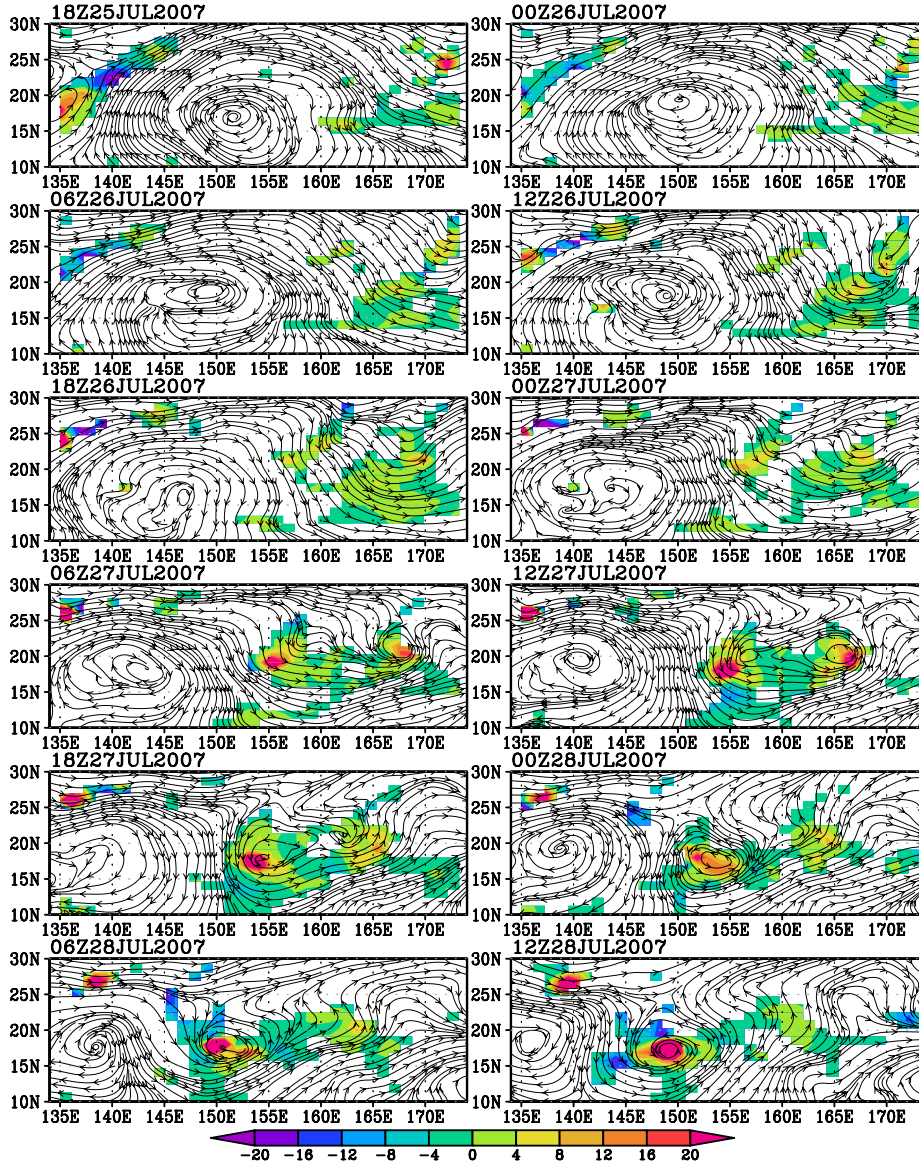
favorable for tropical cyclone formation and to provide guidance on additional or mesoscale factors that may enhance or inhibit tropical cyclone development in the WNP.

## APPENDIX A. OW PLOTS



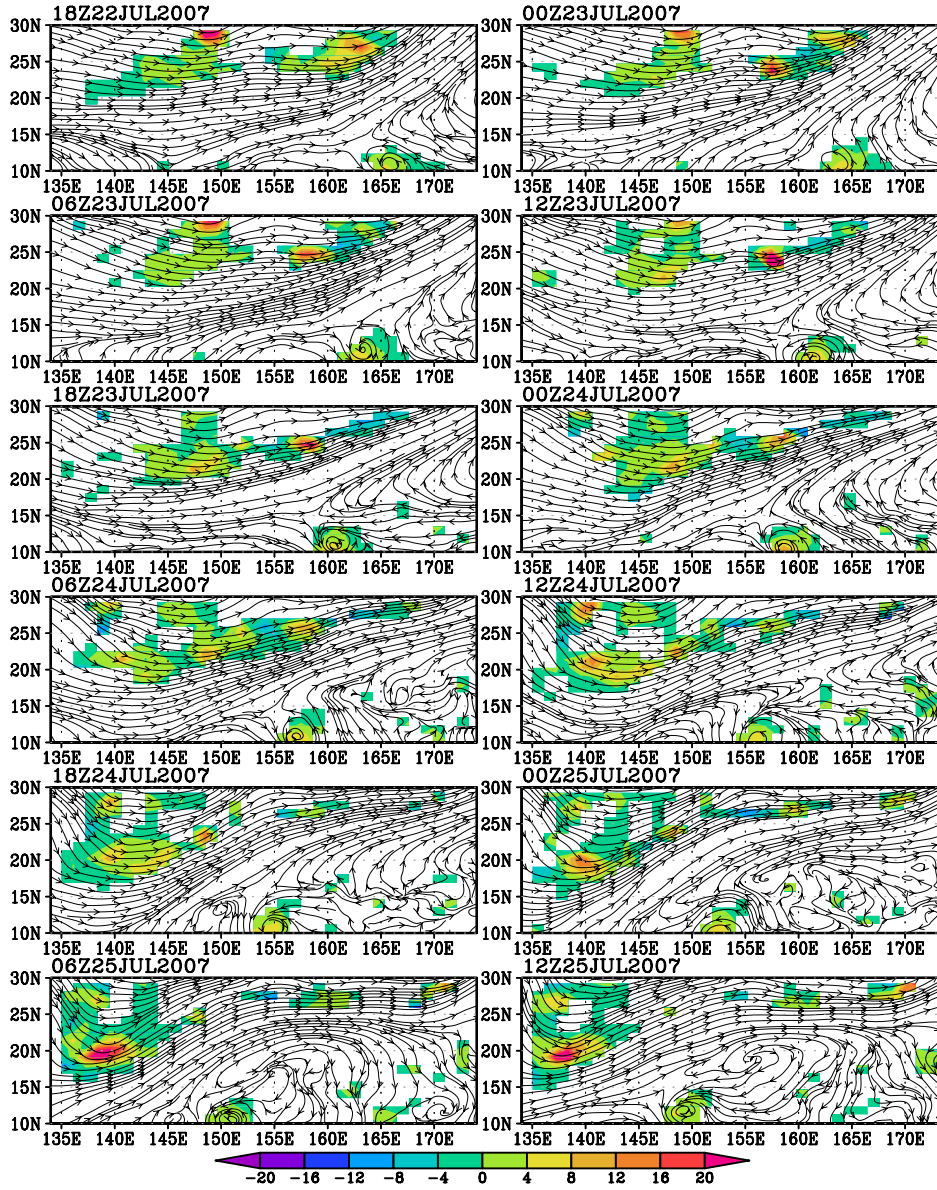
Streamlines of horizontal flow at 600 hPa for the genesis sequence of the non-developer from 1800 UTC 23 July to 1200 UTC 24 July. The shadings indicate high values of OW parameter (units:  $10^{-10} \text{ s}^{-2}$ ) as defined in Eq. (1.1). This quantity, like vorticity, is invariant with respect to translation, therefore identical in translating and moving frames. Red areas are strong values and blue values.

# OW (600 mb; Moving)

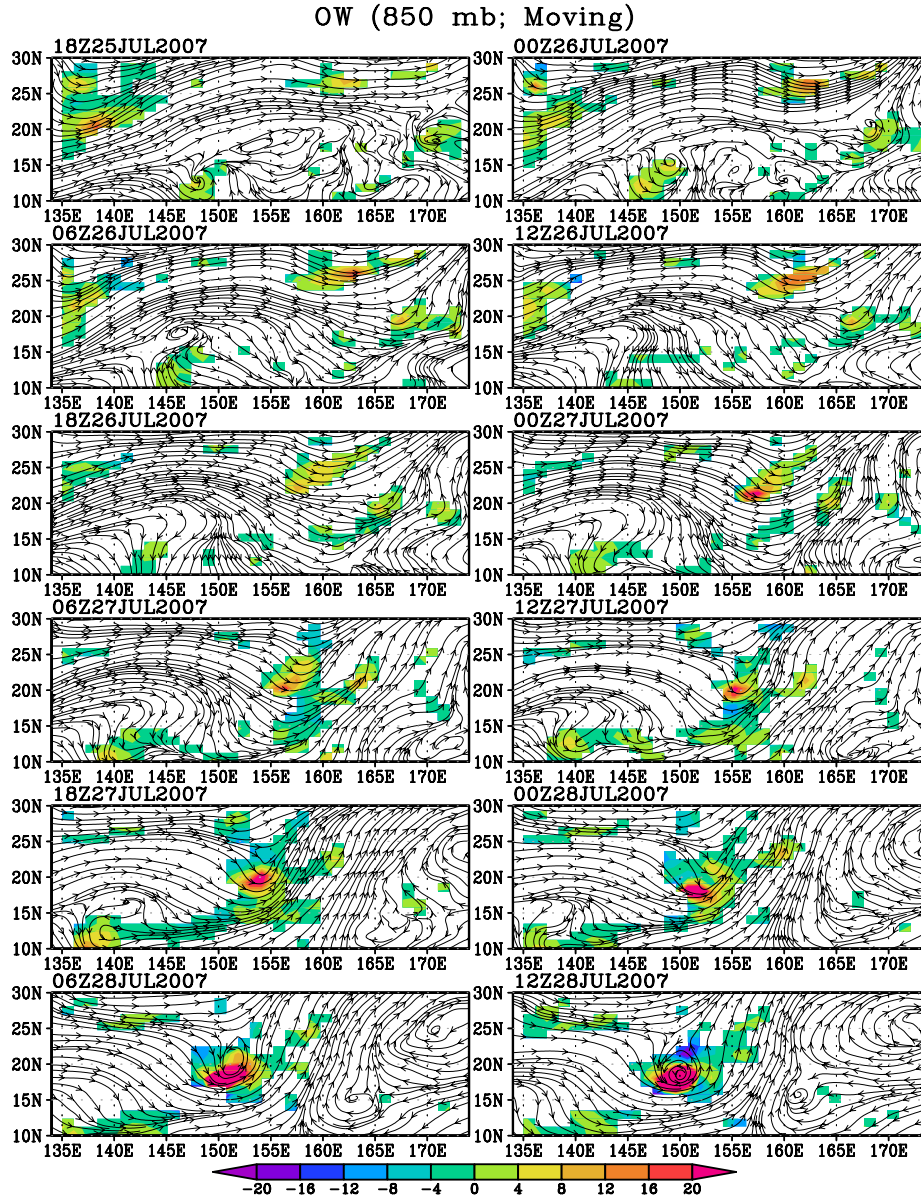


Streamlines of horizontal flow at 600 hPa for the genesis sequence of the non-developer from 1800 UTC 23 July to 1200 UTC 24 July. The shadings indicate high values of OW parameter (units:  $10^{-10} \text{ s}^{-2}$ ) as defined in Eq. (1.1). This quantity, like vorticity, is invariant with respect to translation, therefore identical in translating and moving frames. Red areas are strong values and blue values areas are weak.

OW (850 mb; Moving)

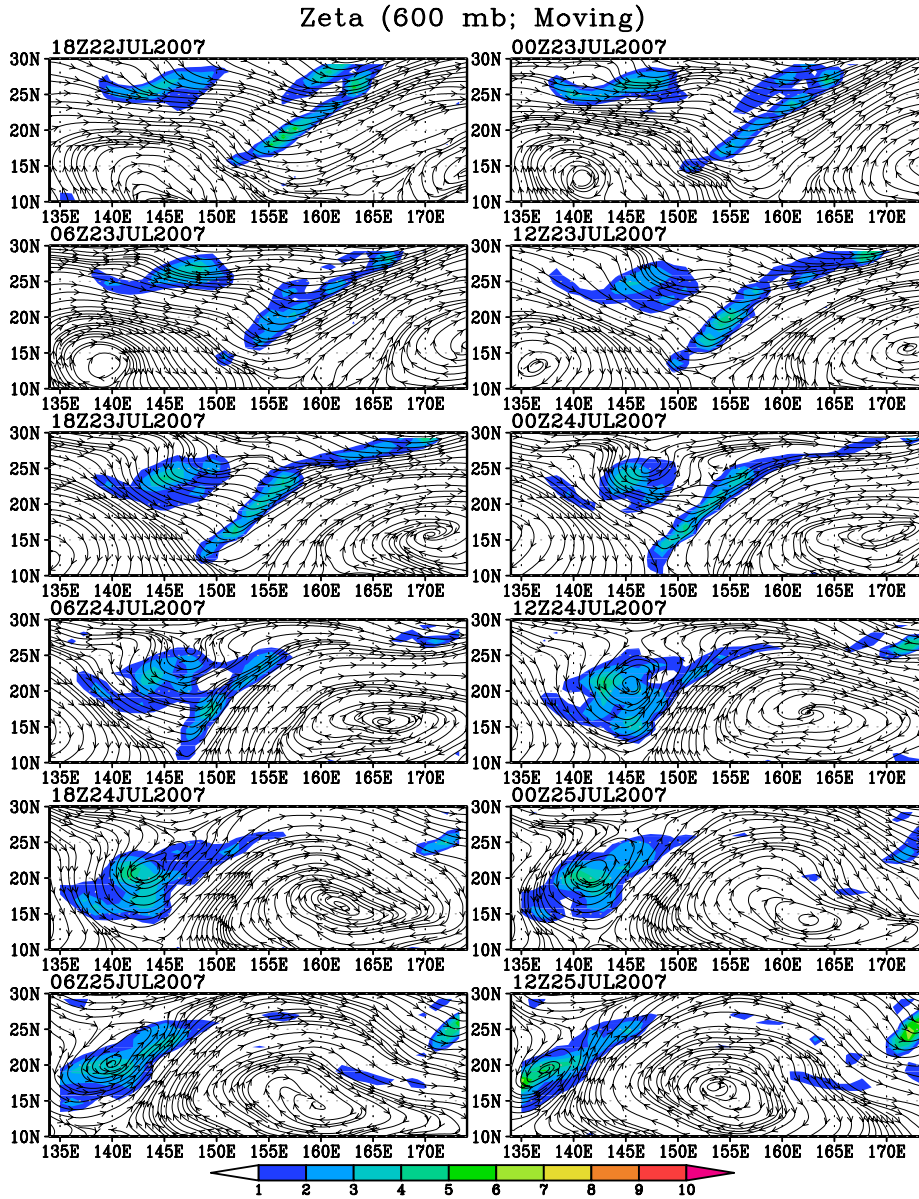


Streamlines of horizontal flow at 600 hPa for the genesis sequence of the non-developer from 1800 UTC 23 July to 1200 UTC 24 July. The shadings indicate high values of OW parameter (units:  $10^{-10} \text{ s}^{-2}$ ) as defined in Eq. (1.1). This quantity, like vorticity, is invariant with respect to translation, therefore identical in translating and moving frames. Red areas are strong values and blue values areas are weak of non-developer from 1800 UTC 22 July – 1200 UTC 25 July.



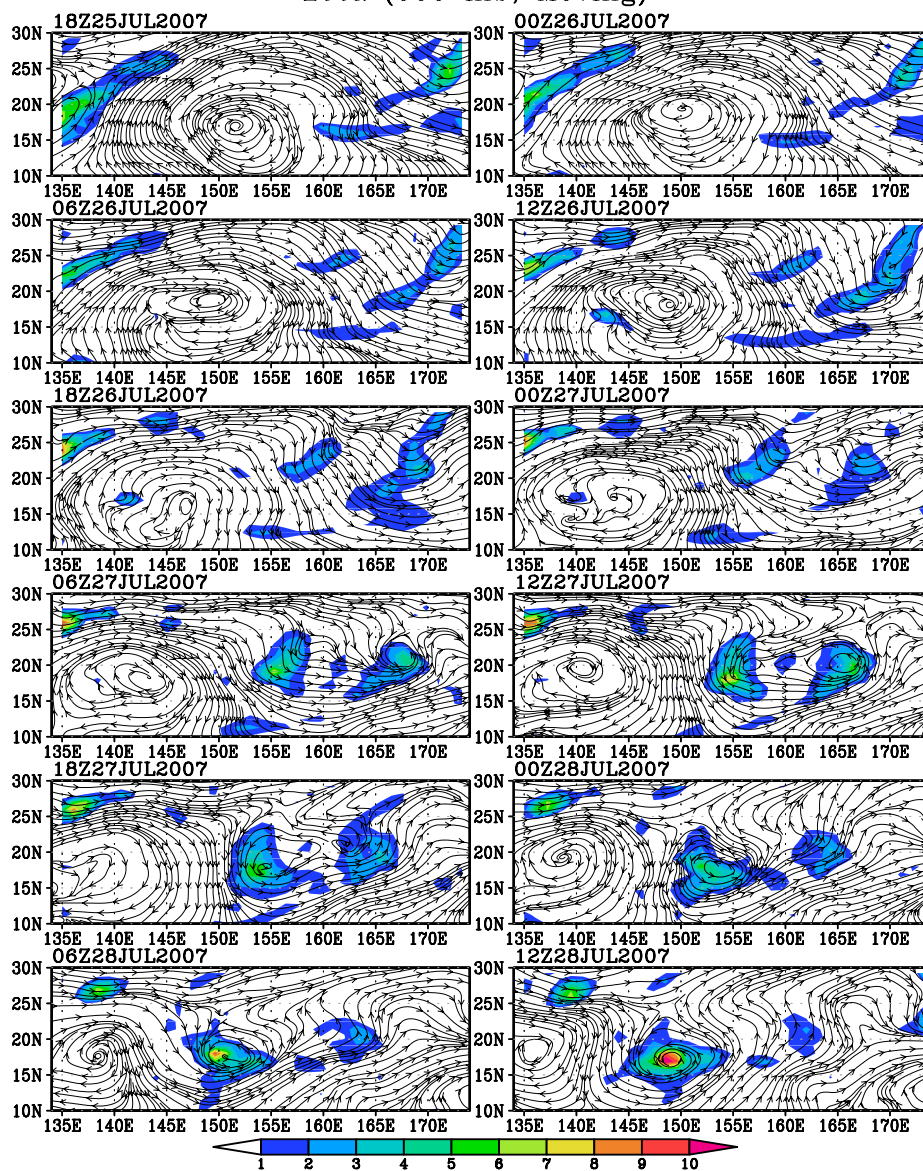
Streamlines of horizontal flow at 600 hPa for the genesis sequence of the non-developer from 1800 UTC 23 July to 1200 UTC 24 July. The shadings indicate high values of OW parameter (units:  $10^{-10} \text{ s}^{-2}$ ) as defined in Eq. (1.1). This quantity, like vorticity, is invariant with respect to translation, therefore identical in translating and moving frames. Red areas are strong values and blue values areas are weak.

## APPENDIX B. RELATIVE VORTICITY PLOTS



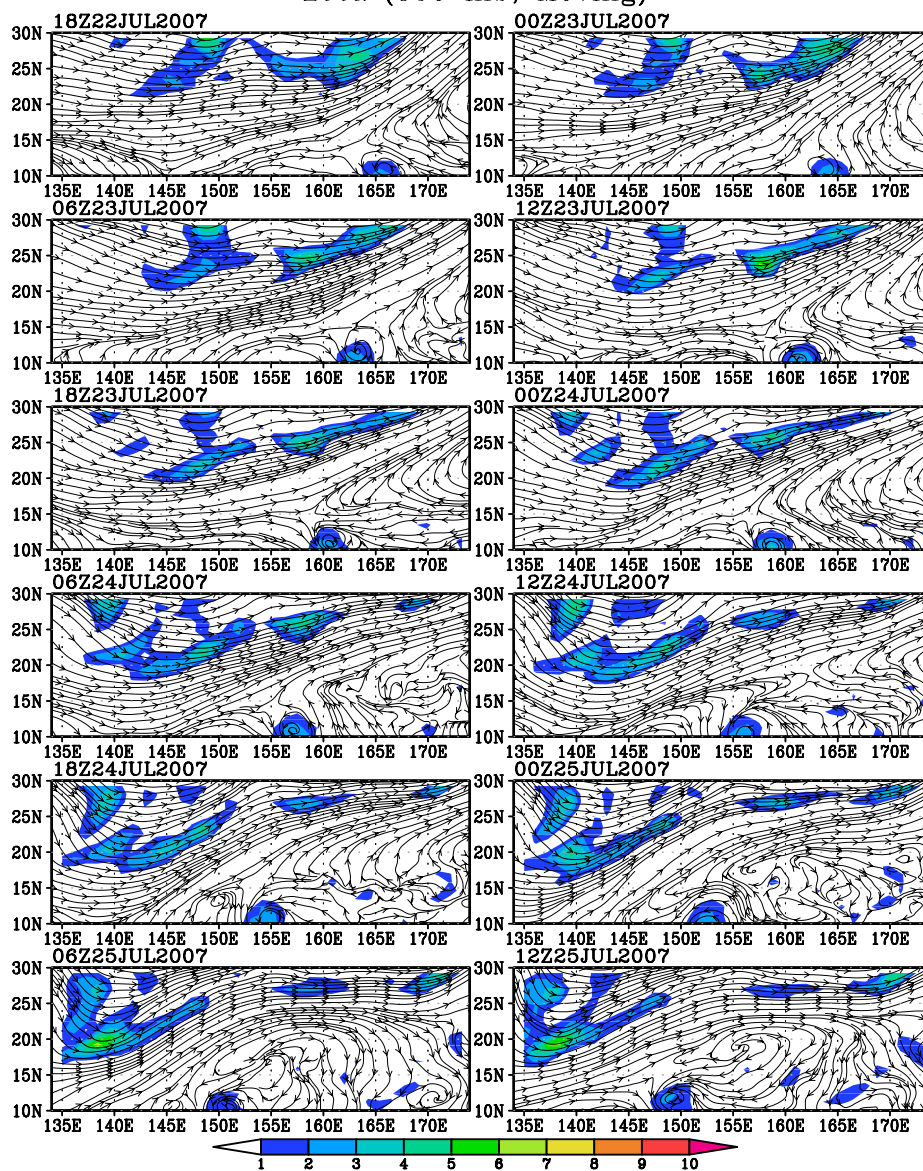
Streamlines of horizontal (rotational+divergent) flow and Zeta at 600 hPa of the non-developer from 1800 UTC 22 July to 1200 UTC 25 July. Shading indicates relative vorticity (units:  $10^{-5} \text{ s}^{-1}$ ).

# Zeta (600 mb; Moving)



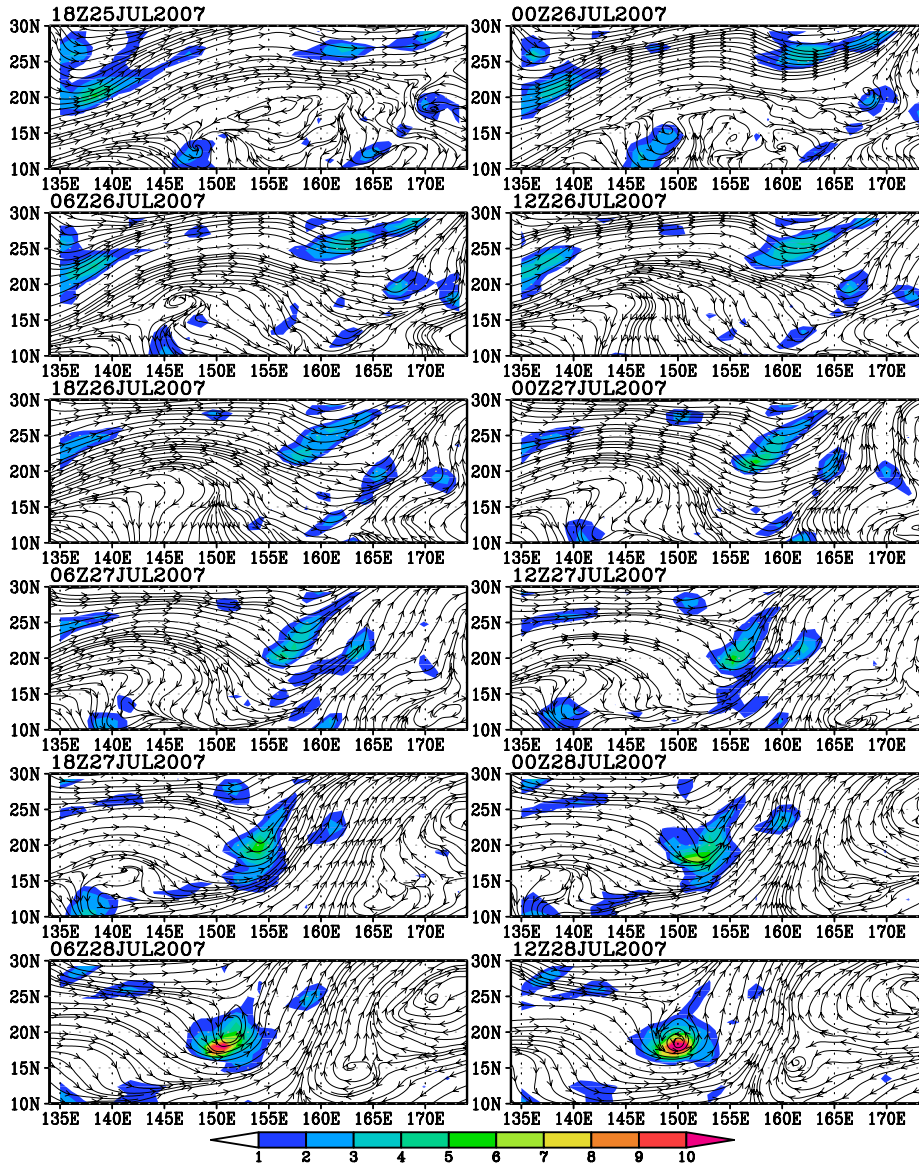
Streamlines of horizontal (rotational+divergent) flow and Zeta at 600 hPa of the non-developer from 1800 UTC 25 July to 1200 UTC 28 July. Shading indicates relative vorticity (units:  $10^{-5} \text{ s}^{-1}$ ).

# Zeta (850 mb; Moving)



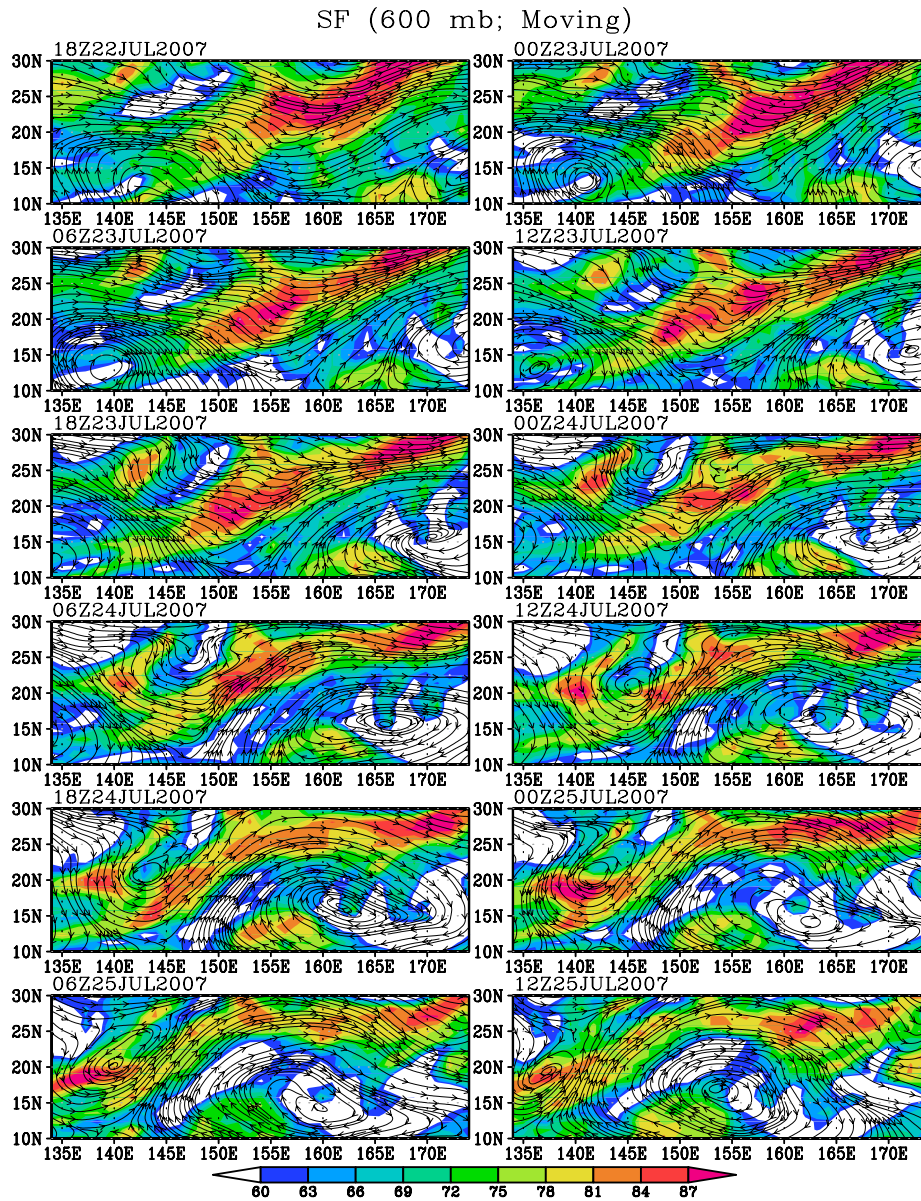
Streamlines of horizontal (rotational+divergent) flow and Zeta at 600 hPa of the non-developer from 1800 UTC 22 July to 1200 UTC 25 July. Shading indicates relative vorticity (units:  $10^{-5} \text{ s}^{-1}$ ).

# Zeta (850 mb; Moving)

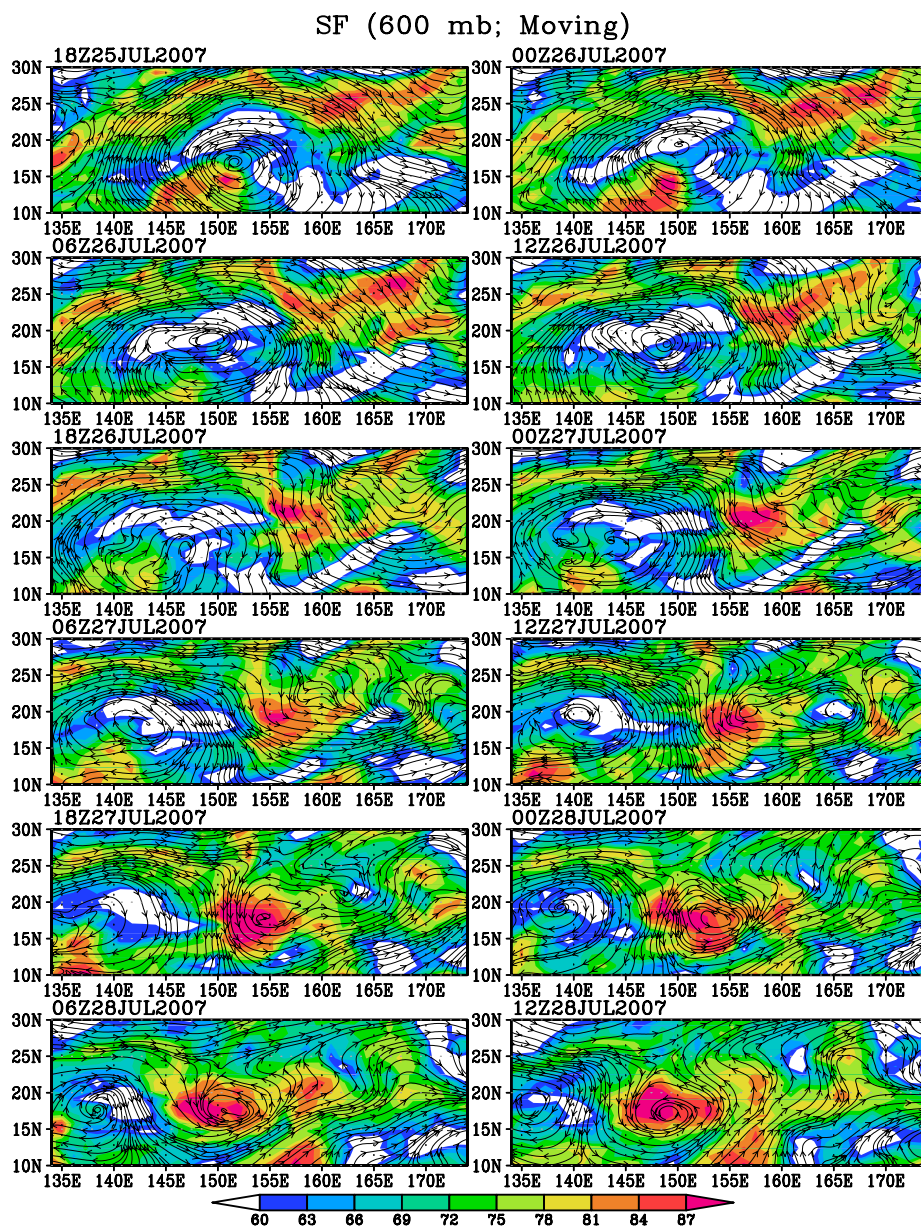


Streamlines of horizontal (rotational+divergent) flow and Zeta at 850 hPa of the Usagi system from 1800 UTC 25 July to 1200 UTC 28 July. Shading indicates relative vorticity (units:  $10^{-5} \text{ s}^{-1}$ ).

## APPENDIX C. SF PLOTS

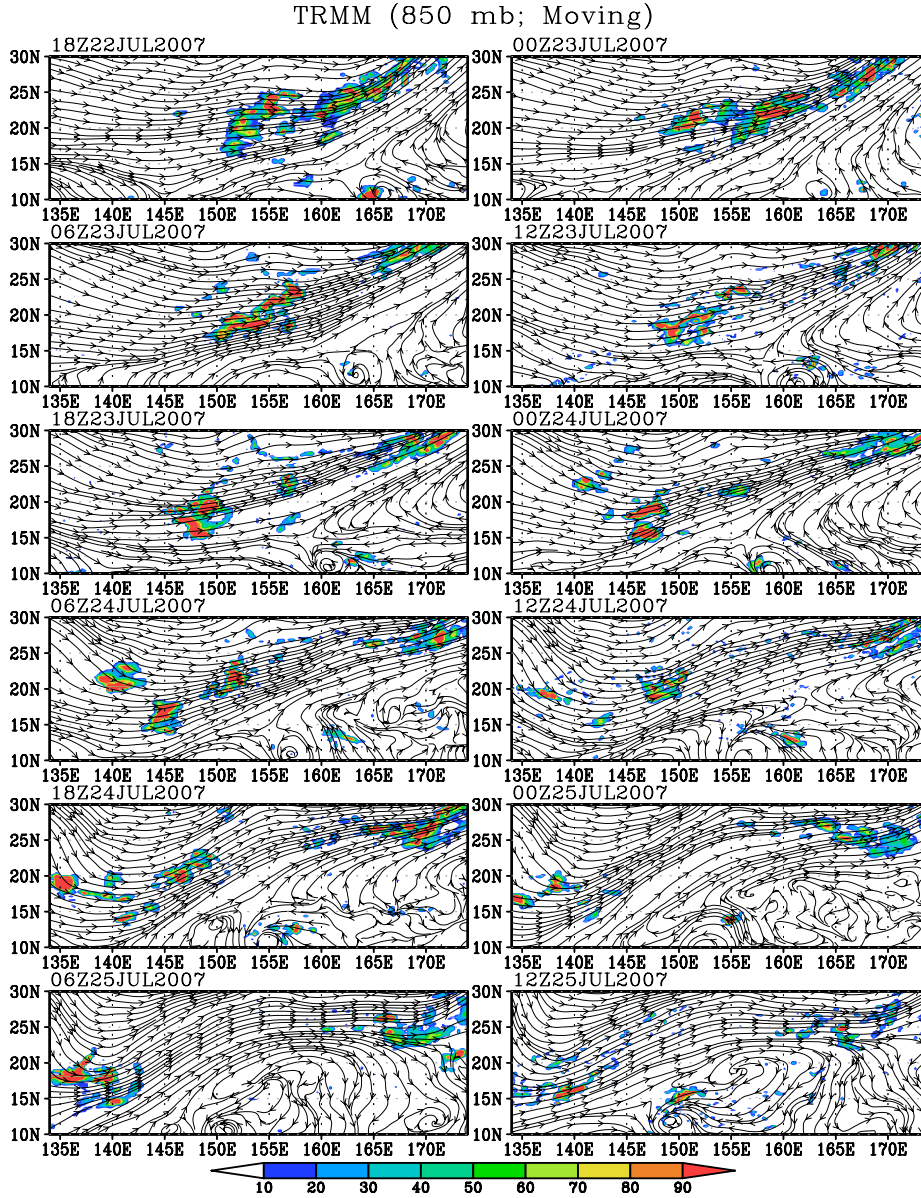


Streamlines of horizontal flow 600 hPa for the genesis sequence of the non-developer, with high values of saturation fraction indicated by shading (unit: percent) from 1800 UTC 22 July to 1200 UTC 25 July. Red areas are strong values and white areas are weak values of SF.



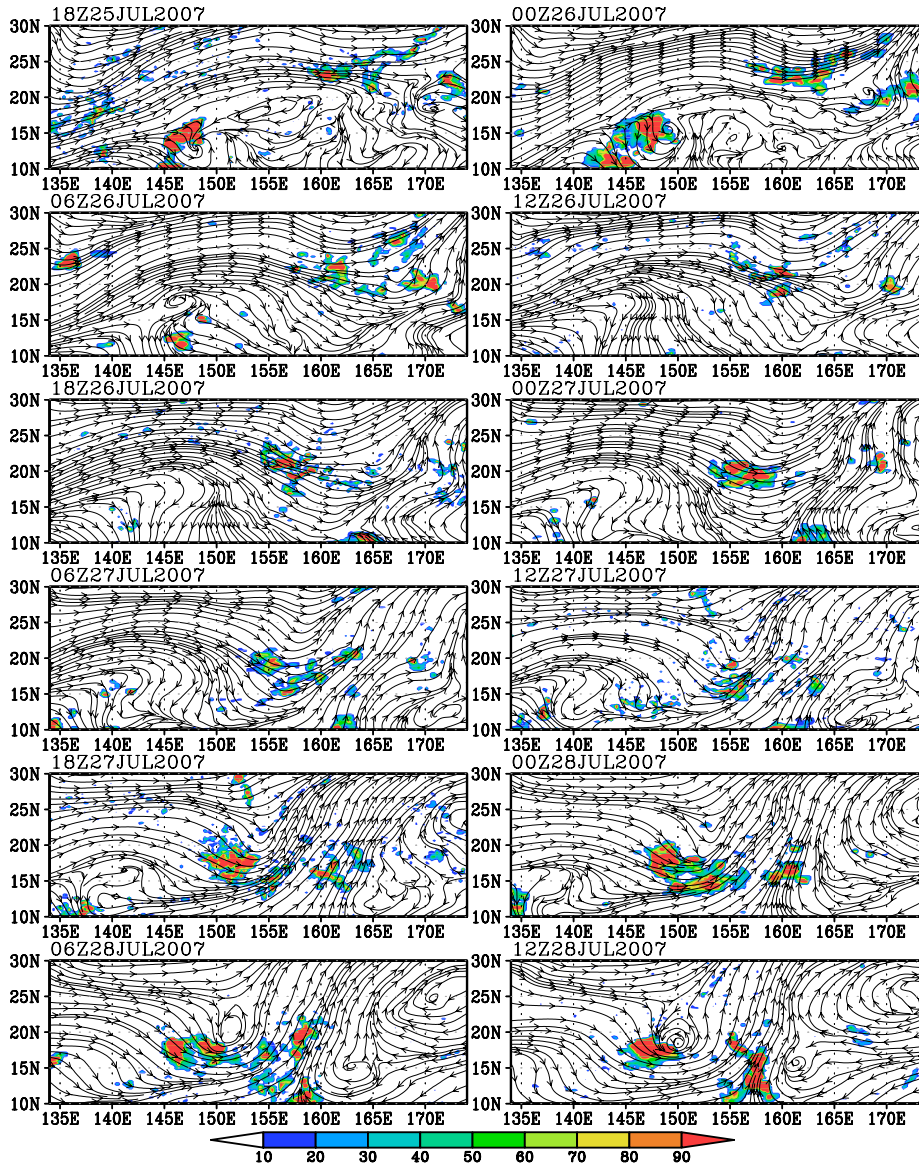
Streamlines of horizontal flow 600 hPa for the genesis sequence of the Usagi system, with high values of saturation fraction indicated by shading (unit: percent) from 1800 UTC 25 July to 1200 UTC 28 July. Red areas are strong values and white areas are weak values of SF.

## APPENDIX D. TRMM PLOTS



Streamlines of horizontal flow 850 hPa for the genesis sequence of the non-developer, with high values of TRMM 3-hour accumulated precipitation indicated by shading from 1800 UTC 22 July to 1200 UTC 25 July. Red areas are strong values and white areas are weak values of precipitation.

TRMM (850 mb; Moving)



Streamlines of horizontal flow 850 hPa for the genesis sequence of the Usagi system, with high values of TRMM 3-hour accumulated precipitation indicated by shading from 1800 UTC 25 July to 1200 UTC 28 July. Red areas are strong values and white areas are weak values of precipitation.

## LIST OF REFERENCES

- BOM, Cited 2008: BOM Website [Available online at [http://www.bom.gov.au/bmrc/pubs/tcguide/ch2/ch2\\_1.htm](http://www.bom.gov.au/bmrc/pubs/tcguide/ch2/ch2_1.htm)], 14 February 2008.
- COLA, cited 2004: Grid Analysis and Display System (GrADS). [Available online at <http://grads.iges.org/grads/>], 14 February 2008.
- Davis, C.A., and L.F. Bosart, 2003: Baroclinically induced tropical cyclogenesis. *Mon. Wea. Rev.*, **131**, 2730-2747.
- Davis, C.A., and L.F. Bosart, 2004: The TT problem: Forecasting the tropical transition of cyclones. *Bull. Amer. Meteor. Soc.*, **85**, 1657-1662.
- Dunkerton, T. J., M. T. Montgomery and Z. Wang, 2008: Tropical cyclogenesis in a tropical wave critical layer: easterly wave, Naval Postgraduate School, **102**, submitted.
- ECMWF, cited 2007: ECMF Website [Available online at [http://www.ecmwf.int/products/forecasts/guide/The\\_Ensemble\\_Prediction\\_System\\_EPS.html](http://www.ecmwf.int/products/forecasts/guide/The_Ensemble_Prediction_System_EPS.html)], 14 February 2008.
- Elsberry, R. L., 2007: Tropical meteorology class notes, Dept. of Meteor., Naval Postgraduate School, Monterey.
- Emanuel, K. A., 2007: The hurricane embryo. Talk presented at short program workshop entitled Small scale and extreme events: The Hurricane, NSF Institute for Pure and Applied Mathematics (IPAM), UCLA.
- Gray, W.M., 1968: A global view of the origin of tropical disturbances and storms, *Mon. Wea. Rev.*, **96**, 669-700.
- Halverson, J., and co-authors, 2007: NASA's Tropical Cloud Systems and Processes Experiment. *Bull. Amer. Meteor. Soc.* **88**, 867-882.
- Hendricks, E. A., M. T. Montgomery, and C. A. Davis, 2004: The role of vortical hot towers in the formation of tropical cyclone Diana (1984). *J. Atmos. Sci.*, **61**, 1209-1232.
- Hoskins, B. J., M. E. McIntyre, and A. W. Robertson, 1985: On the use and significance of isentropic potential vorticity maps. *Quart. J. Roy. Meteor. Soc.*, **111**, 877-946.

- JTWC, cited 2007: Collaboration Site. [Password protected <https://metocph.nmci.navy.mil/collab/jtwc.html>], 14 February 2008.
- Krishnamurti, T. N., H. S. Bedi, M. Subramaniam, 1987: The Summer Monsoon of 1987. *Amer. Meteor. Soc.*, **2**, 321-340.
- McBride, J. L., and W. M. Gray, 1980: Mass divergence in tropical weather systems. Paper I: Diurnal variation. *Quart. J. Roy. Meteor. Soc.*, **106**, 501–516.
- McWilliams, J.C., 2006: Fundamentals of Geophysical Fluid Dynamics, 250, Cambridge, 92-93.
- McWilliams, J.C., 1984: The emergence of isolated coherent vortices in turbulent flow. *J. Fluid Mech.*, **140**, 21-43.
- METED, cited 2007: Buoyancy and CAPE. [Available online at <http://www.meted.ucar.edu/mesoprime/cape/print.htm>], 7 March 2008.
- Montgomery, M.T., and J. Enagonio, 1998: Tropical cyclogenesis via convectively forced vortex rossby waves in a three-dimensional quasigeostrophic model. *J. Atmos Sci.*, **55**, 3176-3207.
- Montgomery, M. T., and R. J. Kallenbach, 1995: Symmetrization, vortex rossby waves, and hurricane motion in an asymmetric balance model. Dept. of Atmospheric Science Paper, **588**, Colorado State University, 78 pp.
- Montgomery, M. T., Nicholls, T. A. Cram and A. B. Saunders, 2006: A vortical hot tower route to tropical cyclogenesis, *J. Atmos. Sci.*, **63**, 335-386.
- NCEP, cited 2003: The GFS Atmospheric Model. [Available online at <http://www.emc.ncep.noaa.gov/gmb/moorthi/gam.html>], 14 February 2008.
- NRL, cited 2004: Development of a Massively Parallel NOGAPS Forecast Model. [Available online at <http://www.nrlmry.navy.mil/sawmill/index.html>], 8 December 2007.
- Powers, J. G., and C. A. Davis, 2002: A cloud-resolving regional simulation of tropical cyclone formation. *Atmos. Sci. Let.*, **3**, 15–24.
- Raymond, D. J., 2007: A Rational Approach to Cumulus Parameterizations. *J. Atmos. Sci.*, submitted.

- Simpson, J., E. Ritchie, G. J. Holland, J. Halverson, and S. Stewart, 1997: Mesoscale interactions in tropical cyclone genesis. *Mon. Wea. Rev.*, **125**, 2643–2661.
- Tory, K. J., and M. T. Montgomery, 2006: Internal influences on tropical cyclone formation. Topic 2.2 in *Sixth International Workshop on Tropical Cyclone*, San Jose, Costa Rica, World Meteorological Organization, 22 pp.
- TRMM, cited 2008: Tropical Rainfall Measuring Mission. [Available online at <http://trmm.gsfc.nasa.gov/>], 8 December 2007.
- Vancas, M. D., 2006: Extratropical transition of tropical storm banyan. M.S. Thesis, Dept. of Meteor., Naval Postgraduate School, Monterey, CA, 72 pp.
- Vis5D, cited 2007: Vis5D documentation site. [<http://vis5d.sourceforge.net/doc/ch01.html>], 14 February 2008.
- Weiss J. B., A. Provenzale, and C. Pasquero, 2002: Vortex statistics from eulerian and lagrangian time series, *Phy Rev Let*, **89**, 1-4.
- Wheeler, M. C., and H. H. Hendon, 2004: An all-season real-time multivariate MJO index: development of an index for monitoring and prediction, *Mon. Wea. Rev.*, **132**, 1917-1932.
- Zehr, R. M., 1992: Tropical cyclogenesis in the Western North Pacific. NOAA Technical Report NESDIS 61, NOAA, Washington, D.C., 181 pp.

THIS PAGE INTENTIONALLY LEFT BLANK

## INITIAL DISTRIBUTION LIST

1. Defense Technical Information Center  
Ft. Belvoir, Virginia
2. Dudley Knox Library  
Naval Postgraduate School  
Monterey, California
3. Superintendent  
Naval Research Laboratory  
Monterey, California
4. Professor Michael Montgomery  
Naval Postgraduate School  
Monterey, California
5. Professor Patrick Harr  
Naval Postgraduate School  
Monterey, California
6. Professor Russell Elsberry  
Naval Postgraduate School  
Monterey, California
7. Professor Phil Durkee  
Naval Postgraduate School  
Monterey, California
8. Professor Karl Pfeiffer  
Naval Postgraduate School  
Monterey, California
9. Doctor Zhuo Wang  
Naval Postgraduate School  
Monterey, California
10. Doctor Tim Dunkerton  
Northwest Research Associates  
Bellevue, Washington
11. Director, Joint Typhoon Warning Center  
Naval Pacific Meteorology and Oceanography Center  
Pearl Harbor, Hawaii

12. Captain Raymund DeLeon  
AFSOUTH Weather Flight  
Davis-Monthan Air Force Base, Arizona